A Study of the Erosion Mechanisms of Silicone Rubber Housing Composites

by

Refat Ghunem

A thesis
presented to the University of Waterloo
in fulfillment of the
thesis requirement for the degree of
Doctor of Philosophy
in
Electrical and Computer Engineering

Waterloo, Ontario, Canada, 2014

AUTHOR'S DECLARATION

I hereby declare that I am the sole author of this thesis. This is a true copy of the thesis, including any required final revisions, as accepted by my examiners.

I understand that my thesis may be made electronically available to the public.

Abstract

Silicone rubber insulators have been replacing conventional insulators made from toughened glass and porcelain in the power system, due to the non-wetting properties of silicone rubber insulation housing. However, silicone elastomers will eventually wet-out leading to leakage current and dry-band arcing giving rise to erosion of the silicone housing material, and eventually insulation failure. Well-established formulations of insulation housing composites have been developed and validated for erosion performance using the standard inclined plane tracking and erosion test, yet no such formulations have been developed and validated for DC. With the assumption that equivalent performance will be obtained, an adjustment to the creepage distance has been the measure taken in using the AC insulators for DC, without taking into consideration the differing aspects of the DC as compared to the AC dry-band arcing. This practice questions the existing DC insulators as an unknown entity that requires further investigation to ensure the reliability of the power supply. In addition recent demands have been raised to develop housing composites specifically for DC outdoor insulation, particularly with the increased interest in DC. It follows that developing a standard DC inclined plane tracking and erosion test is necessary for the development of more suitable materials for outdoor DC insulation applications.

This thesis provides a thorough study of the DC dry-band arcing mechanism as opposed to the well understood mechanism of the AC dry-band arcing and provides a mechanistic understanding to the dry-band arcing leading to erosion as a foundation for the development of a standard DC inclined plane tracking and erosion test. To this end, the influence of inorganic fillers in silicone rubber on resisting erosion due to dry-band arcing is also presented, as an essential step towards obtaining more suitable silicone composite for DC outdoor insulation applications.

Acknowledgements

First and foremost all the gratitude goes to almighty God for providing me with the strength and spirit to complete my thesis study successfully.

My appreciation goes to my dear thesis supervisors, Prof. Shesha Jayaram and Prof. Edward Cherney, for their support and guidance throughout my study. Talking about erosion, the knowledge and experience I have gathered from my supervisors have been essential in eroding my path towards finalizing my research study. I wish to thank them for the effort they have given for supervising my research study and I wish I would be always meeting their expectations.

My thanks go to the examining committee, Prof. Behzad Kordi, Prof. Magdy Salama, Prof. George Freeman and Prof. Leonardo Simon for their beneficial comments on my thesis study. I wish to express my appreciation to Prof. Edward R. Vrscay for the invaluable discussions. I would like also to express my deep thanks to my teachers and elder brothers Dr. Ayman El-Hag and Dr. Khalid Assaleh for the pieces of advice that enlightened my track.

I can't forget my colleagues and friends in the high voltage engineering lab (HVEL) and at the University of Waterloo for the truthful discussions during my PhD study.

Last but not least, I wish to express my deep appreciation to my dear parents, brother and sister, who were always behind the scenes providing me with all the support and self-esteem needed to conduct my study successfully.

Dedication

To my first and foremost teacher, my father Atef, and beloved mother Hanan,

To My dear brother, Mohammad (Ghuna Motatawera),

To my sweet sister and cousin, Daed (sweet Dodo) and Bilal (Abu Nabil),

and to my eagerly awaited beautiful niece, lovely Naya.

Table of Contents

List of Figures

List of Tables

List of Acronyms and Symbols

Acronyms

Chapter 1

AC	Alternating current
ASTM	American Society for Testing Materials
ATH	Alumina Tri-Hydrate
CV	Coefficient of Variation
DBA	Dry-Band Arcing
DC	Direct current
DSC	Differential Scanning Calorimetry
EDBA	Eroding Dry-Band Arcing
EPDM	Ethylene Propylene Diene Monomer
HTV	High-Temperature Vulcanizing
IEC	International Electrotechnical Commission
IPT	Inclined Plane Tracking and Erosion Test
IR	Infrared
ITV	Initial-Tracking Voltage
LC	Leakage Current
LMW	Low-Molecular Weight
LSR	Liquid Silicone Rubber
MRA	Multiresolution Analysis
PDMS	Polydimethylsiloxane
rms	Root Mean Square
RTV	Room-Temperature Vulcanizing
SiR	Silicone Rubber
TGA	Thermogravimetry Analysis
UV	Ultraviolet

Chapter 3

DTG	Differential Thermogravimetry
HA25	Commercial High-Temperature Vulcanizing Silicone Rubber+25 wt% Alumina Tri-Hydrate

HA58	Commercial High-Temperature Vulcanizing Silicone Rubber+58 wt% Alumina Tri-Hydrate
RA10	Liquid Silicone Rubber+10 wt% Alumina Tri-Hydrate
RA30	Liquid Silicone Rubber+30 wt% Alumina Tri-Hydrate
RA50	Liquid Silicone Rubber+50 wt% Alumina Tri-Hydrate
RA30L	Laser Sample-Liquid Silicone Rubber+30 wt% Alumina Tri-Hydrate
RA50L	Laser Sample-Liquid Silicone Rubber+50 wt% Alumina Tri-Hydrate
RA30TC	Thermal Conductivity Sample-Liquid Silicone Rubber+30 wt% Alumina Tri-Hydrate
RA35TC	Thermal Conductivity Sample-Liquid Silicone Rubber+35 wt% Alumina Tri-Hydrate
RA40TC	Thermal Conductivity Sample-Liquid Silicone Rubber+40 wt% Alumina Tri-Hydrate
RA45TC	Thermal Conductivity Sample-Liquid Silicone Rubber+45 wt% Alumina Tri-Hydrate
RA50TC	Thermal Conductivity Sample-Liquid Silicone Rubber+50 wt% Alumina Tri-Hydrate
RA55TC	Thermal Conductivity Sample-Liquid Silicone Rubber+55 wt% Alumina Tri-Hydrate
RS10	Liquid Silicone Rubber+10 wt% silica
RS30	Liquid Silicone Rubber+30 wt% silica
RS50	Liquid Silicone Rubber+50 wt% silica
RS30L	Laser Sample-Liquid Silicone Rubber+30 wt% Silica
RS50L	Laser Sample-Liquid Silicone Rubber+50 wt% Silica
TE	Time-to-Eroding
Chapter 4	
RI	Residue Intact
RR	Residue Removed

Symbols

Chapter 1

^{o}C	Degrees Centigrade
CH_3	Methyl Group
CH_4	Methane
CO_2	Carbon Dioxide
Si-O	Siloxane Bond
wt%	Percentage weight
cm	Centimeter
NH_4Cl	Ammonium Chloride

V	Volt
Ω	Ohm
kΩ	Kilo ohm
%	Percent

Chapter 3

A	Surface area
A_j	Reconstructed wavelet-based approximation at the j^{th} resolution
a_k	Approximation expansion coefficients
A_{rms}	Root-mean-square of the approximation expansion coefficients
cm^3	Centimeter cube
$COV(Y_1,Y_2)$	Covariance between Y_1 and Y_2 data sets
C_p	Heat capacity
D_j	Reconstructed wavelet-based detail at the j^{th} resolution
$d_{j,k}$	Detail expansion coefficients
d_{jrms}	Root-mean-square of the j^{th} detail expansion coefficients
f_s	Sampling frequency
g	gram
h_o	Coefficients of the scaling function
h_1	Coefficients of the wavelets
Hz	Hertz
i	Dry-band arcing current
I_w	Wetting current
j	Resolution Level
k	Translation Factor
K	Windowed width of the leakage current signal
kHz	Kilohertz
kV	Kilovolt
kVA	Kilo volt-ampere
K_s	Fraction of total power absorbed by the tested silicone rubber sample in the inclined plane test
kW	Kilowatt
L	Distance between metallic electrodes
L_a	Dry-band arcing length

m	Integer
mA	Milliampere
min	minute
ml	Milliliter
mm	Millimeter
μm	Micrometer
mK	Millikelvin
mV	millivolt
N_2	Nitrogen
P_d	Dry-band arcing power
P_s	Power Dissipated on the tested silicone rubber by dry-band arcing during the inclined plane test
psi	Per square inch
Q	Heat flow
r	Correlation coefficient
R	Voltage ratio
R_b	Ballast resistance
r_d	Dry-band arcing resistance per unit length
r_p	Wetting resistance per unit length
R_T	Thermal resistance
s	second
T_{max}	Maximum surface temperature
T	Temperature
t	Dry-band arcing duration
thk	Thickness
V_d	Dry-band arcing voltage
V_s	Source voltage
V_w	Wetting voltage
W	Watt
Y_1	First set of data used in the calculation of the correlation coefficient
Y_2	Second set of data used in the calculation of the correlation coefficient
ρ	Density
↓2	Down sampling by 2

∇	Gradient
$\frac{\partial T}{\partial t}$	Partial derivative of temperature with respect to time
Φ_k	Scaling function
ΔT	Temperature drop
ψ_k	Wavelet

Chapter 5

%Diff	Percentage Difference
i	Current waveform
$\bar{i}$	Mean of the current
i_{rms}	Root-mean-square current
N	Number of samples
n	number of samples
V^{ref}	Reference Voltage
σ	Standard Deviation

Chapter 1
Introduction

1.1 Preface

High voltage direct current can be an economical mode of power delivery, but justification for its use must address the aspect of reliability. The reliable performance of outdoor insulators, which are recognized as one of the backbone components of the transmission and distribution line systems, has accordingly become a crucial demand. Currently, outdoor silicone rubber (SiR) insulators are replacing the conventional ceramic insulators, as SiR housing materials have demonstrated an electrical performance superior to porcelain and glass. However, in polluted conditions, SiR insulators are prone to dry-band arcing (DBA) eroding the housing material, which may lead to insulation failure and consequently interruption of the power supply.

Extensive investigation into the erosion mechanism has been conducted in the development of SiR insulators with acceptable erosion performance. In particular the reliable evaluation of erosion in the standardized inclined plane tracking and erosion test (IPT) has led to well established formulations of SiRr housing for AC outdoor insulation applications. On the other hand, creepage distance has been the specification considered for polymer DC as compared to AC line insulators, with lesser attention given to the relative erosion performance and despite the very different DBA characteristics under DC as compared to AC voltages. Due to the rapid growth taking place in the power system network, power delivery in DC is becoming an option for utilities, raising the importance of standardizing the DC IPT and thus developing new and improved silicone rubber housing composites for DC outdoor insulation.

The diagram in Figure 1.1 summarizes the fundamental requirements of developing SiR housing composites with acceptable erosion performance, indicating the determination of the erosion indicators and the use of the thermal characterization methods are additional tools that construct for more solid base of SiR insulation housing design in the IPT. It follows that understanding the eroding DBA (EDBA) mechanism and the effects by which inorganic fillers suppress SiR erosion in the DC IPT are critical tasks in the development of SiR insulation housing composites for DC outdoor insulation. Therefore, the intent in this study is to investigate the mechanisms and develop the necessary tools leading to the development of the standard DC IPT, which obviously facilitates designing reliable SiR housing composites for DC outdoor insulation.

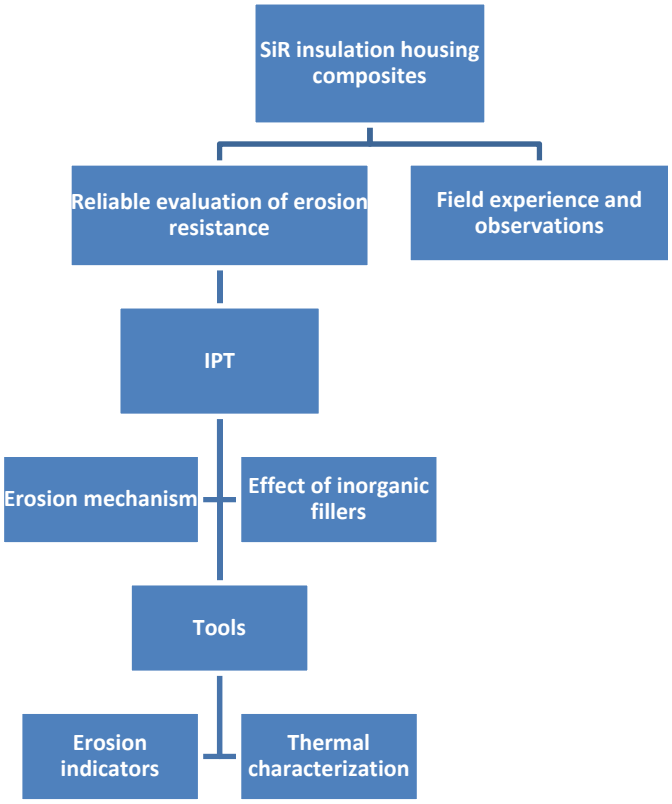

Figure 1.1. Simplified procedures of the development of SiR insulation housing composites.

1.2 Motivation

DC mode of power delivery has been taken into consideration for long distances, mainly due to the economical costs of installation. Such a limited application for DC transmission of electricity has justified the lesser emphasis on developing insulation housing withstanding the DBA under DC voltages. In particular, relatively few studies have evaluated SiR formulations to gain an understanding of the physical mechanism of DBA under DC, with focuses mainly given on the validation of AC-designed composites for outdoor DC insulation. This practice, which has been adopted for utilities and insulator manufacturers, has reduced the incentive to develop insulators that can function specifically for stresses under DC voltages.

With the increased interest in DC mode of power delivery, a new concern has been raised about the validity of the current practice in applying the AC-designed insulators for DC. Such a concern is justified, given the traditional belief about the DBA being more severe under DC as compared to AC voltages, particularly with the recent concerns given to the existence of severe erosion at the end seals of the insulators designed for AC and yet have been used under DC voltages.

Most importantly, a new demand has recently been raised for the development of new and improved insulators for DC as the rapid development in the area of power electronics has further facilitated transmitting power in DC. In addition, the penetration of distributed generators into the deregulated power system network, producing DC as the output mode of power, has even promoted the DC microgrid paradigm in a hybrid scheme with the existing AC grid. These new concepts of power delivery require reliability of operation as an essential requirement, which eventually requires insulation housing to possess acceptable erosion performance, thus withstand the stresses under DC effectively.

Although, observations leading to characterization of DBA under field conditions are important, standardized tests, such as the inclined plane tracking and erosion test (IPT), salt-fog test and rotating-wheel-dip test are the primary tools through which outdoor insulation housing are designed in the material development stage. Of these standards, the IPT has been widely utilized in the industry and even at the research scale due to its low-conduction time to rank materials that are suited for field applications. It follows that understanding the eroding EDBA mechanism and the effects by which inorganic fillers suppress SiR erosion in the DC IPT are critical tasks in the development of SiR insulation housing composites for DC outdoor insulation. On the other hand, relatively few studies have been conducted to determine the DC performances of SiR in the IPT, with almost no attention given to the development of the equivalent standard DC IPT. Such development task is very important not only to provide reliable outcomes for DC stresses, but also to ensure practical testing that will lead to optimal rather than overdesigns of SiR housing composites.

1.3 Objectives

In this thesis, a thorough study of the DC DBA mechanism as opposed to AC DBA, for which the latter is well understood, is conducted. In the above mentioned contest, the study will closely examine the role of inorganic fillers, which are vital for suppressing the effects of DBA. Such an understating leads to building solid guidelines of developing the equivalent DC IPT, as a foundation for the development of optimum polymeric composites for outdoor DC insulation.

In particular the objectives of this thesis are as follows:

- Understanding the DC DBA mechanism as compared to the well-understood AC DBA, thereby validating the existing standard apparatus of the IPT for DC voltages and developing equivalent guidelines for the DC IPT.

- Understanding the EDBA mechanism in the DC IPT and determining the corresponding erosion indicators in LC.
- Investigating the role of inorganic fillers, in particular, the filler level and type (silica vs. ATH) on suppressing the heat ablation by DBA under DC voltages.

1.4 Thesis Organization

The organization of this thesis can be summarized as follows:

- In Chapter 2, "Materials and Methods", the SiR composites utilized in the study are described in terms of the base material and the fillers incorporated. The IPT setup and methods are described. The IPT is utilized beyond the determination of the erosion resistance of the tested composite to investigate the EDBA mechanism and the corresponding suppression effects of fillers. An infrared (IR) camera is used to monitor surface temperature during the IPT, and thermal characterization of the composites is conducted. Laser heating experiments, thermogravimetry analysis (TGA), DSC and thermal conductivity measurements as per ASTM D5470 is described as the thermal characterization methods.
- Chapter 3, "Results", presents the experimental findings obtained in the IPT and thermal characterizations tests. The results include the eroded depth and area of the tested SiR under DC as compared to AC voltages of the IPT, the simultaneous LC and temperature measurements during the IPT, and the eroding hotspot temperature as obtained by TGA and DSC.

- Chapter 4, “Discussion”, analyzes the results presented in Chapter 3 and explains the erosion mechanism of the DC DBA and its influential factors with respect to the voltage type. In addition, the role of inorganic fillers in reducing the effect of the DC DBA in the IPT is described. These mechanistic studies are shown through establishing correlation between the IPT outcomes and the thermal characterization conducted. Analysis of the hotspot temperature induced by the DBA of the AC, +DC and –DC IPTs is provided.
- Chapter 5, “Conclusions and Future Work”, provides conclusions to the findings obtained throughout the study and recommendations for the future work pertaining to the investigated topics.

Chapter 2

Background and Literature Survey

2.1 Outdoor Insulators in the Power System

Outdoor insulators in the power system function to hold the bare conductors that are mechanically supported by the grounded overhead line towers and to provide the electrical isolation between the energized conductors and the towers. Outdoor insulators have been commonly classified based on the type of the insulation housing material as conventional ceramic with porcelain or glass housing and non-ceramic with polymeric weathersheds, as depicted in Figure 2.1. The core in polymer insulators is an insulating fiberglass rod; whereas, as an example, the cap and the pin in the suspension type porcelain insulators are joined through cement. Both insulator types are equipped with mechanical fitting as the hardware parts.

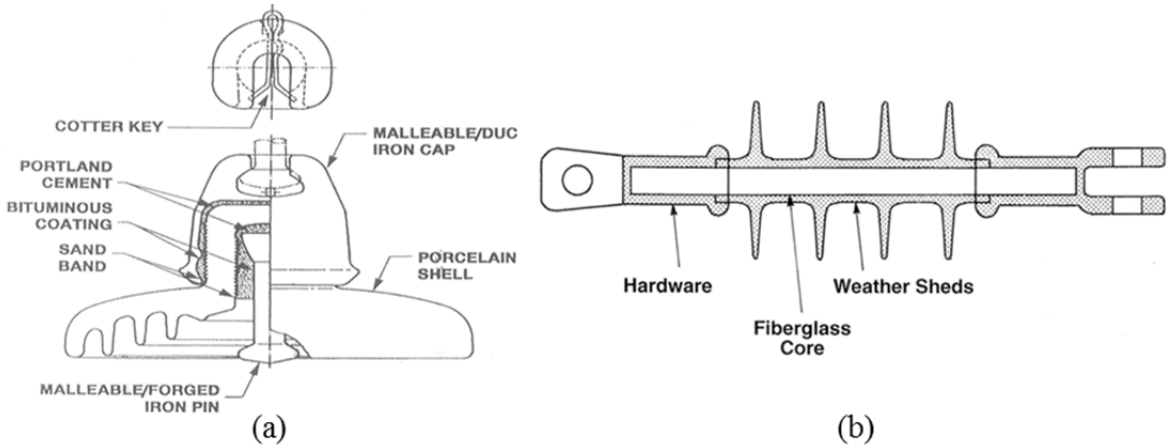

Figure 2.1. Schematic diagram of (a) cap-and-pin suspension type procelain and (b) polymer insulators [1].

2.1.1 Contamination Performance of Outdoor Insulators

Outdoor insulators are subject to electrical, mechanical, thermal, chemical and environmental stresses, which may lead to insulation failure and thus interruption of the power supply. Therefore outdoor insulation designs of different geometries and hosing material compositions are developed to withstand these stresses, with a careful consideration given to the possible synergistic effects of combined stresses in polluted environments.

In outdoor polluted conditions, contaminants are deposited on the surface of the insulation housing mainly due to the force of the wind, and the type of contaminants is dependent on the location of the insulators installed in commercial, industrial or residential areas [1]. Due to wetting of the pollutants, conductive filaments giving rise to leakage current (LC) may develop. As a result, evaporation by joule heating of the conductive layer may take place, forming dry bands across which most of the energization voltage will appear. If the dry-band voltage is sufficient to initiate ionization, dry-band arcing (DBA) takes place. The DBA may severely degrade the housing material or propagate to bridge the insulator surface leading to flashover, and eventually interruption of power supply.

Polymer insulators have demonstrated superior pollution performance due to the low surface tension (hydrophobicity) of the housing materials, while ceramic insulators are prone to wetting. On hydrophobic surfaces, wet contaminants tend to shape as intermittent droplets (Figure 2.2), thereby suppressing the development of conductive paths for LC. Of the polymeric insulating materials in use, silicone rubber (SiR) has shown superior hydrophobicity, most importantly, due to the diffusion of a low-molecular weight (LMW) fluid from the bulk to the surface, washing off the contaminants and retaining the hydrophobicity of the housing material [2]. The hydrophobicity recovery of SiR not only delays the induction of DBA, but also reduces the operational costs of conducting hot-line

washing as a preventive maintenance for the insulators. Therefore, the silicone-based composites are the preferred housing material formulations for outdoor insulators.

Figure 2.2. Hydrophobic surface of a polymer inslator [3].

2.1.2 Tracking and Erosion of Silicone Rubber Insulation Housing

When continuous wetting destroys the hydrophobicity of SiR insulators, the housing material may be susceptible to DBA leading to tracking and erosion. Surface tracking is defined as the development of carbonized channels that causes an irreversible loss of insulation properties [4]. The carbonaceous tracks may propagate as moving DBA electrodes or, alternatively, may be removed from the surface due to the wind or other effects, whereby erosion becomes dominant [5]. Inorganic fillers, which constitute a major portion of the housing material, play a role in reducing the amount of the polymer, thus the organic components, which suppresses tracking. In particular, SiR has an inorganic backbone as compared to other insulating materials, such as ethylene propylene diene monomer (EPDM); therefore, erosion should be the concern over tracking in the case involving SiR insulators.

CHAPTER 2 BACKGROUND AND LITERATURE SURVEY

Erosion is the permanent loss of insulation mass, dominantly, through heat. Heat ablation of the housing material may leave the fiberglass core vulnerable to moisture and voltage, which are conducive to tracking failure of the rod, thus to insulation failure. Development of SiR composites with acceptable erosion resistant has, therefore, been the essential task investigated in the development of SiR housing materials for outdoor insulation applications.

Figure 2.3 depicts the erosion mechanism of SiR due to DBA, showing moisture to play the key role by dissolving the deposited contaminants, thus, forming conductive channels for LC [6]. It follows that the thickness of the conductive channels affects the surface resistance of electrical insulation and thus the DBA current magnitudes imposing heat. The induced DBA as well as localized hot spots enhance the effect of thermal degradation, which, along with other mechanisms such as ultraviolet (UV) radiation and corona erodes the housing material.

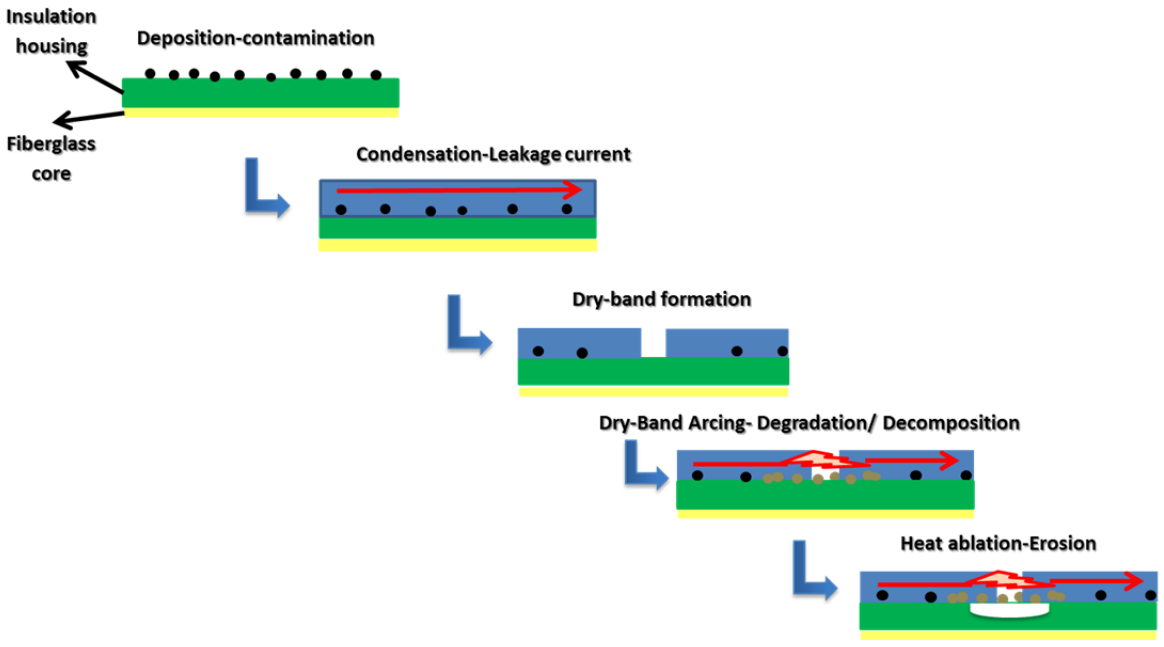

Figure 2.3. Erosion mechanism of SiR insulators by DBA.

2.2 Silicone Rubber for Outdoor Insulation Housing

The backbone structure of SiR is composed of alternating inorganic siloxane bond (Si-O) with methyl groups (CH_3) added, forming polydimethylsiloxane (PDMS) as shown in Figure 2.4. Substitution of the methyl groups with other organic functional groups facilitates the application of SiR in outdoor insulation. For example, vinyl groups can be useful to improve the crosslinking during curing of the housing material. Therefore, vinylpolydimethylsiloxane is a common silicone elastomer used in the manufacturing of housing materials for outdoor insulators [1].

Silicone-based insulation housing can be classified with respect to the curing temperature to high-temperature vulcanizing (HTV), room-temperature vulcanizing (RTV) and liquid SiR (LSR). The HTV SiR is cured at high temperature, at 180 ^{o}C, and pressure, and is commonly used in outdoor transmission and distribution as well as station post insulators. The RTV SiR can be supplied either in one- or two-component compounds. The first is cured at room temperature and commonly used in coating of ceramic insulators; whereas, the two-part RTV SiR cures at lower temperature as compared to the HTV SiR, and is widely used for insulation housing of large equipment, such as transformer bushings in power stations. Unfilled LSR is supplied in two parts including the base polymer and curing agent, and can be cured at 200 ^{o}C within few minutes [1].

SiR insulation housing includes reinforcing silica and additives such as colorants and UV stabilizers, which are added relatively in small amounts. Inorganic fillers are also added both to reduce the cost of the insulator, as they replace the specialty silicone-base polymer in the composite, and to improve the erosion resistance.

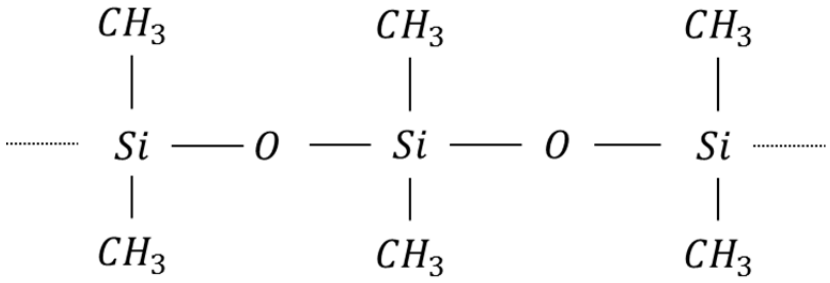

Figure 2.4. Molecular structure of the PDMS [1].

2.2.1 Thermal Degradation of Silicone Rubber

Bond Scission

Heat due to the DBA can cause scission of the siloxane bond, which leads to the formation of cyclic SiR oligomers that are volatile. These oligomers can be formed as result of three possible mechanisms, which are (1) unzipping, (2) random scission and (3) hydrolysis [7, 8]. Unzipping takes place in the SiR that contains silanol end groups as shown in Figure 2.5 [7]. In the random scission, cleavage of the siloxane bond occurs until the resultant chain is too short to form cyclic oligomers or the volatile oligomers evaporate, oxidize in the gas phase, and as a result leave silica residue (Figure 2.6) [7]. Hydrolysis may also depolymerize the siloxane bond yielding methane (CH_4) in addition to the oligomers as shown in Figure 2.7 [8-10].

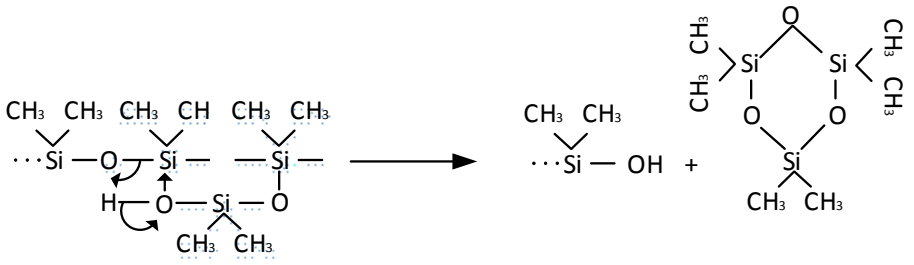

Figure 2.5. Depolymerization of SiR containing silanol end groups due to unzipping [7].

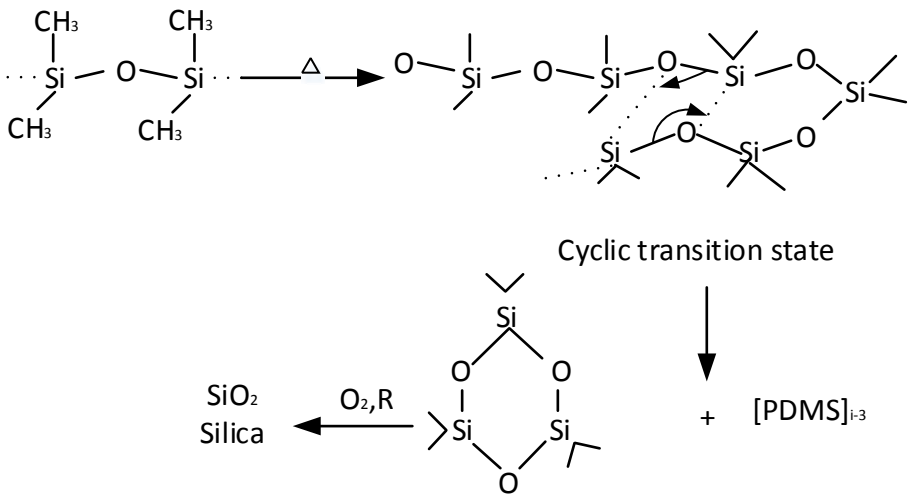

Figure 2.6. Depolymerization of SiR by random scission [7].

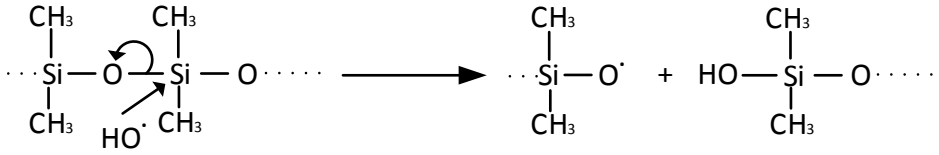

Figure 2.7. Hydrolysis of the SiR by hydroxil group [7].

Andrinov Mechanism

The Andrinov mechanism proposes thermal oxidation of the methyl groups in SiR to take place at temperatures below 149 ^{o}C. The thermal oxidation leads to scission of the Si-C bond, which results in the formation of both peroxide and a free radical. The peroxide can be decomposed to hydroxide and formaldehyde, eventually producing volatile components, carbon oxides, hydrogen and water. Reaction of the hydroxide and the free radical together or with other methyl groups yields the inert silica residue [11, 12], which is considered to play a significant role in the erosion of SiR, in this study.

Degradation in Air versus Inert Atmospheres

The nature of the thermal degradation of SiR, either in air (oxidative) or inert atmospheres, is dependent on the heating rate and the nature of the composition. At low heating rate, oxidative degradation takes place in two stages; at 239 ^{o}C and 400 ^{o}C, respectively. For inert atmospheres, thermal degradation has been reported to initiate at 400 ^{o}C and possess a significant rate at 539 ^{o}C [7-10]. Siloxane oligomers are the byproducts of the inert degradation; whereas, water, carbon dioxide (CO_2) and silica are produced from the oxidative degradation in addition to the oligomers. At higher heating rates, the oxidation degradation tends to take place in one stage at higher decomposition temperatures. Small traces (4wt% [9, 10]) of black residue, mainly identified as silicon carbide, are formed in the inert degradation. This black residue has been found to exist in insignificant amounts (1wt% [7]) during the oxidative degradation, confirming erosion is dominant over tracking of SiR under the effect of heat.

2.2.2 The Role of Inorganic Fillers

Being known as effective flame retardants, inorganic fillers have been employed to suppress the heat ablation of the DBA. The physical and volume effects of the fillers have been highlighted to play the major role in suppressing SiR erosion [13, 14]. The volume effect has been found responsible for improving thermal properties of the composite, such as thermal conductivity, heat capacity and thermal stability; whereas, the physical effect refers to the surface cleaning mechanism associated with the production of water of hydration in composites containing hydrated fillers. Volume effect is further enhanced with increased filler loading promoting percolation between filler particles in the host polymer, thereby dissipating heat. As such, the type of the inorganic filler and its amount can be defined as important aspects by which erosion is suppressed. Several SiR formulations have been

accordingly developed utilizing the two commonly employed fillers in outdoor insulation applications, which are silica and alumina tri-hydrate (ATH).

Although optimum and reliable housing material designs of SiR for AC outdoor insulation applications have been proposed and verified in field conditions [15], a concern about the performance of the same designs for DC has been raised. The concern can be justified since different characteristics of DC as opposed AC DBA can occur in field conditions. Factors, such as the dynamics of the DBA under the effect of voltage polarity, electrolytic corrosion, electrowetting, and arc extinction with AC, affect DBA power and make equivalence between the two voltage types challenging. Therefore, it is important to investigate into the validity or the development of SiR housing composites for DC outdoor insulation applications.

2.2.3 Silicone Rubber Housing for DC Outdoor Insulation

In earlier studies, SiR insulation housing composites have been examined under DC, with no difficulties reported as long as the insulator creepage distance is selected according to the relative pollution performance with respect to the voltage type [16]. On the contrary, severe erosion has been recently reported under DC as compared to AC [17-20], even with the creepage distance criterion considered [19]. Beyond the validation of composites, understanding the DBA phenomenon leading to erosion and the corresponding suppression effect of inorganic fillers under DC voltages is an important aspect in the establishment of sound principles to develop SiR housing composites for DC outdoor insulation.

2.3 The Inclined Plane Tracking and Erosion Test

Figure 2.8 (a) and (b) show the schematic circuit of the standard IPT setup as per the ASTM D2303 and arrangement of the test samples, respectively, where the electrode-assembly facilitates the use of

different voltage ranges, which allows evaluating wide spectrum of materials with different erosion performances. Standard accelerated aging conditions can be imposed during the IPT by controlling the flow rate of the contamination applied by the peristaltic pump. DBA occurs in the presence of ballast resistors to stabilize the discharge activity and protect the surface [21]. The contaminant used is an aqueous solution of ammonium chloride (NH_4Cl), with a resistivity kept in the range of 370 to 400 Ω.cm, containing 0.02 wt% nonionic wetting agent (Triton X-100) [22].

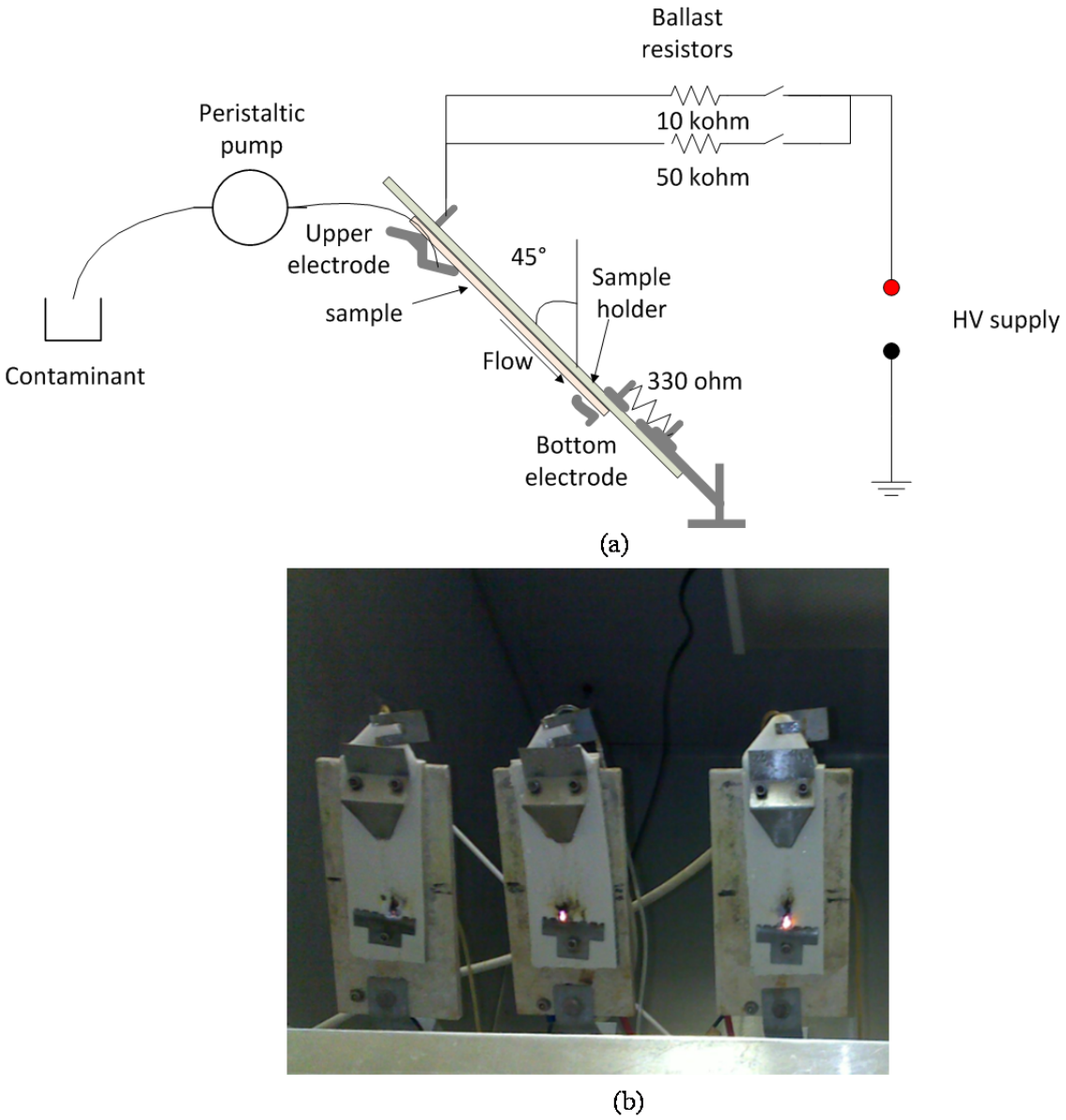

Figure 2.8. (a) A schematic diagram of the standard IPT and (b) laboratory arrangment of test samples in the IPT.

To study erosion using the IPT, two methods are implemented, which are the initial-tracking-voltage (ITV) and constant voltage methods. The ITV can be outlined in the following steps where

the process begins once a continuous channel of the liquid contaminant on the surface is observed [22].

- Voltage is applied in one-hour steps with a level increment of 250 V in each proceeding step.
- If a failure criterion (as defined below) is met within the first two voltage steps, the test is terminated and repeated with a lower starting voltage.
- The ITV is the voltage at which a failure criterion is met, given that the failure has occurred no sooner than the third voltage step.

The voltage is chosen with respect to contaminant flow rate and ballast resistor values in order to induce continuous and effective DBA. Depending on the material composition, a specific amount of power has to be dissipated to initiate failure. The failure criterion is defined by obtaining a 2.54 cm (1-inch) track propagated on the surface as per ASTM D2303. Other criteria can be implemented as per IEC 60587, for example, obtaining deep erosion or flaming of the sample [23].

Time-to-track and erosion depth or area can be the outcomes of the constant voltage method, for which the initial-tracking-voltage method is used first to determine the test voltage level [22]. It is therefore preferred to conduct the constant voltage method on different composites by applying voltages that reflect the tracking voltage classes. The IPT has been also utilized to investigate the mechanism of the EDBA under AC [24, 25], with lesser attention given to the DC EDBA. In particular composites have been tested under DC, with no clear guidelines provided for the DC IPT.

2.4 Literature Review

In order to construct a knowledge base for developing the DC IPT, understanding erosion of insulation housing composites along with observations and characterization of corresponding dry-band arcing has to be obtained. Therefore, in this chapter literature review pertained to the erosion mechanism in the IPT is conducted. Also, a review of erosion indicators in standard AC tests is presented. Literature review for the studies pertained to the effect of fillers on the erosion resistance is presented. Finally, a review for the analysis conducted in the investigation into the physical mechanism of the DBA in the AC and DC IPTs is presented.

2.4.1 Erosion of Silicone Rubber under AC and DC Voltages

Erosion of SiR under AC and DC voltages was compared using the constant voltage method of the IPT, where +DC was found the most severe voltage followed by –DC [18, 20, 26, 27]. The severity of the positive polarity of DC on various formulations of SiR was also confirmed in field aging tests [28]. Time-to-track method was also implemented to compare erosion under AC and DC where the shortest time-to-track is considered an indication of an inferior performance. The shortest time-to-track was always measured under -DC for different contaminant types, conductivities and flow rates [26, 29].

In a laboratory test proposed to have an arrangement similar to that of the IPT [30], the increased discharge current magnitude and period were the factors reported by which erosion is more severe under DC as compared to AC [31]. DBA with increased currents and longer periods have been reported by Moreno *et al.* as the mechanism that causes greater erosion of SiR under DC than AC [31]. Gorur *et al.* reported similar eroding mechanism in salt fog leading to most inferior performance under -DC, but interestingly a similar performance under AC and +DC was obtained [32]. Similar findings on

insulators have also been found by Gustavson *et al.* but with voltage determined to be the governing parameter irrespective of the type of voltage [28]. Mailfert *et al.* recommended that the composite design should be modified from those used currently because stable and rooted discharges were observed under DC [33].

Regarding DC polarity, the period and current magnitude of the DBA have also been the primary properties identified governing erosion of SiR. Employing a wavelet transform, Sarathi *et al.* detected longer periods of DBA activity that led to earlier failure under –DC than +DC [29]. Corrosion of the upper test electrode under +DC due to electrolysis was reported to cause an increase in the conductivity of the liquid contaminant leading to higher magnitude of LC and consequently more damage on the surface [18, 20]. Higher LC under +DC was also reported in [34], but with shorter discharge duration with respect to –DC. LC measurements revealed a greater number of intermittent discharges under +DC [18], with LC magnitude emphasized as the main factor [18, 20]. Rowland *et al.* verified the impact of the magnitude of the DBA current, based on the use of optical detection to verify a greater number of intermittent discharges under +DC [34]. However, it is important to understand the reproducible and deep erosion patterns under DC relative to AC [18, 19], and in particular, the inception of the EDBA.

Zhang *et al.* proposed that rapid and deep erosion of SiR may be attributed to the wind effect allowing an inception of a compressed DBA with an increased energy density rather than a gradual erosion process [35]. In both laboratory tests and field conditions, concentrated discharges were shown to severely degrade SiR insulators, even at low DBA currents [36]. Kumagai *et al.* proposed a critical standard material testing voltage level to generate a stable DBA that severely erodes SiR [37].

Therefore, beyond the simple characterization of the DBA under DC, it is more crucial to investigate the promoting physical mechanism of the EDBA, particularly the formation of residue.

Gorur *et al.* highlighted the influence of the residue during salt fog test with respect to the development of stable DBA, which leads to earlier failure [32]. The residue was identified as conductive deposits as a result of contaminant evaporation [32]; whereas, residue of SiR has been reported to be dominantly non-conductive in nature [38]. Therefore the residue reported in [32] may be considered as apparatus-related rather than from the sample itself. Alternatively, the effect of conductive deposits can be prevented using the standard liquid contaminant specified in the IPT, which constitutes mainly of ammonium chloride salt that evaporates [21]. Mathes *et al.* reported no evidence of conductive deposits on the surface by DBA and therefore no biased effect in the IPT [21].

2.4.2 The Equivalent DC Inclined Plane Test

Although less erosion resistance under DC as compared to AC was confirmed, a contradiction with respect to polarity effect can be recognized. This contradiction may be dependent on the test method applied or even the existence of any experimental source of bias. Given that monopolar is one of the common modes of HVDC transmission, it is important to determine the polarity effect on SiR performance, with the reliable and fair selection of test parameters. The selection of the equivalent DC voltages was an important factor investigated to eliminate sources of experimental bias while investigating erosion under DC as compared to AC.

Most of the studies have considered applying equal voltages of rms AC and DC [20, 26, 29, 31-33, 39] since erosion by DBA is an energy driven degradation process [24, 25]. Alternatively, it was emphasized that relative specific creepage distance that is selected based on withstand voltages is the criterion suitable for the selection of the DC voltages [40, 41]. The problem of obtaining frequent DC

flashovers on insulators has supported the inadequacy of equalizing DC and root-mean-square (rms) AC voltages in aging tests [40]. Area-under-voltage was another criterion proposed in the IPT, where both the AC and equivalent DC voltage waveforms possess equal areas under the curves [18].

However, in applying the power approach, selecting DC voltages to be equal to the corresponding rms AC is oversimplifying the case. There are two components of LC if separated, energy approach may be useful for comparing the DC to AC voltages. The first component is the non-discharge current that leads to joule heating and evaporation of the contaminant, forming dry-bands [42], while the second is the DBA component which contributes to heat ablation of the material surface. The effective component in the energy approach is, therefore, the DBA component. Unlike in the case of field aging tests, using relative specific creepage distance to select DC IPT voltages may not be accurate. In the IPT, insulating materials are ranked with respect to heat ablation rather than hydrophobicity as wetting agents are employed [43]. With regards to the area-under-voltage, it is evident that this criterion compensates for the alternating nature of the 60Hz AC voltage as opposed to the constant DC, yet with no consideration to the polarity effect. It is important, therefore, to propose a reliable method by which the equivalent DC IPT voltage can be selected.

2.4.3 Leakage Current Indicators of the Eroding Dry-Band Arcing under DC Voltages

The LC as an indicator of DBA on SiR has been extensively analyzed with AC but not to the same extent with DC. With AC, the third harmonic component has been shown to be a useful indicator of DBA [44-46] with the energy of the DBA correlated to erosion as well as the DBA temperature [25]. Furthermore, the energy of the LC harmonics obtained in a wavelet based multiresolution analysis (MRA) has been correlated to erosion of SiR [47, 48].

The analysis of LC under DC has been applied in the context of comparing erosion under AC to erosion under DC. The time-to-track of SiR was compared in the IPT with +DC and –DC by analyzing the spectral energy with time using the wavelet transform [29]. Increasing trend of the average LC with time, thus degree of intermittency of LC, was correlated with greater damage on SiR samples tested in the DC IPT [29]. The degree of intermittency in LC was accordingly proposed as a useful indicator of the severity of the erosion under DC [18]. The normal distribution was fitted to the discharge current signature in the DC IPT [18] and the coefficient of variation (CV) was proposed as an indicator by which DBA severity could be compared to AC, and accordingly, equivalent DC IPT voltages were defined. The CV was verified using the ITV, which was also found to be a useful indicator of DBA energy with DC [19].

In addition, simultaneous measurements of LC and surface temperature is one way of studying the EDBA as monitoring the temperature detects degradation leading to erosion [25], and LC characterizes the DBA. To date, no indicators to understand the stages through which DBA progresses to significant erosion have been suggested. Continuous scintillations have been shown to be an important condition leading to erosion [21]. Significant erosion was also hypothesized to occur when the hot spot temperature due to DBA is greater than 400^{o}C as thermo-oxidation takes place where exothermic heat can be generated [37]. Oxidation was also proposed elsewhere to contribute to erosion in a complex fashion [49]. Therefore, it is important to investigate for possible indicators in the DBA current through which significant erosion takes place under DC.

2.4.4 The Effects of Inorganic Fillers under DC Voltages

The role of fillers in SiR has been extensively studied for AC outdoor insulation applications. Gorur *et al.* determined an increase in the erosion resistance of SiR composites containing higher

amounts of ATH and silica [14, 32], due to the corresponding volume effect of the filler [32]. The hydrated fillers were also speculated to suppress erosion, through a physical cleaning mechanism of surface residue, thereby reducing the temperature on the surface [13, 14]. Meyer *et al.* showed reduced erosion of SiR composites due to increased thermal conductivity achieved by the addition of ATH or silica, with no significant effect for the type of the filler at 50 wt% of filler loading [50, 51]. Kumagai *et al.* suggested a critical ATH level of 40 wt% by which the erosion resistance of SiR can be increased, through internal oxidation, shown by differential scanning calorimetry (DSC) [37]. Schmidt *et al.* showed an optimal composition of ATH-free SiR with acceptable erosion resistance can be achieved considering a balance between the filler amount, filler dispersion, and bonding with the base matrix [52]. However, more insight into the mechanisms by which fillers affect erosion due to the EDBA under DC is investigated in this study.

2.4.5 Thermal Analysis of the Eroding Dry-Band Arcing

Erosion of SiR under AC and DC voltages has been reported to be a thermally driven degradation mechanism of the DBA [18-20, 24, 25]. It follows that investigating the characteristics of DBA as a source of heat under AC and DC stresses is an important task in the understanding of the ensuing erosion of insulating materials.

Gorur *et al.* proposed an analytical model to determine the surface temperature of SiR in salt fog, taking into consideration heat transfer by conduction and convection between the DBA plasma and the material under test [32]. Significant influence of the thermal conductivity has been found, as improved by the addition of ATH or silica filler, reducing erosion [32]. Correlation was obtained between the DBA current and the surface temperature, thereby establishing a relationship between LC and the onset of erosion [32]. A similar approach was proposed by Kim *et al.*, with the assumption

that heat conduction is the primary mechanism giving rise to surface temperature, showing agreement between the proposed model and experimental findings [53]. Meyer *et al.* utilized the energy of the DBA, determined by its third harmonic power of LC, to predict the extent to which SiR was damaged in the IPT [53].

Other than fillers, additional factors such as wind have been incorporated into modeling the DBA power. Wind was found to compress the DBA, thus increasing its current and power [54]. In addition, compression was found to increase the energy density dissipated on SiR, allowing higher temperatures to develop.

Corrosion of the IPT electrodes under +DC has been proposed as the primary factor giving rise to increased DBA current, and therefore power, as compared to AC. On the other hand, studying the DBA length, under DC as compared to AC, may lead to broader understanding of the corresponding DBA characteristics. [35]. However, other factors such as the voltage polarity on the DBA heat have yet to be investigated.

2.5 Summary

The development of a reliable erosion screening technique under AC stresses has been an essential step taken in the development of SiR composites for outdoor insulation applications, and over years the IPT has been one of the most standardized techniques utilized. Based on an extensive investigation into the DBA mechanism leading to erosion under AC voltages of the IPT, SiR housing material designs for AC outdoor insulation applications have been developed and commercialized using inorganic fillers. Nevertheless, there is a lack of reported experience and studies about the effect of DBA induced on the insulators' surface stressed under DC voltages. Composites that have been designed for AC are being applied to DC, with simple consideration given to the relative withstand

AC and DC voltages. Relatively few studies have evaluated polymeric materials to gain an understanding of the physical mechanism of DBA under DC. Recent studies have focused mainly on the validation of AC-designed composites for outdoor HVDC but with less emphasis on determining the mechanism of dry band formation and heat ablation of polymeric materials associated with DBA under DC; both areas to be studied in this thesis.

In this thesis, a mechanistic framework towards the development of the DC IPT is established as a foundation for the development of housing material composites of SiR, a widely utilized elastomer in outdoor insulation applications. As such, a thorough understanding of the physical mechanism of the DBA mechanism under DC is investigated. To this end, the study will closely examine SiR with inorganic fillers, which are vital for suppressing the effects of DBA, as a foundation for the development of optimum polymeric composites for outdoor DC insulation applications.

Chapter 3
Materials and Methods

The IPT, which has been used for evaluating polymeric materials for outdoor AC insulation applications, is utilized in this research. The study has begun with measurements of the LC, enabling an analysis of the modified wetting characteristics of surfaces under DC; thus, testing voltage levels can be suitably chosen under DC with respect to the corresponding standard AC.

During the IPTs, temperature measurements have been made to couple the thermal mechanism of erosion with the DBA characteristics, and TGA and DSC have been used to predetermine the temperature at which the erosion process begins. The performance of SiR composites are also studied. In addition, with the goal of determining the suppression mechanism of the DBA under DC, the study will include the effects of various types and levels of fillers, employing those commonly used for outdoor insulation applications: ATH and silica. Then, a modified setup of the IPT is utilized to understand the physical mechanism of the DBA under DC as compared to AC.

3.1 Material Samples

The IPT samples utilized have 127 mm length × 50 mm width and a thickness of 5 mm. The samples can be categorized with respect to the base material into LSR composites that were prepared in the lab (set no.1) and commercial HTV SiR composites (set no.2), as shown in Table 3.1. The prepared samples were formulated using LSR (GE RTV 615), a two-part vinylpolydimethylsiloxane without fillers. The two parts (A and B) were mixed using a high shear mixer maintaining a weight ratio of 10:1 between part A and B, respectively. Unfilled and filled with 10, 30 and 50 wt % samples that were filled with either ATH or silica were prepared maintaining a total sample weight of 50 g.

More information about the silica and ATH fillers employed can be found in [3].The material weights were measured using an electronic balance, Sartorius model AC 211S-00MS, that has an accuracy of 0.1 g. The prepared composites were degassed and then cured at room temperature in molds possessing sizes similar to those of the samples. The cross-linked composites were heated in an oven at an approximate temperature of 85 ^{o}C for three hours, and then the samples were cleaned using ethanol and deionized water prior to use. The commercial composites were ATH-filled SiR at 25 and 58 wt%. Table 3.1 lists the material samples used in the IPT throughout the study along with their identification names. The IPT was conducted with five samples as per ASTM D230 and each IPT was conducted three times, so a total of 15 samples of each composition were tested in the mechanistic investigation.

Laser samples of the LSR were prepared using ATH and silica, with similar properties to that in Table 3.1, but with the addition of 2.5 wt % iron oxide with reference to the filler amount to ensure similar absorptance to the laser beam by the composites [55]. The laser samples were disk shape with radius and thickness of 8 and 0.5 cm, respectively.

Table 3.2 shows the sample compositions for the laser experiments. Thermal conductivity was also measured for the LSR samples filled with ATH in order to investigate the influence of the filler level on the thermal conductivity.

Table 3.3 shows the thermal composition of the samples for which the thermal conductivity was measured. The TGA/DSC samples were extracted from the composites described in Table 3.1 to possess a weight <5g.

Table 3.1. Description of the IPT material samples used in the study.

Set No.	Sample identification	Type of SiR	Filler			
			Type	Level (wt%)	Median particle size (µm)	Density (g/cm^3)
1	Unfilled SiR	LSR	None	0	None	
	RA10		ATH	10	1.5	2.5
	RS10		silica		1.4	2.65
	RA30		ATH	30	1.5	2.5
	RS30		silica		1.4	2.65
	RA50		ATH	50	1.5	2.5
	RS50		silica		1.4	2.65
2	HA25	HTV	ATH	25	Not available/same source	
	HA58			58		

Table 3.2. Sample compositions used in the laser heating experiments.

Sample Identification	Fillers			
	ATH (wt%)	Silica (wt%)	Iron oxide (wt%)	Total Filler (wt%)
RA30L	29.25	None	0.75	30
RS30L	None	29.25		
RA50L	48.75	None	1.25	50
RS50L	None	48.75		

Table 3.3. Samples used in the thermal conductivity measurements.

Sample Identification	Fillers		
	ATH (wt%)	Iron oxide (wt%)	Total Filler (wt%)
RA30TC	29.25	0.75	30
RA35TC	34.12	0.88	35
RA40TC	39.00	1.00	40
RA45TC	43.87	1.13	45
RA50TC	48.75	1.25	50
RA55TC	53.62	1.38	55

3.2 Experimental Apparatus

3.2.1 The Inclined Plane Test

Figure 3.1 shows the IPT setup used in the study. In the AC IPT, a 75 kVA distribution transformer with rated voltage of 8 kV is used and the applied voltage is adjusted with a variac. In the DC IPT, a dual polarity, 5 kV and 1 kW regulated Glassman® DC supply with a ripple less than 5% of rated voltage at full load is used. The DC supply has a 0.05% resolution and an accuracy of 0.5% of reading + 0.2% of rated voltage with voltage regulation of less than 0.005% for the specified line variations and 0.01% + 1mV/mA for load variations.

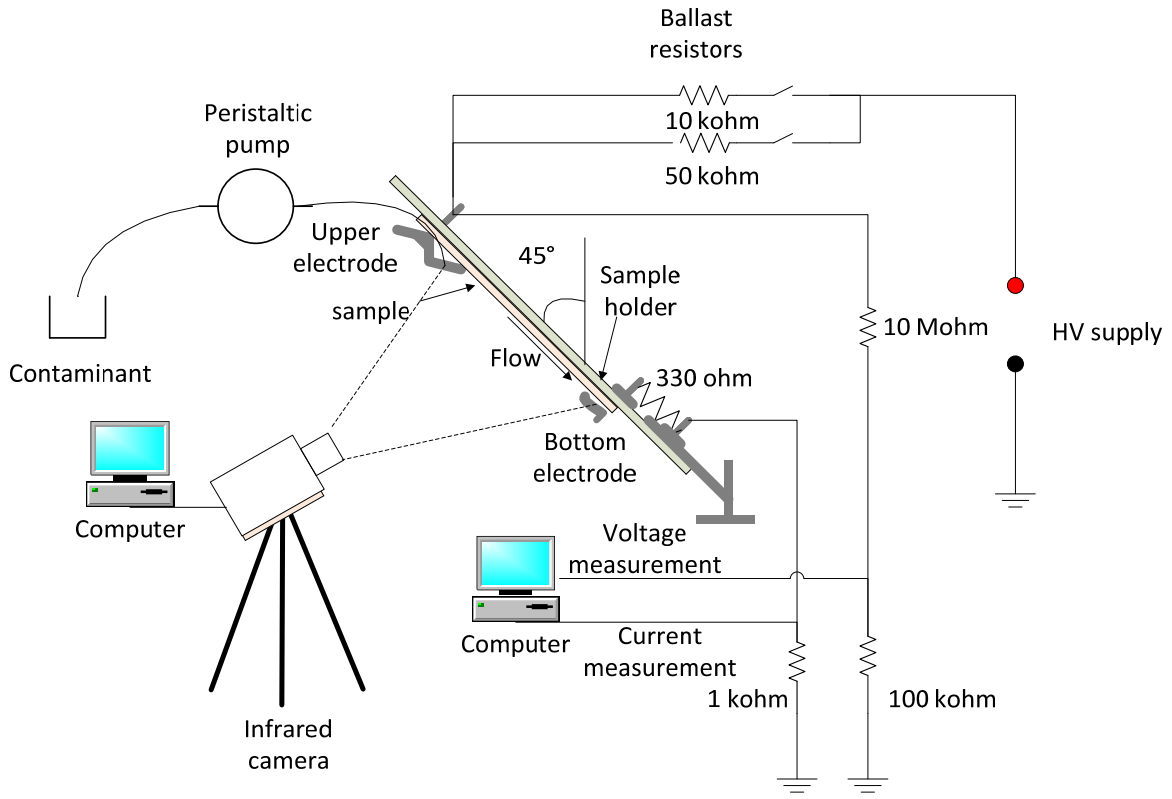

Figure 3.1. Schematic circuit diagram of the IPT setup used in the study.

The LC was acquired at a sampling frequency f_s of 7.68 kHz, with a window of 512 samples stored every second. A FLIR® SC500 thermal IR camera was used to measure the maximum surface temperature (T_{max}) which was acquired at fs of 1Hz. The obtained waveforms as analyzed with T_{max} were smoothed using the moving average technique in order to allow a trend analysis [25]. The emissivity factor of the test sample was set to 0.98 [25].

For track-resistant materials, erosion or tracking combined with erosion (erosion path) is a typical failure mode in the IPT [21]. Therefore, two standard failure criteria pertaining to both modes are considered for the silicone samples. The failure criteria assigned for stopping the test are (1)

obtaining a 2.54 cm (1-inch) erosion path [22], and (2) a hole due to intensive erosion or ignition of the sample surface [22, 23].

3.2.2 Laser Heating Experiments

In order to investigate the thermal properties of the prepared composites, temperature profiles in laser experiments were obtained on the samples before reaching the decomposition temperature of SiR or ATH. As such, the laser power (Figure 3.2) was applied for 30 seconds and the relative thermal conductivity was obtained through a relative comparison of the temperature profiles [14, 50, 51]. To investigate the suppression mechanism of fillers at elevated temperatures, the laser beam was applied for approximately ten minutes until a steady state T_{max} was reached. The laser powers applied to the 30 wt% filled samples were 1.60, 3.50 and 4.50 W, and laser powers of 3.50 and 4.50 W were used for the 50 wt% samples.

Figure 3.3 depicts the methodology of extracting T_{max}. Thermal images were taken using a FLIR T650SC IR camera at a rate of 7.5 frames/second, a resolution of 640×480 pixels and thermal sensitivity <30 mK at 303.15 K. Post processing was applied to the images using FLIR R&D software for extraction of the temperature profiles and T_{max}. Within an assigned area (E1) in the thermal image, the location of the T_{max} was obtained, and the evolution of the T_{max} was acquired as shown in Figure 3.3. A line (L1) passing through the point of T_{max} was used for the temperature profiles (Figure 3.3).

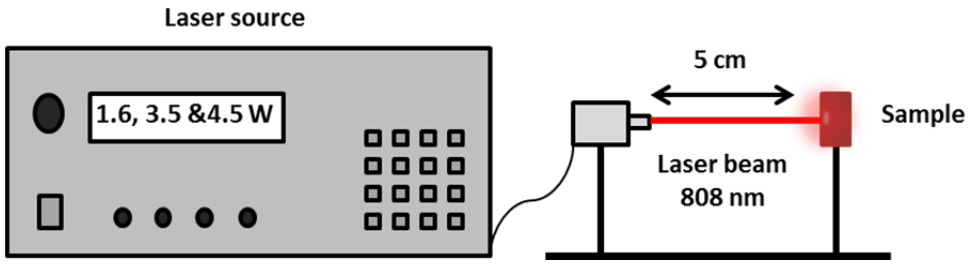

Figure 3.2. Schematic diagram of laser heating experiments.

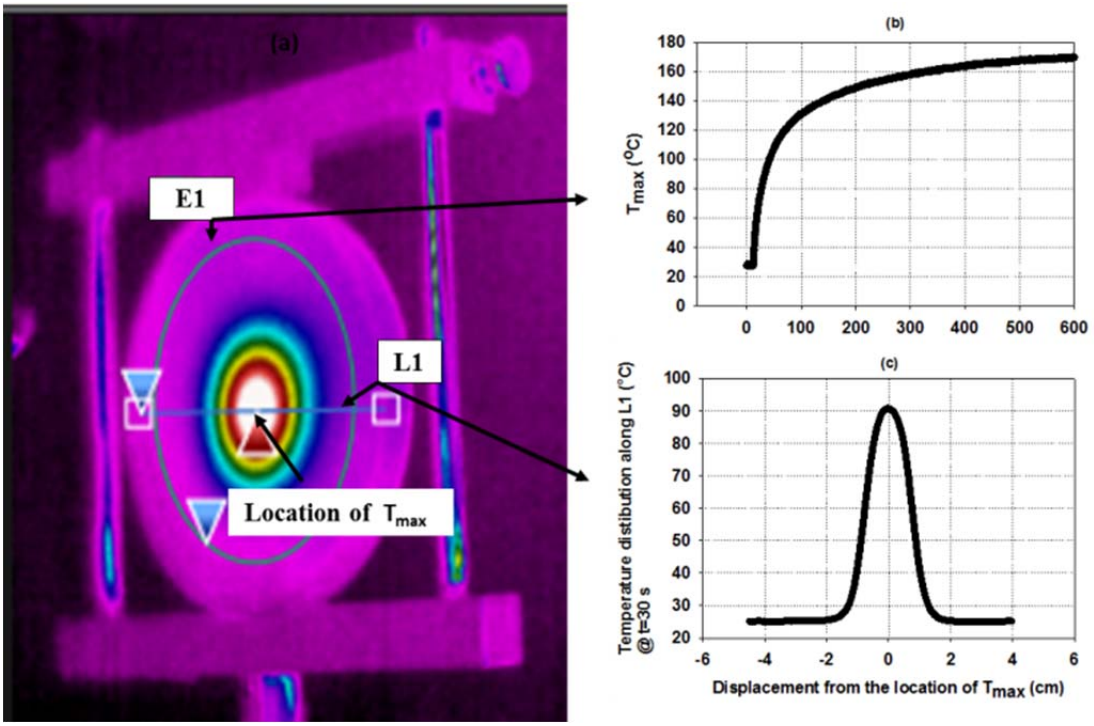

Figure 3.3. Measurement of T_{max} and temperature profiles of laser heating experiments, (a) thermogram of the tested sample by laser power, (b) measurement of the evolution of T_{max} in the allocated area (E1) and (c) temperature profile across line (L1) at t=30 s for relative thermal conductivity indication.

3.2.3 Thermogravimetry and Differential Scanning Calorimetry

TGA and DSC were conducted, in the SDT Q600 Simultaneous model of TA®, to identify the thermal mechanisms associated with the evolution of T_{max} during the IPT [37, 56]. TGA and DSC were conducted simultaneously for the SiR composite in a test pan heated as per a pre-set ramping temperature protocol. The IPT samples were heated in both air and nitrogen (N_2) atmospheres at a rate of 10°C/minute between 10 and 500°C [37, 56]. The weight loss from the tested sample is the outcome of the TGA as a function of temperature, indicating thermal degradation of the tested SiR. The differential thermogravimety (DTG) curve was obtained to indicate the rate of the degradation by taking the derivative of the thermogravimetry curve. The thermal degradation mechanism associated with weight loss was identified through DSC curve, possessing exothermic humps or endothermic

dents. The hump indicates a thermo-oxidation; whereas, the endothermic dent was identified as a thermal decomposition of the tested composite [37].

3.2.4 Thermal Conductivity Measurement using the ASTM D5470 Method

Determination of thermal conductivity was conducted for each composition described in Table 3.3 at 100 oC and 200 psi as per the ASTM D5470 method [57], in which the test sample forms a joint and the thermal resistance R_T of the joint (test) sample was determined, as

$$R_T = \frac{\Delta T}{Q},$$

and ΔT and Q are the temperature drop and heat flow across the joint, respectively. With both the thickness thk and the surface area A of the joint measured using a Mitutoyo® laser, LSM 503, thermal conductivity, given by

$$Thrmal\ conductivity = \frac{thk}{R_T A}$$

was determined.

3.3 Study Approach

3.3.1 Electrowetting of the Liquid contaminant in the AC and DC Inclined Plane Tests

Electrowetting refers to the reduction of the contact angle of an electrolyte on the surface of a solid due to the application of a DC electric field but is completely applicable to AC at power frequency [58, 59]. Electrowetting behavior of liquid contaminant in the IPT was studied under AC, +DC and –DC voltages through LC measurements. The main purpose of LC measurements was to detect and analyze the modified DBA characteristics in the DC IPT. These modified characteristics may affect the relative comparison with AC to be biased and, therefore, should be understood. The measurement was conducted for two stages prior to and after DBA inception. Analysis of DBA at both stages

allows broader analysis of the test conditions that affect the DBA. The measurements were conducted for 5 minutes in order to insure sufficient time for electrification and DBA inception. In addition, the conduction time was selected such that no significant damage on the surface takes place due to DBA, thus biasing due to surface condition can be prevented. Three tests were performed and in each test, five specimens of RS30 composites were used.

The test was conducted by applying voltages in steps of 0.25 kV from 0.25 to 3.00 kV maintaining a contaminant flow rate of 0.30 ml/min. Intermittent discharges could be observed around a starting voltage of 2.00 kV. Therefore, the electrowetting behavior of IPT liquid contaminant is analyzed below 2.00 kV for an applied voltage range of 0.25-1.75kV. Since no significant DBA activity was observed for test voltages between 0.25-1.75 kV, the average current can be a dependable measurement representing the wet layer current.

Based on the understanding of the behavior of the liquid contaminant under voltage [19], the wetting current I_w during the standard IPT can be represented by the LC measured prior to the evaporation of the liquid contaminant forming dry-bands [60]. Accordingly, I_w was determined for flow rates between 0.30 and 1.65 ml/min by increasing the applied voltage insteps of 0.25 kV until dry-band are formed at the wetting voltage applied V_w.

3.3.2 Equivalent DC Voltages of the Inclined Plane Test

Selection of the appropriate voltage level in the constant voltage methods of the IPT is an important aspect whereby outcomes can be altered. The applied voltage should not be out of the tracking/erosion class of the material, as a higher voltage applied may lead to rapid failure or burning and a lower voltage may not provide an efficient DBA [49]. In addition, the liquid contaminant in the IPT, an aqueous solution of 0.1 wt% NH_4Cl, has been selected to promote tracking over erosion, so a lower voltage applied than the ITV should be selected for a reliable study of erosion [4, 21, 49].

CHAPTER 3 MATERIALS AND METHODS

According to ASTM D2303, in using the constant voltage methods, materials must be stressed below the ITV by 0.75 kV. The same voltages can be applied to materials that have a similar tracking/erosion class, but if the materials are different in their tracking/erosion classes, the corresponding voltages must be different with respect to the ITV [22, 49]. For example, if the ITVs for materials A and B are 4 kV and 3.5 kV respectively, then the voltages that should be applied are 3.25 kV and 2.75 kV, respectively.

Likewise, the ITV can be also used to select the equivalent DC IPT voltages as the ITV may be dependent on the voltage mode. The adapted approach from the ASTM D 2303 is proposed for choosing the erosion test voltage in the DC IPT as described in the following procedures.

- The initial-tracking AC voltage for a specific material composition is determined as per the aforementioned ITV protocol in section 2.3 [22]. The starting voltage is usually chosen based on experience [22]; therefore, in this study the starting rms AC, +DC and –DC voltages are 3.25 kV, 2 kV and 2.5 kV (2.25 kV on the pure SiR samples), respectively.
- The ratio between the ITVs under the +DC and AC voltages, defined by

$$R_{+DC}^{ITV} = \frac{ITV_{+DC}}{ITV_{AC}} \quad (2.1),$$

  can then be determined, where the subscript and superscript indicate the voltage mode and test method, respectively. Likewise,–DC to AC ration of the ITVs can be obtained. All the equations shown in this section are given for +DC for the sake of brevity.
- The AC erosion test voltage V_{AC}^{ITV} is determined by decrementing the $\mathrm{ITV_{AC}}$ by 0.75 kV as per ASTM D2303.
- The DC erosion test voltage V_{+DC}^{ITV} can be accordingly obtained as follows:

$$V_{+DC}^{ITV} = V_{AC}^{ITV} \times R_{+DC}^{ITV} \quad (2.2).$$

It is important to note that the equivalent DC IPT voltages are not found directly by decrementing the DC ITV by 0.75 kV as is the case under AC since different characteristics may occur between AC and DC DBA. This difference may affect this offset value of 0.75 kV to be less under DC. Therefore, the ratios are proposed to prevent biasing the obtained equivalent DC voltages through the ITV method and coupling the selection method with the tracking/erosion class.

The unfilled SiR, RS10 and RS30 composites were used in this part of the study to develop the equivalent DC IPT voltages. Erosion was then investigated for the RS30 and RA30 samples under the equivalent DC voltages obtained with respect to the ITV for relative comparison with AC erosion. The erosion was evaluated using the maximum erosion depth and erosion area.

3.3.3 The Role of Surface Residue

A correlation between the formation of DBA residue, surface temperature, and the EDBA was examined under DC as compared to AC. Six HA58 samples were used in a special protocol of the constant voltage method in the IPT. The DBA residue was removed periodically, using an ethanol and deionized water wipe, from three of the six samples under test by switching off the voltage and contaminant flow for about one minute. Figure 3.4 illustrates the IPT conducted following the described protocol in the study of the role of surface residue. TGA and DSC were utilized to determine the degradation temperatures of the tested SiR and identify the degradation observed with respect to the measured temperatures during the IPT [37].

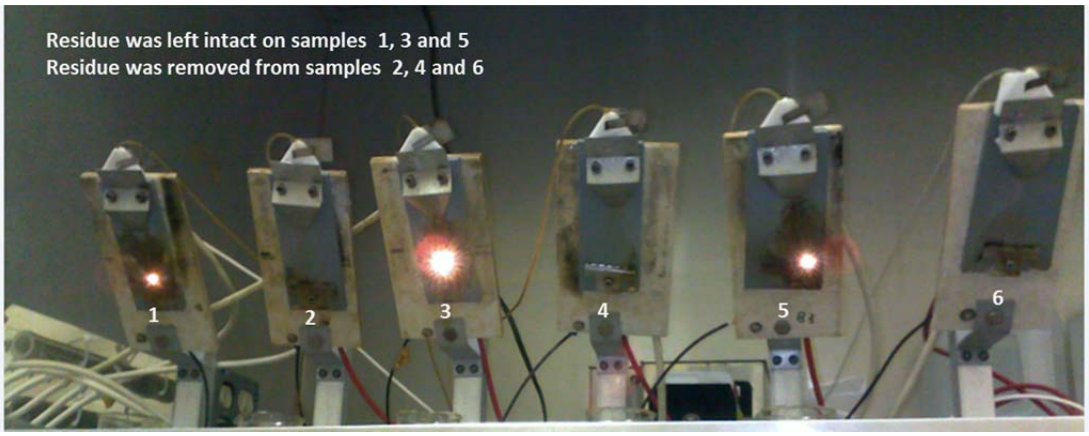

Figure 3.4. Tested samples in the investigation of the influence of the surface residue; this case is under the equivalent +DC voltage.

3.3.4 Wavelet-Based Multiresolution Analysis

Simultaneous measurement of LC and surface temperature is one way of studying the EDBA as monitoring the temperature detects degradation leading to erosion [25, 37]. Short-time analysis and in particular the wavelet-based multiresolution analysis (MRA) can be an effective technique through which the evolution of the DBA characteristics and the corresponding physical mechanism can be understood.

In the MRA, the windowed LC waveform $i(t)$ can be decomposed into its linear series expansion for j resolution levels as follows:

$$i(t) = \sum_{k=-\infty}^{\infty} a_k \varphi(t-k) + \sum_{k=-\infty}^{\infty} \sum_{j=0}^{\infty} d_{j,k} \psi\left(2^j t - k\right) \tag{3.1}$$

where $\varphi_k(t)$ and $\psi_{j,k}(t)$ are the scaling function and wavelets derived from the scaling function, respectively and k, a_k, and $d_{j,k}$ are the translation, approximation, and detail expansion coefficients, respectively [61]. Daubechies 4 wavelet was applied in this study [47, 48]. The approximation and detail expansion coefficients in equation (3.1) can be calculated from $\sum_m h_o(m-2k)a_{j+1}(m)$

and $\sum_m h_1(m-2k)a_{j+1}(m)$, respectively, where m is an integer and $h_o(n)$ and $h_1(n)$ are the coefficients of the scaling function and the wavelets, respectively. MRA was implemented using Matlab® through cascaded $h_o(n)$ and high pass $h_1(n)$ filters, with each phase being followed by a down sampling step by two (↓2). The approximation and detail coefficients were accordingly expanded to constitute a specific frequency band at each resolution level with respect to fs.

As an example, Figure 3.5 depicts the MRA applied up to three resolution levels, on a windowed LC current waveform acquired during the IPT under +DC. The LC waveform can be observed to be pulsative of square shape that can be classified into main and random pulses. The main pulse can be resolved into three components as shown in Figure 3.5a corresponding to the fronts, tails and flat tops; whereas, the random pulses are also recognizable to be imbedded on the flat tops as for the case involving the train of pulses indicated in Figure 3.5a.

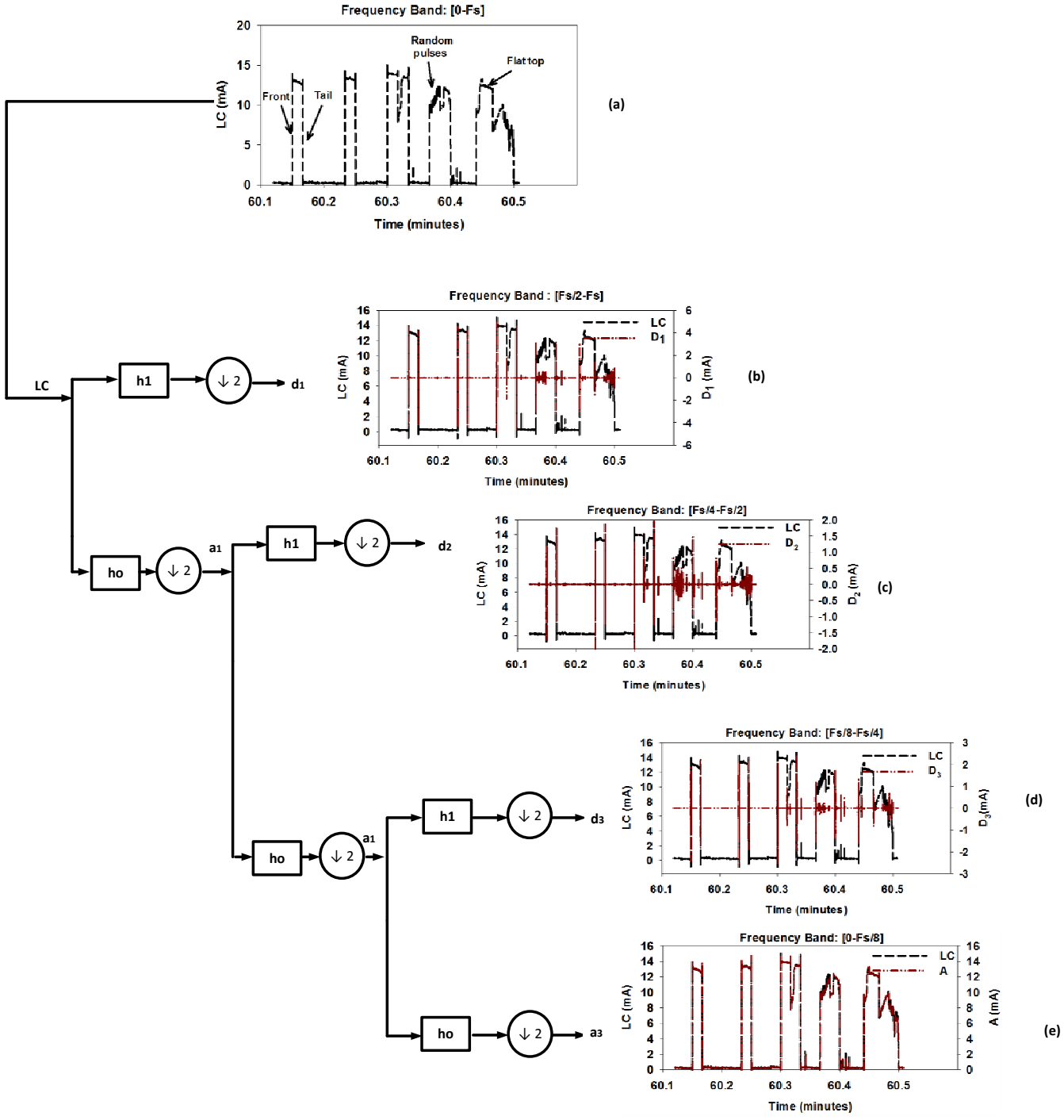

Figure 3.5. Multiresolution analysis applied at three resolution levels on a LC window acquired during the DC IPT showing (a) the windowed LC waveform, (b) the first detail (D_1), (c) second detail (D_2), (d) third detail (D_3) and (e) the approximation (A); this example is for an RA30 sample tested at +DC.

The details (D_1, D_2, and D_3) and the approximation (A_3) illustrated were reconstructed using the inverse discrete wavelet transform [61], with the wavelet denoising applied at a threshold of 0.21 mA at all the resolution levels. The low-frequency waveform A is useful to indicate the frequent occurrence of the main pulses, and therefore to analyze the stability of the DBA or in other words the sustainability of the flat top. The peaks imbedded in D_1, D_2, and D_3 are associated with the fronts and tails of the main and the random pulses at the three resolution levels; whereas, diminishing sensitivity is evident for the details to detect the random pulses at lower frequency bands (moving from D_1, Figure 3.5a to D_3 in Figure 3.5d). Possible distinction can be therefore suggested for the corresponding physical mechanism of the main and the random pulses. The LC acquired can be defined to be originated mainly from the DBA and surface wetting, with random ionizations imbedded on the DBA component. Rowland *et al.* defined through optical detection the discharge and wetting activities on the surface as the main sources of the LC pulses acquired during the DC IPT [34], and Kumagai *et al.* described ionizations to take place in DBA plasma [37].

In this study, the rms value of the approximation coefficients A_{rms}, given by

$$\sqrt{\frac{1}{K}\sum_{K}|A_7(k)|^2},$$

was obtained for each window, where K is window width of 512 samples (1 second). Similarly, the rms value of the detail expansion coefficients d_{jrms}, defined by

$$\sqrt{\frac{1}{K}\sum_{K}\left|d_j(k)\right|^2},$$

can be determined. The rms waveforms were smoothed using the moving average technique [25]. It should be noted that insignificant effect was found for the noise component, which was extracted at

different levels of the wavelet thresholding technique, on the trend of the smoothed rms waveforms. The MRA was therefore applied directly on the acquired LC waveforms. The LC waveform was analyzed at seven resolution levels with each level representing a specific frequency band as indicated in Table 3.4.

The decomposed LC waveforms, A_{rms} and d_{jrms} , were analyzed simultaneously with T_{max} during the hotspots and the eroding hotspots to characterize the EDBA. The proposed time-to-eroding parameter, TE, for which longer times indicate higher resistance to the EDBA was ascertained for ATH and silica filled samples for both DC polarities by measuring the time at which an eroding hotspot was obtained. Five samples of each composition were tested as per ASTM D2303 [22] and the hotpot temperature was identified through TGA and DSC analyses [37].

Table 3.4. Frequency bands of the resolution levels employed in the MRA.

Waveform	Frequency band (Hz)
d1rms	3840-7680
d2rms	1920-3840
d3rms	960-1920
d4rms	480-960
d5rms	240-480
d6rms	120-240
d7rms	60-120
A rms	< 60

3.3.5 The Role of Inorganic Fillers

The reduction in erosion by fillers has been traditionally understood in the context of their flame retardancy [52]. The flame retardancy of composites has been investigated through understanding the suppressive effects of fillers during the combustion phase in the degradation of polymers [7, 62]. Correlation has been obtained between the flame retardancy of fillers and the improved thermal

effects of fillers inhibiting combustion [63]. Similarly, with the erosion dominantly defined to be a thermal mechanism [28], investigating SiR erosion under DC requires understanding the suppressive effects of fillers during hot spots development by DBA under DC. The understanding of the development of hot spots in the DC IPT is proposed in this study through wavelet-based MRA of the LC waveform [64]. As such, the corresponding effect of fillers is investigated in this part of the study. While improvement of the thermal conductivity and heat capacity has been attributed to the dilution in the condensed phase, production of diluent gases has been shown to increase the heat capacity of the gas phase after the decomposition [7, 62, 63]. Therefore, measurement of the T_{max} using the IR camera during the IPT is important.

The stable DBA was obtained to be promoted under +DC as compared to the –DC voltages in the IPT [65]; therefore, +DC voltages were applied. Voltage level of 2.25 kV was applied, and a level of 2.75 kV was used to compare the highly filled composites in set no. 1 of Table 3.1. Suppression of erosion was investigated in this study rather than evaluating the erosion resistance; therefore, testing was stopped with the initiation of erosion, unless the sample failed.

It should be noted that the formation of an inert char due to the thermal decomposition of SiR, which forms a thermal barrier between the DBA and the surface and thus suppresses further heat ablation [7, 62, 63], is an important aspect in the erosion suppression mechanism. However, the thermal effects of the fillers impeding the initiation of deep erosion due to stable and intense DBA under DC is important, rather than showing the influence of the inert char insulating heat from the DBA after erosion.

To understand the thermal effects of ATH and silica in SiR, laser heating experiments were conducted utilizing the constant power approach. In addition, DSC analysis was utilized to identify

the thermal effects obtained for the fillers [37, 56], and ASTM D5470 method was used to investigate the volume effect of the filler on thermal conductivity.

3.3.6 Thermal Analysis of the Dry-Band Arcing under AC and DC

The test apparatus is similar to the IPT apparatus described in Figure 3.1. Five RS30 samples were mounted at an angle approaching 90^{o}C, thereby accelerating the effects of DBA [35]. Contaminant flow rates between 0.3 and 1.65 ml/min and a test voltage of 5 kV, which lies within the critical testing voltage range of SiR [37, 66, 67], were used in this part of the study on the RS30 samples [19]. Simultaneous measurement of LC, visual observations, and thermal analysis were conducted. Video recordings from a web camera and from an IR camera (FLIR T650SC) captured the DBA, with the T_{max} extracted from the thermal images using FLIR software.

The DBA power dissipated on the SiR surface can be written as

$$P_s = P_d K_s$$

where K_s and P_d are the fraction of the total DBA power absorbed by the SiR sample, which has been assumed to be 0.9 [68] and the DBA power, respectively. Such a high absorbance reflects the irradiated heat losses to be quite small due to the inverted orientation of the sample. The P_d was determined using the DBA voltage V_d and current i as follows:

$$P_d = V_d i,$$

with the capacitive current under AC assumed to be negligible due to the conductive liquid contaminant (2.5 - 2.7 mS/cm) , which includes Triton X100 as a wetting agent. Considering the circuit model of the impinged surface by the DBA, the V_d can be obtained from the relationship

$$V_d = V_s - iR_b - ir_p(L - L_a),$$

where $V_s,\ R_b, r_p, L\ and\ L_a$ are the source voltage, ballast resistance, surface resistance of the liquid contaminant per unit length, 5 cm distance between the electrodes, and the DBA length, respectively. The r_p of the liquid contaminant was determined using the measured I_w at different flow rates, as

$$r_p = \frac{\left[\frac{V_s}{I_w} - R_b\right]}{L} \quad (2.3).$$

In addition, to investigate the effect of metallic ions from electrode corrosion under +DC, and likely under AC, the linear resistance of the DBA r_d can be defined as follows:

$$r_d = \frac{V_d}{L_a i}.$$

The DBA in the IPT is viewed as the source of heat for ablation of SiR. It follows that the temperature on the surface due to DBA is dependent on the geometry, power and thermal properties of the SiR samples. The heat transfer equation, which can be expressed for the thermal analysis conducted in this study as

$$\rho C_p \frac{\partial T}{\partial t} = \nabla.(k\nabla T) + Q,$$

was applied to analyze the surface temperature T, where $\rho, C_p,\ t, k\ and\ Q$ are the density, specific heat capacity of the composite, duration of the DBA, thermal conductivity, and the DBA heat impinging the surface respectively. T_{max} was found to increase with the period of the DBA and observed to saturate after short periods. This behavior of T_{max} may be attributed to the influence of the formation of char behaving as a heat shield between the DBA and the SiR surface. Based on the visual observations and thermal analysis, saturation of T_{max} seems to be limited to about one second in duration for flow rate ≤ 1ml/min; whereas, periods of 4-7 seconds could be observed at higher flow rates. The dominant DBA with period of 1.2 and 0.7 s was observed in the –DC and +DC IPTs, respectively [34]. Therefore T_{max} was estimated and compared to the experimental findings with

respect to the DBA period of one second at flow rates ≤1 ml/min. Comsol® software was utilized to analyze the temperature rise (Figure 3.6), with the DBA power experimentally obtained under AC and DC. The DBA length has been always found to be small, i.e. < 1cm, therefore, the corresponding affected surface area was assumed to be rectangular having the dimensions of $L_a \times w_a$ cm^2, where L_a and w_a are respectively the length and width of the DBA. Based on visual observations, an average value of 0.2 cm was taken for w_a.

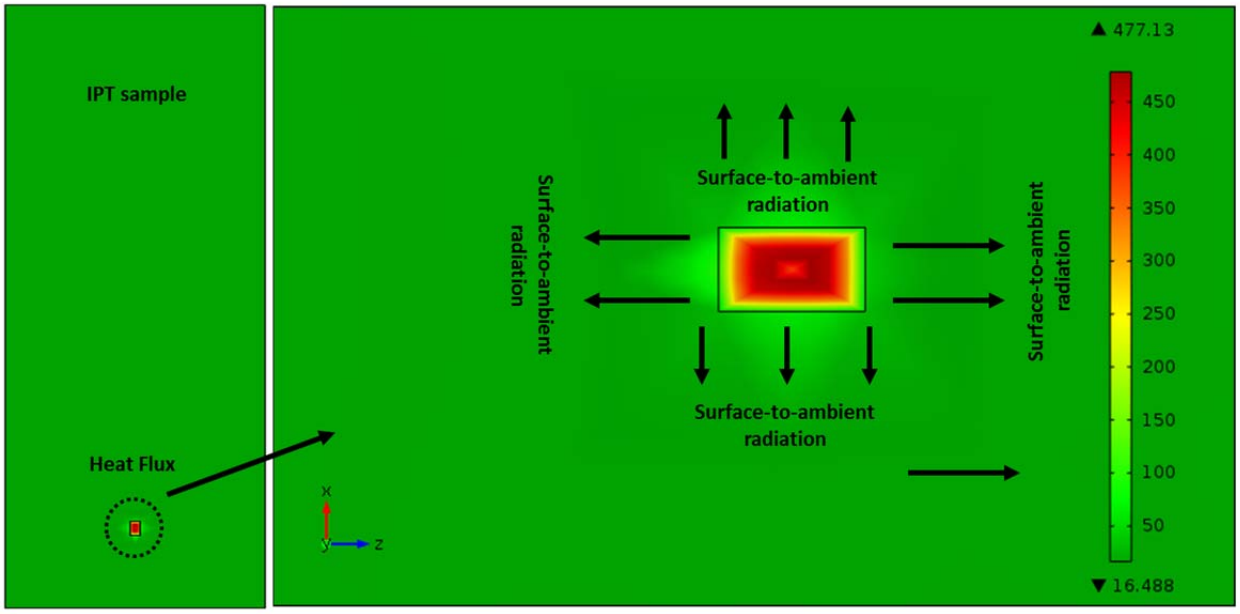

Figure 3.6. Comsol ® model used to estimate the T_{max}, This example for the case of +DC (5 kV).

It should be noted that a comparative analysis of the thermal effect of the DBA with respect to voltage type was investigated rather than providing an analytical solution for the absolute hotspot temperature induced by the DBA. Therefore, the study considered the thermal effect of the DBA on the SiR condensed phase and correlation analysis was used for validation. The correlation coefficient r, defined by

$$r = \frac{\mathrm{COV}\,(Y_1, Y_2)}{(\sigma_{Y_1}.\sigma_{Y_2})}, \tag{2.4}$$

was obtained for the estimated and the experimentally determined T_{max}, respectively Y_1 and Y_2, where $\mathrm{COV}\,(Y_1, Y_2)$ represents the covariance.

The tests conducted and the corresponding approaches taken in the study can be summarized in the diagram shown in Figure 3.7.

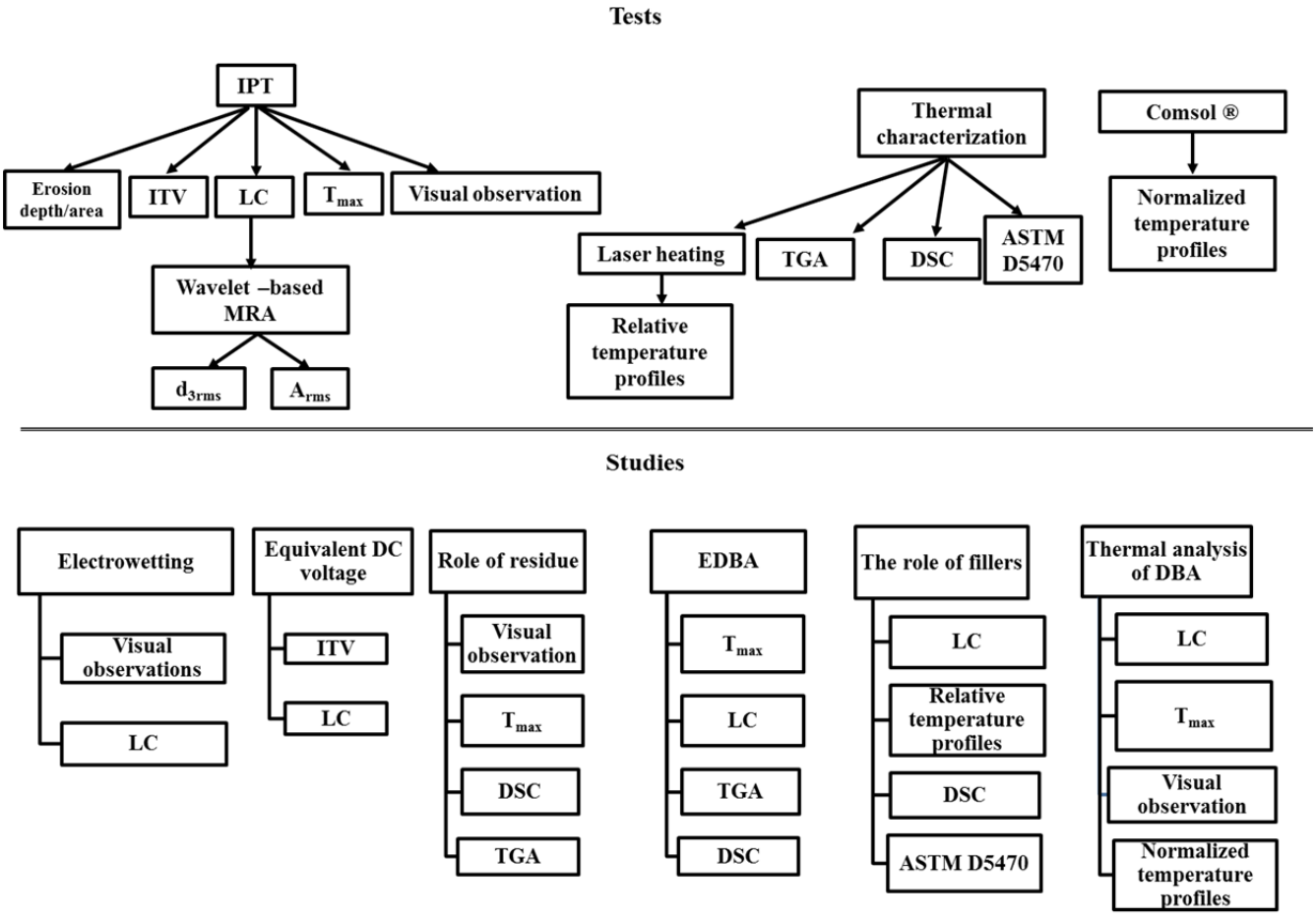

Figure 3.7. Diagram of the conducted tests and the corresponding studies.

Chapter 4
Results

Development of the equivalent DC IPT requires the integration of both the experimental findings elucidating the erosion mechanisms and parametric study of the DBA characteristics under DC as compared to AC stresses. In particular, the factors influencing erosion under DC as compared to AC, such as the electrowetting of the liquid contaminant, the voltage polarity, surface condition and physical characteristics of the DBA have to be investigated. Therefore, in this chapter, results of analyzing the LC and temperature measured during the IPT, identification of the corresponding thermal degradation mechanisms and understanding the erosion suppression effects of fillers are presented.

4.1 Initial-Tracking Voltage in the AC and DC Inclined Plane Tests

The ITVs determined for the Unfilled, RS10 and RS30 as descried in 3.3.2 are shown in Table 4.1. It is evident that the erosion class of a specific SiR composition is dependent on the voltage mode, and is largely independent of the filler loading. Figure 4.1 shows typical erosion patterns on RS30 samples tested under AC, +DC and -DC voltages. In all three voltage modes, the eroded path is initiated from the bottom electrode and longer channels of residue are found to accumulate under +DC as compared to –DC.

Table 4.1. ITVs of the tested SiR composites under AC, +DC and –DC voltages.

Sample identification	ITV (kV)		
	AC	+DC	-DC
Unfilled SiR	3.5-3.75	2.25*	2.75-3.0
RS10	3.75	2.5-2.75	3.25
RS30	3.75-4.0	2.5-2.75	3.25

*Obtained sooner than third voltage step and noted as ITV since DBA initiated at 2.0 kV

(a) AC

(b) +DC

(c) -DC

Figure 4.1. Failure patterns on three different RS30 samples failed in the ITV test under (a) AC, (b) +DC and (c) –DC.

4.2 Leakage Current in the +DC, -DC and AC Inclined Plane Tests

Figure 4.2 shows the measured LC as a function of applied voltage (with 95% confidence intervals) for AC, +DC and –DC, in the investigation of the wetting behavior of the liquid contaminant. It is visually observed that when LC saturation occurs, intermittent discharges accompanied significant disruption of the contaminant. Expulsion of small droplets from the contaminant rivulet at a voltage level of 1.25 kV could be clearly observed under AC, +DC and –DC. Typical expulsion pattern is shown in Figure 4.3. As the ejected volume of contaminant increases with applied voltage, reducing the rivulet, and therefore its conductance, the DBA current magnitude also diminishes. Since the average LC is highest under +DC at pre DBA stage, it follows that the lowest ejection occurs at +DC. Foam in the contaminant rivulet under –DC has been observed which appears to be generated at the upper electrode.

Figure 4.4 shows the I_w and the corresponding V_w obtained at flow rates between 0.3 and 1.65 ml/min under the applied 5kV AC, +DC and –DC voltage [60]. Little difference was obtained in the I_w with respect to the voltage type for flow rates of 1, 1.3 and 1.65 ml/min; and therefore the

corresponding r_p values were assumed similar with respect to the voltage type for these flow rates.

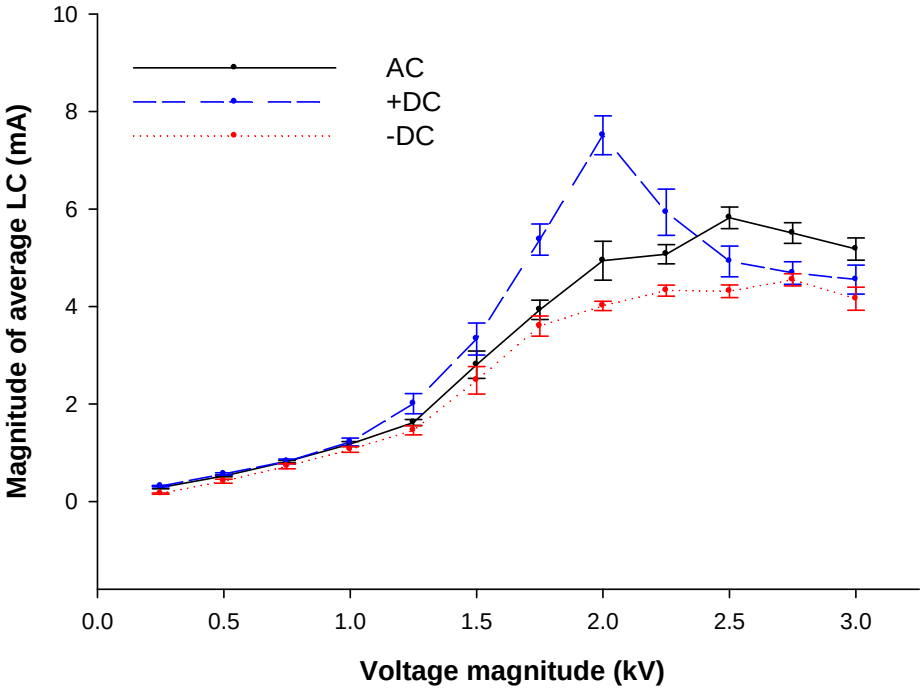

Figure 4.2. Average LC under AC, +DC and –DC for voltage ranges of 0.25-3 kV.

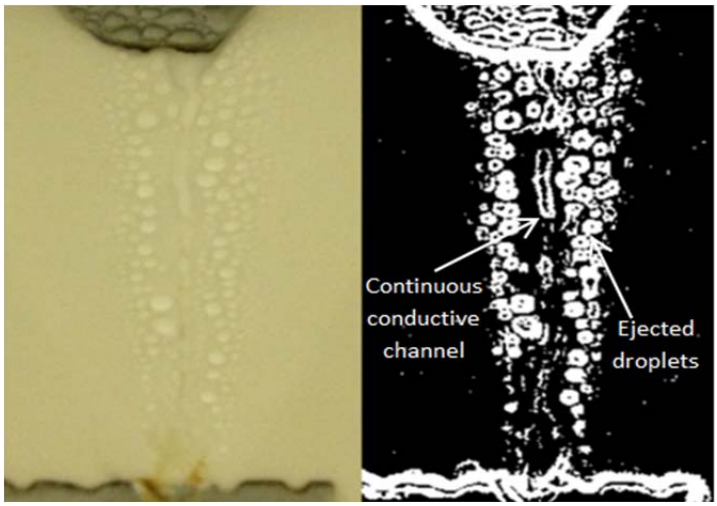

Figure 4.3. Typical expulsion pattern observed during the surface measurement study under the IPT voltage (1.75 kV +DC); left-actual image and right-black-and-white image.

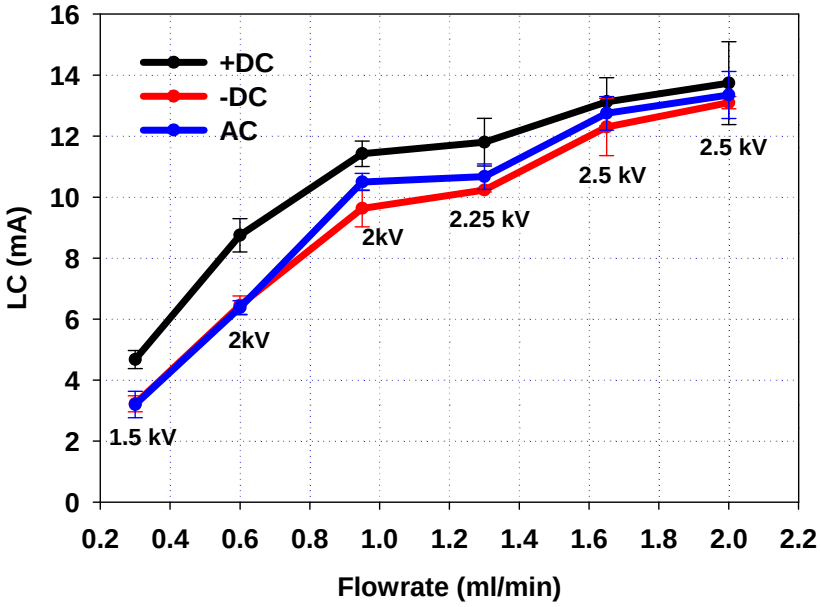

Figure 4.4. I_w as a function of flowrate prior to the formation of dry-bands under +DC, -DC and AC voltages.

4.3 AC and DC Erosion under the Equivalent Voltages

The average R^{ITV}_{+DC} and R^{ITV}_{-DC} obtained for the tested composites using the ITV method were found to be 67% and 84% of the AC voltage, respectively. The equivalent +DC and –DC voltages were, accordingly, calculated, as in equation (2.1), and are shown in Table 4.2. Figure 4.5 and Figure 4.6 show the erosion pattern for the tested RS30 samples under the equivalent voltages and the corresponding measured erosion depth and area, respectively. Comparable erosions are obtained under +DC and –DC but not for AC despite applying the equivalent test voltages as determined by the ITV method. Bruce *et al.* also reported a comparable erosion under +2.25 kV and -3.25 kV, but with different flow rates (0.15 ml/min and 0.3 ml/min under +DC and –DC, respectively) [18]. Obtaining such an agreement in the erosion resistance shows the potential of finding reproducible outcomes in the DC IPT.

Table 4.2. Average CV ratios for +DC and –DC as compared to the AC IPTs and AC, +DC and –DC voltages to be applied in the constant voltage methods for the tested SiR composites.

Sample identification	R_{+DC}^{ITV} (%)	R_{-DC}^{ITV} (%)	V_{AC}^{ITV} (kV)	V_{+DC}^{ITV} (kV)	V_{-DC}^{ITV} (kV)
Unfilled SiR	60-64	73-86	2.75-3.0	2.0	2-2.5
RS10	67-73	87	3.0	2-2.25	2.5
RS30	63-73	81-87	3-3.25	2-2.25	2.5-2.75
Average	67	84	-	-	-

(a) 3.5 kV AC (rms)

(b) 2.25 kV +DC

(c) 3 kV –DC

Figure 4.5. Erosion patterns for the voltage modes and suggested test voltages in (a) 3.5 kV rms AC; (b) 2.25 kV +DC; (c) 3 kV –DC.

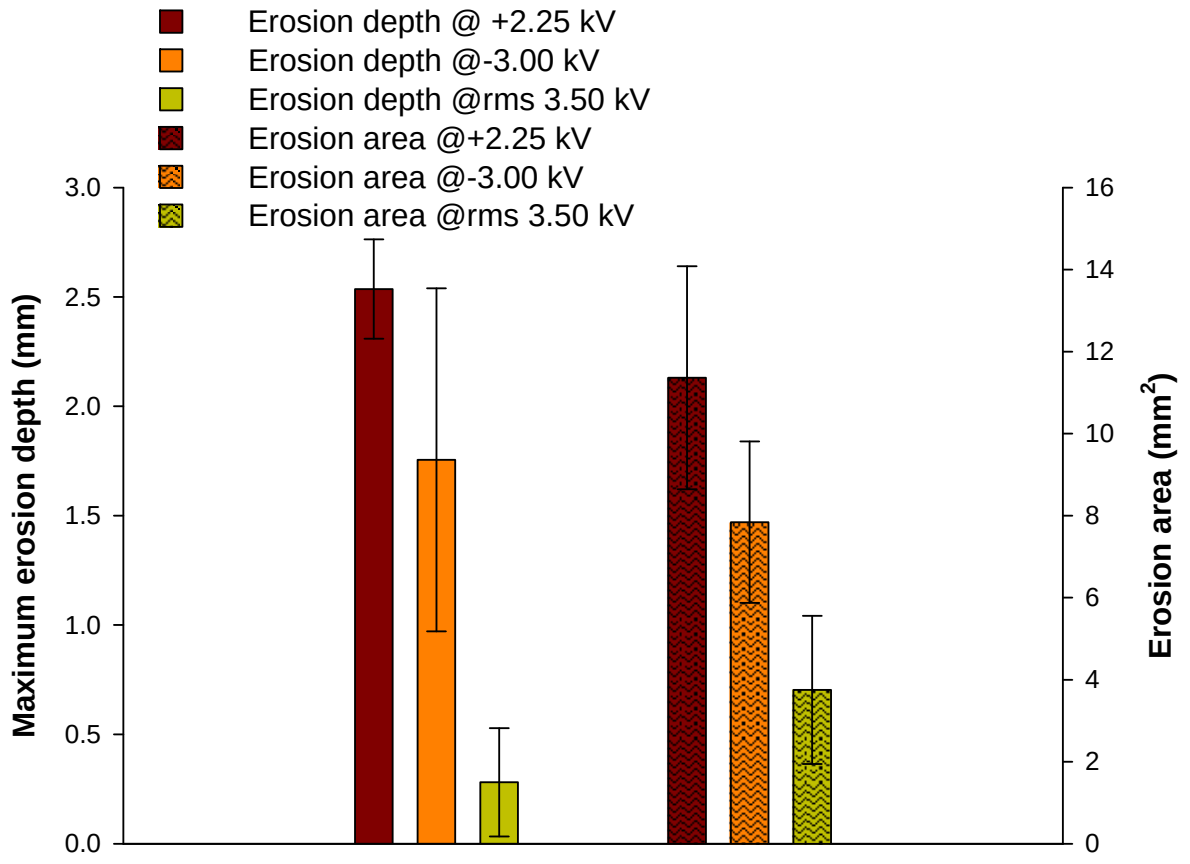

Figure 4.6. Maximum erosion depth and area on RS30 samples tested in the IPT at 3.5 kV AC, 2.25 kV +DC and 3 kV –DC.

4.4 Correlation of Residue, Hotspot Temperature and Eroding Dry-Band Arcing

Figure 4.7 compares the growth of T_{max} on HA58 samples, with residue intact (RI) and residue removed (RR), under the equivalent +DC and -DC to AC voltages. The findings reported were obtained for all the tested samples, and typical results are illustrated for the sake of brevity. The primary observation is that the DBA residue gives rise to hotspots which accelerates erosion of the test samples. Damage was clearly observed for a hot spot temperature > 200 ^{o}C under both AC and DC; however, deep erosion was evident under DC at an eroding hotspot approaching 400 ^{o}C which was not

recorded under AC. In addition, deeper erosion and more concentrated residue were obtained for the samples tested under +DC as compared to –DC as evident in Figure 4.8. Similar relative erosion patterns were reported with respect to the voltage polarity even on different formulations of SiR and at different IPT voltages [18, 20]. Similar degradation with temperature has also been reported for different compositions of filled SiR [37].

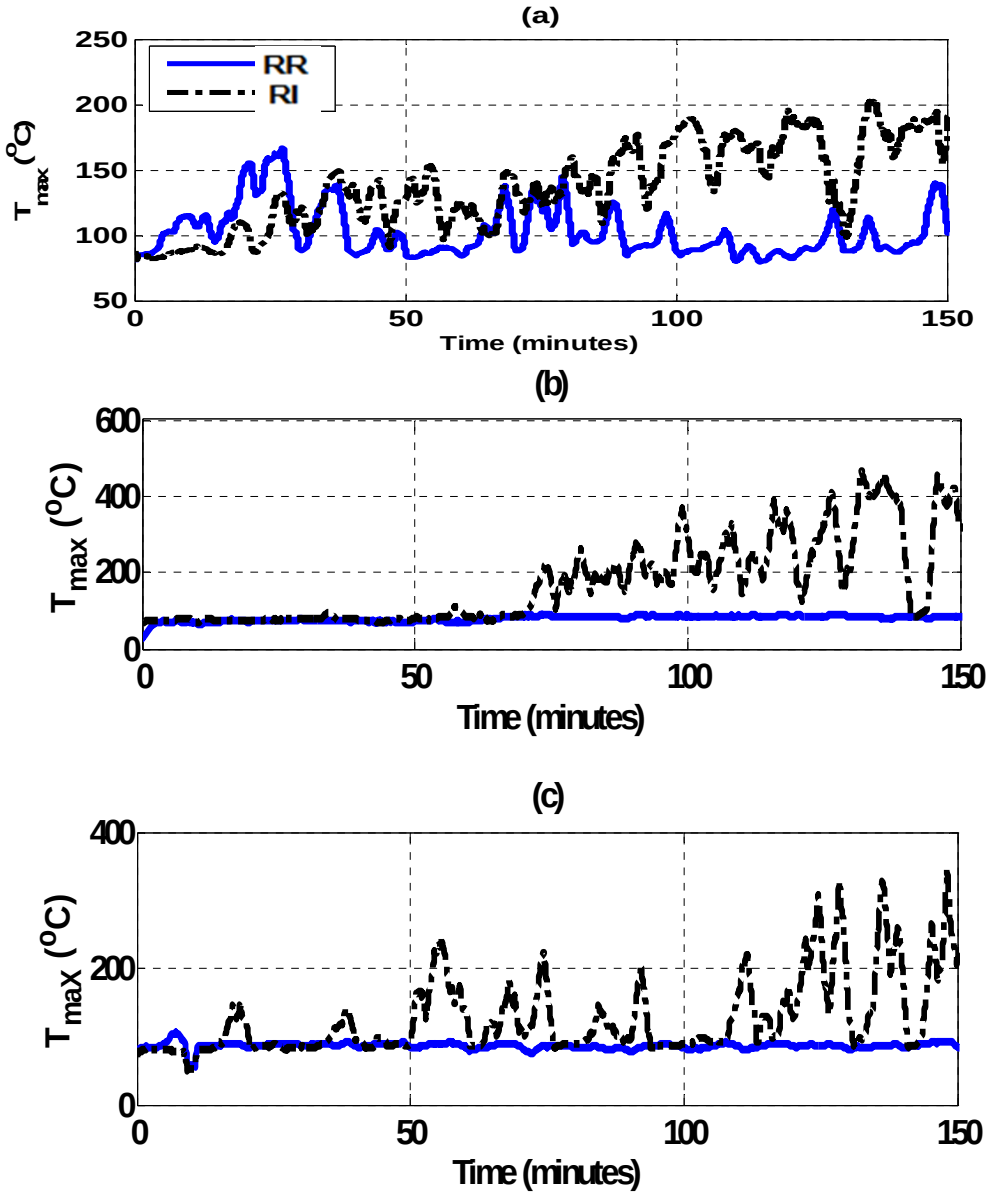

Figure 4.7. T_{max} on HA58 samples with voltages of (a) AC (rms 3.5 kV); (b) +DC (2.25 kV); and (c) –DC (3 kV) with RI and RR.

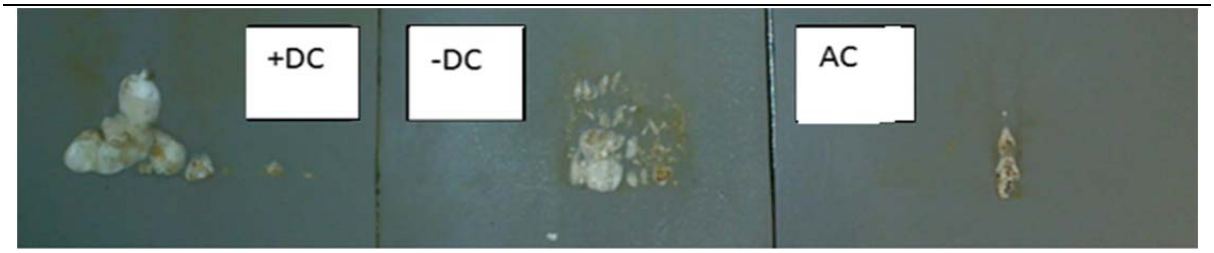

Figure 4.8. Erosion patterns on the tested HA58 composites in studying the influece of the reside formation under the equivalent +DC, -DC and AC voltages.

4.5 The Eroding Hotspot Temperature

Figure 4.9 shows the TGA and DSC results for the HA58 material. The DSC plot shows an endothermic dent in interval A, corresponding to thermal decomposition [37]. Decomposition of the HTV material took place in interval A with an initial loss of weight at approximately 210 ^{o}C. The interval A in the DTG results shows maximum degradation at 340 ^{o}C. Similarly, the initial degradation temperature can be obtained from interval A at 230 ^{o}C with a maximum rate at 317 ^{o}C for the RA30 sample as shown in Figure 4.10. Also, Figure 4.11 shows 200 ^{o}C as an initial degradation temperature and 371 ^{o}C as the temperature of maximum rate of weight loss during A for the RS30 sample. Hotpot spots were therefore defined at T_{max} 200^{o}C; whereas, T_{max} approaching the 400 ^{o}C leading to deep erosion was identified as the eroding hotspot temperature on the tested SiR [37].

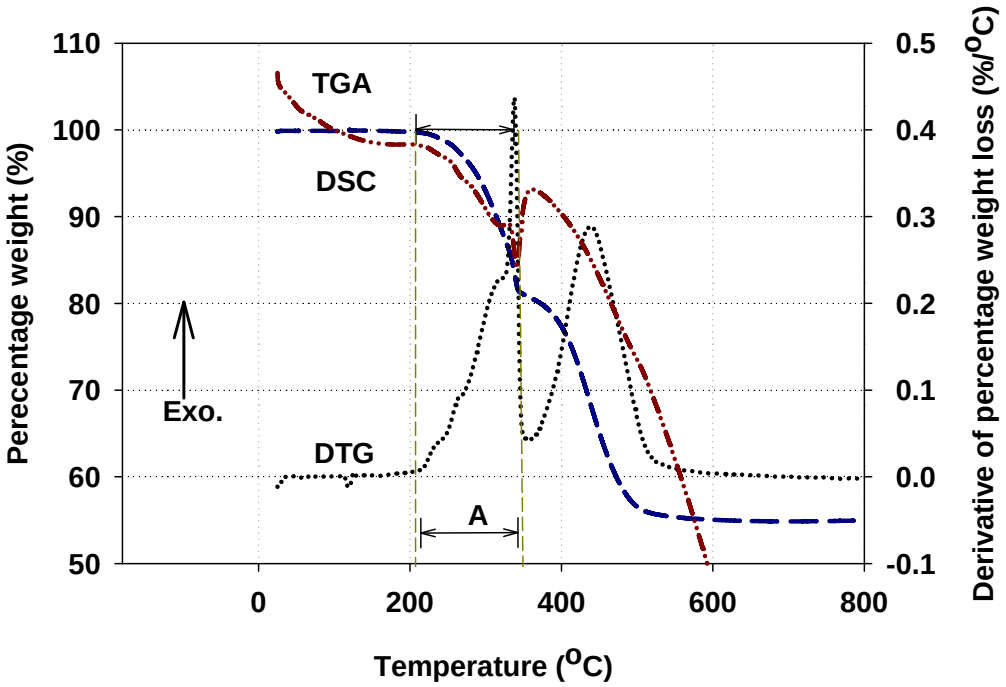

Figure 4.9. TGA and DSC curves of the HA58 composites in air.

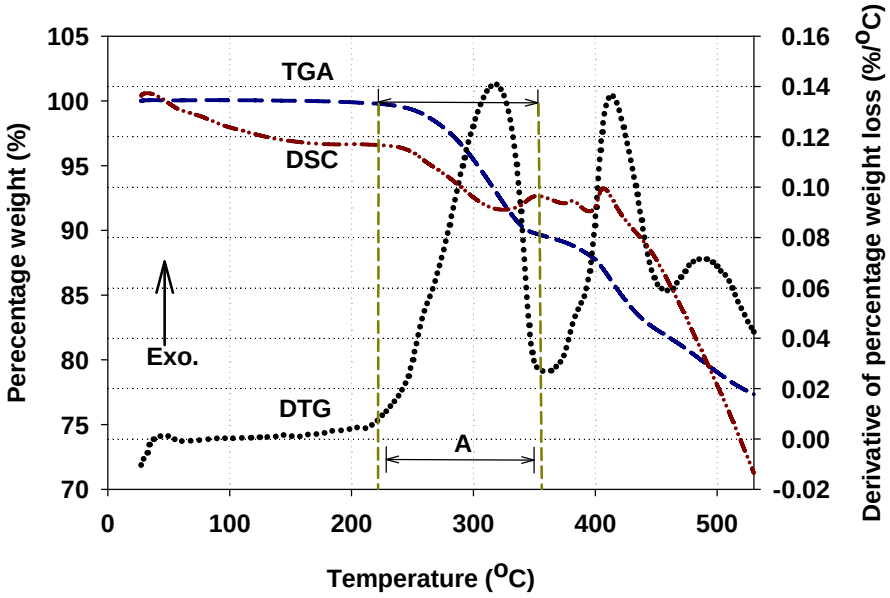

Figure 4.10. TGA and DSC curves of the RA30 composites in air.

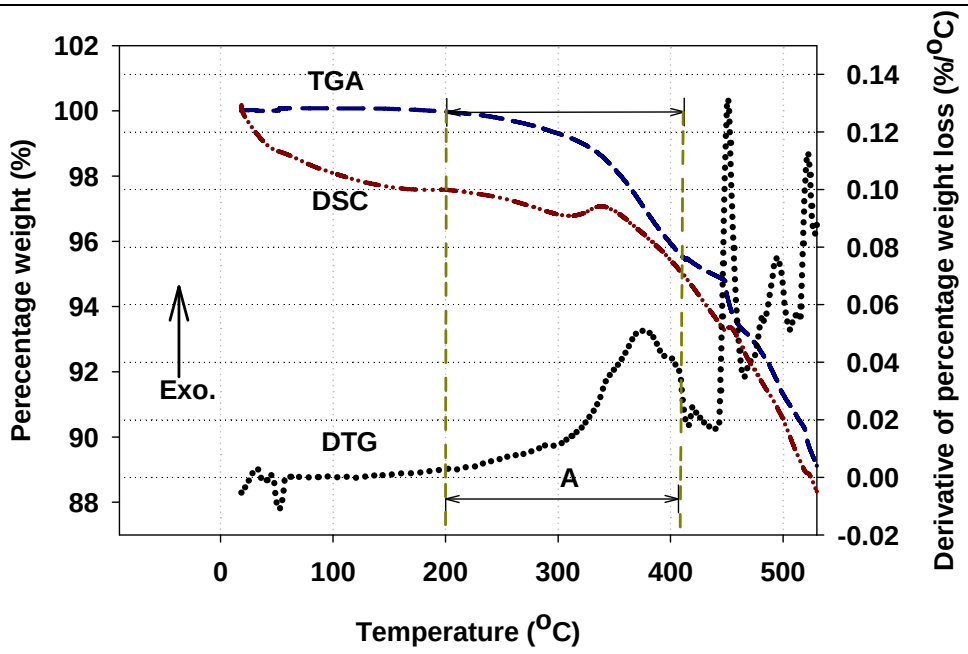

Figure 4.11. TGA and DSC curves of the RS30 composites in air.

4.6 Characterization of the Eroding Dry-Band Arcing

Figure 4.12 shows an example of the correlation between the measured T_{max} and the A_{rms} waveform for an RA30 sample under 2.25 kV +DC. Similar correlations were also obtained for the remaining samples tested under both polarities. Fewer non-conduction periods were found to be associated with hot spot temperature development and ultimately the eroding hotspots. A segment of the EDBA current waveform, shown in Figure 4.13, verifies a stable discharge. Random discharges embedded in the stable DBA current (flat top) are evident in Figure 4.13b. The effect of these discharges is to slightly raise the magnitude of the flat top of the stable DBA current, thereby increasing the intensity of the stable DBA as confirmed by simultaneous monitoring of the surface condition, Figure 4.13c. Therefore, the rms details mainly reflect the intensity of the stable discharge during the EDBA since they detect the transient fronts/tails of the random pulses on the flat top of the stable (main) discharge.

Figure 4.14 compares the T_{max} to d_{1rms}, d_{3rms} and d_{7rms}, in which significant correlation is evident between the rms value and T_{max}. The correlation diminishes with higher order details (lower frequency bands), especially for d_{7rms} in Figure 4.14. This finding is clearly confirmed by the analysis of the unsmoothed waveforms, as indicated by d_{1rms} versus d_{7rms} in Figure 4.15.

At elevated temperatures, it has been shown that volatile cyclic oligomers are produced during the decomposition of SiR and ionization of the resulting plasma phase in the DBA promotes intense discharges [37]. The stable and intense discharges, which were found to initiate deep erosion, were identified through an increase in the LC, forming random pulses that are superimposed on the flattop of the stable LC. Such an increase in the LC enables the evolution of the d_{3rms} (> 0.1 mA [18]) shown in Figure 5.2, and the relative evolution of the d_{3rms} was accordingly proposed as an indicator of the relative inception of the stable and intense DBA. It was observed that higher temperatures coincided with the occurrence of superimposed LC pulses. The correlation between the surface temperature, which is a reflection of the discharge severity and d_{3rms} can be therefore justified, and the magnitude of the d_{3rms} accordingly indicates the extent to which the random pulses take place. Thus, the relative magnitude of d_{3rms} is an indicator of the degree of ionizations in the plasma phase.

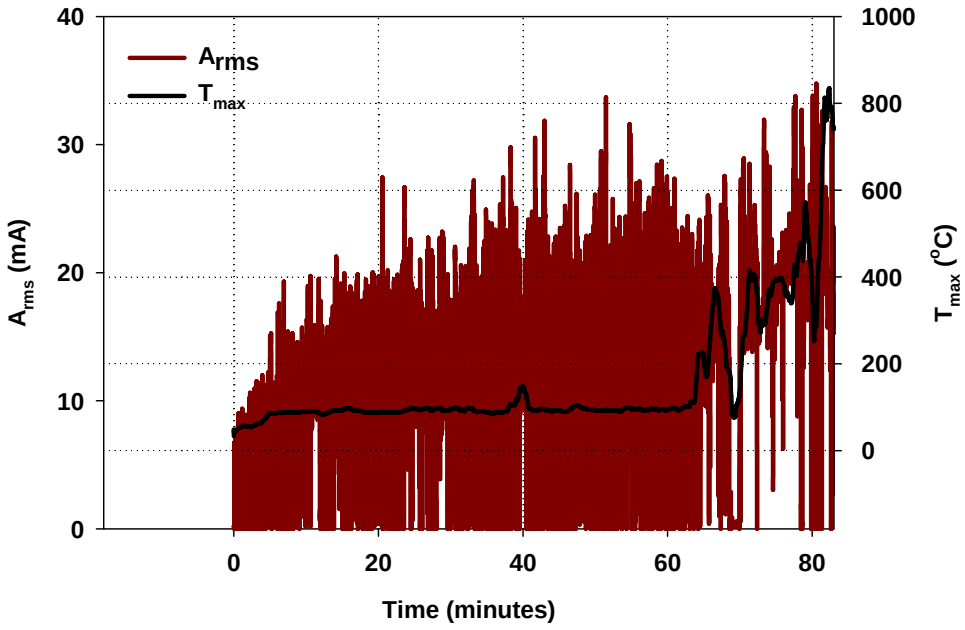

Figure 4.12. A_{rms} waveform of an RA30 sample under 2.25 kV +DC along with the corresponding T_{max}.

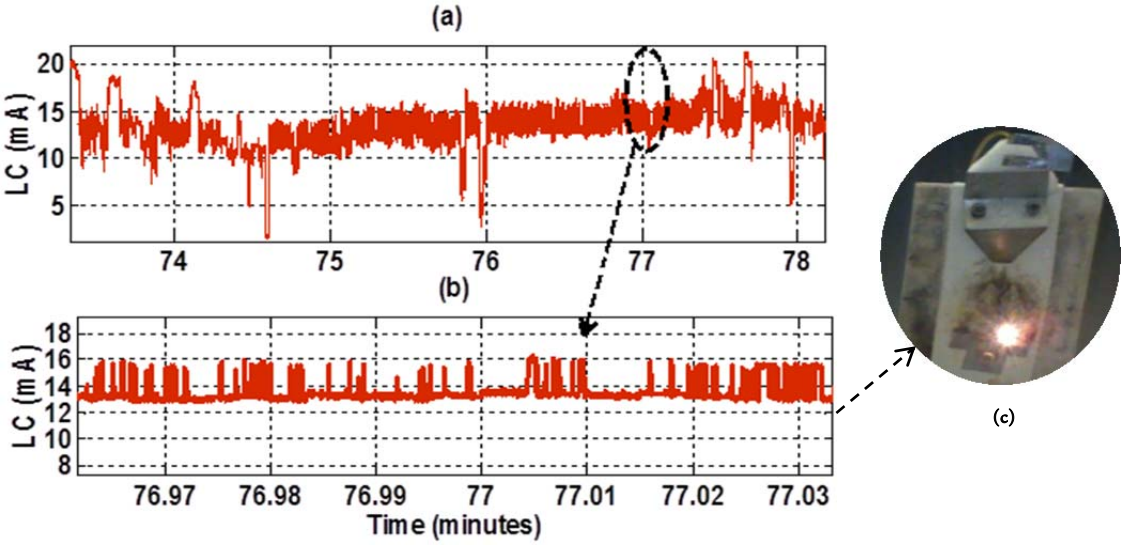

Figure 4.13. (a) Measured LC during the EDBA under DC with time; (b) segment of the EDBA current that shows stable discharge current (flat top) with associated random discharges promoting an intense discharge as shown in (c).

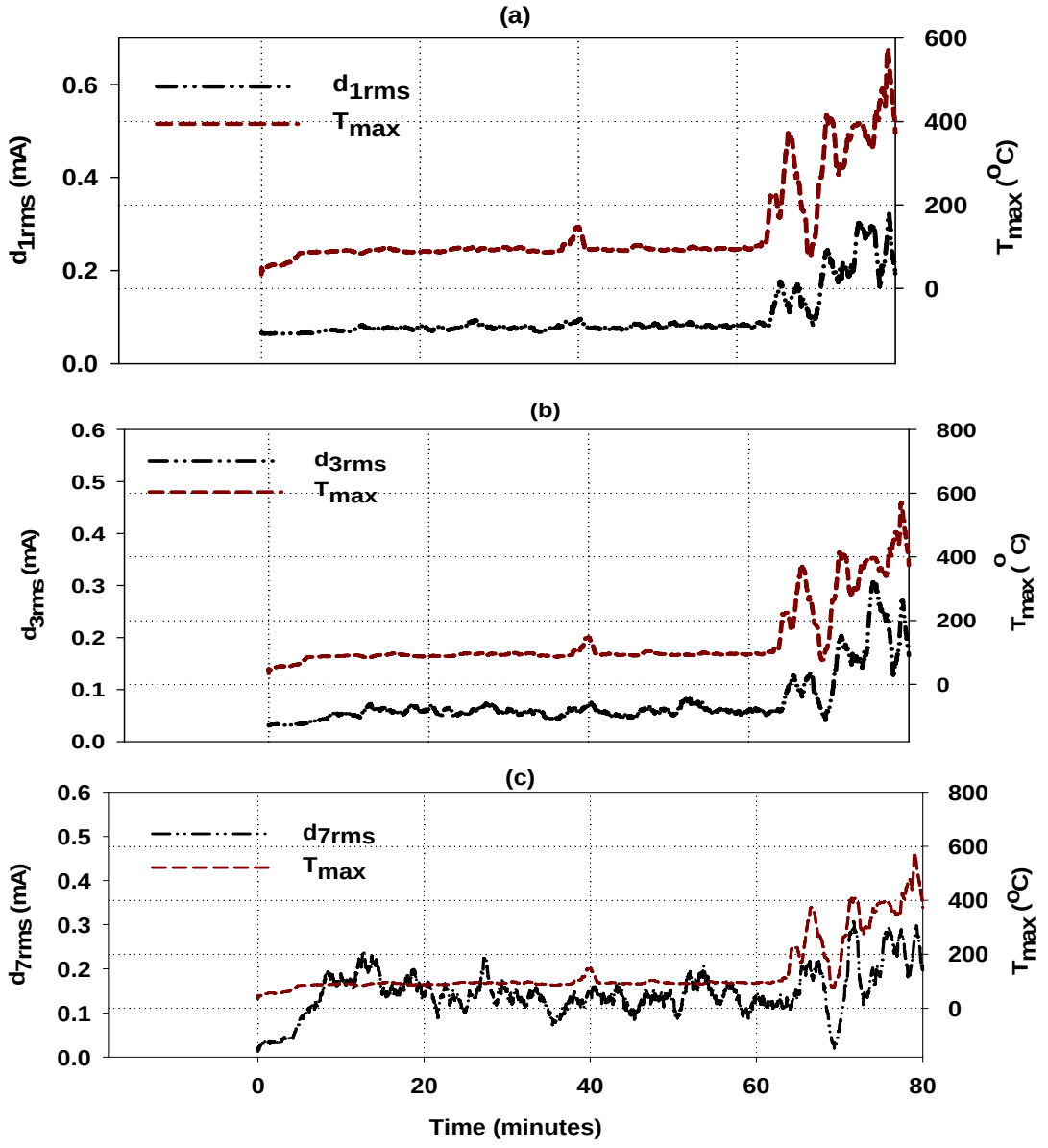

Figure 4.14. Comparison of the T_{max} with time to (a) d_{1rms}, (b) d_{3rms}, and (c) d_{7rms} on sample RA30 at 2.25 kV +DC.

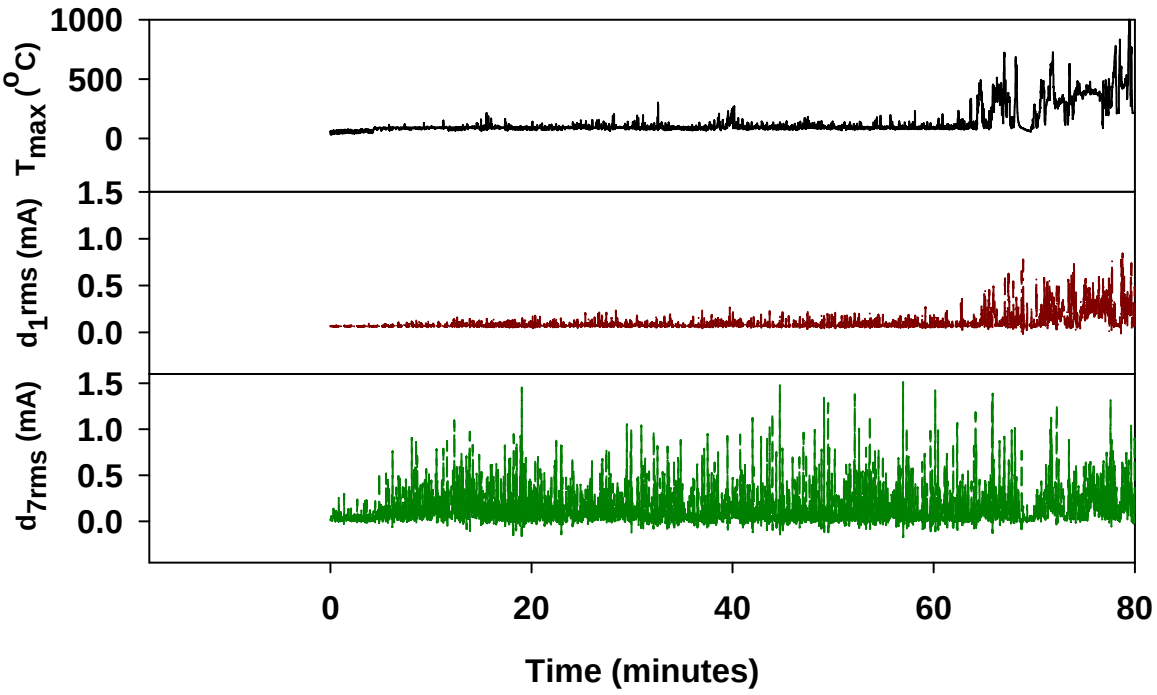

Figure 4.15. Comparison of d_{1rms} and d_{7rms} to T_{max} with time for an RA30 sample at 2.25 kV +DC.

4.7 Suppression of Dry-Band Arcing Erosion by Alumina Tri-hydrate and Silica Fillers in Silicone Rubber under DC

Figure 4.16 shows the TE for RA30 and RS30 samples under +DC and –DC; the –DC show shorter TE. In addition, the silica samples show shorter TE than the ATH samples. TE was also found to increase with filler level irrespective of the filler type. The DBA residue was observed to form in a scattered pattern on the ATH samples as opposed to the silica samples. The water of hydration of ATH released during DBA is believed somewhat to hinder the formation of a concentrated residue, thereby delaying the EDBA [13, 14]. Regarding polarity, despite the higher temperatures observed under +DC, slower formation of residue was observed under +DC than under -DC, leading to longer TE [31].

Figure 4.17 shows the development of d_{3rms} with time in the IPT for unfilled SiR, RA30 and RS30 specimens. The delayed evolution of d_{3rms} observed for both RS30 and RA30 samples shows a delay in the evolution of T_{max} due to the addition of un-hydrated silica and hydrated alumina [50], with a slower evolution of T_{max} evident for RA30 as compared to the RS30 samples. Figure 4.18 shows similar trend for the evolution of T_{max} with time for RA30L and the RS30L samples at laser powers of 3.5 and 4.5 W. Higher magnitudes of d_{3rms} were found for the unfilled SiR as compared to the RA30 and RS30 samples, showing a reduction in the ionizations of the plasma phase on the filled as compared to the unfilled composites. The very little difference in the magnitude of d_{3rms} between RA30 and the RS30 samples indicates an insignificant difference in the degree of ionizations between 30 wt% ATH and silica.

Figure 4.19 shows the development of d_{3rms} for RA30, RS30, RA50 and RS50 samples at 2.75 kV +DC. Sample RS50 shows a longer time for d_{3rms} to develop as with the higher filler loading. However, a lower level of d_{3rms} for the RA50 sample suggests yet another mechanism to be present reducing the degree of ionizations in the plasma phase. Similarly, a lower level of d_{3rms} was found for highly filled HTV SiR with ATH as shown in Figure 4.20.

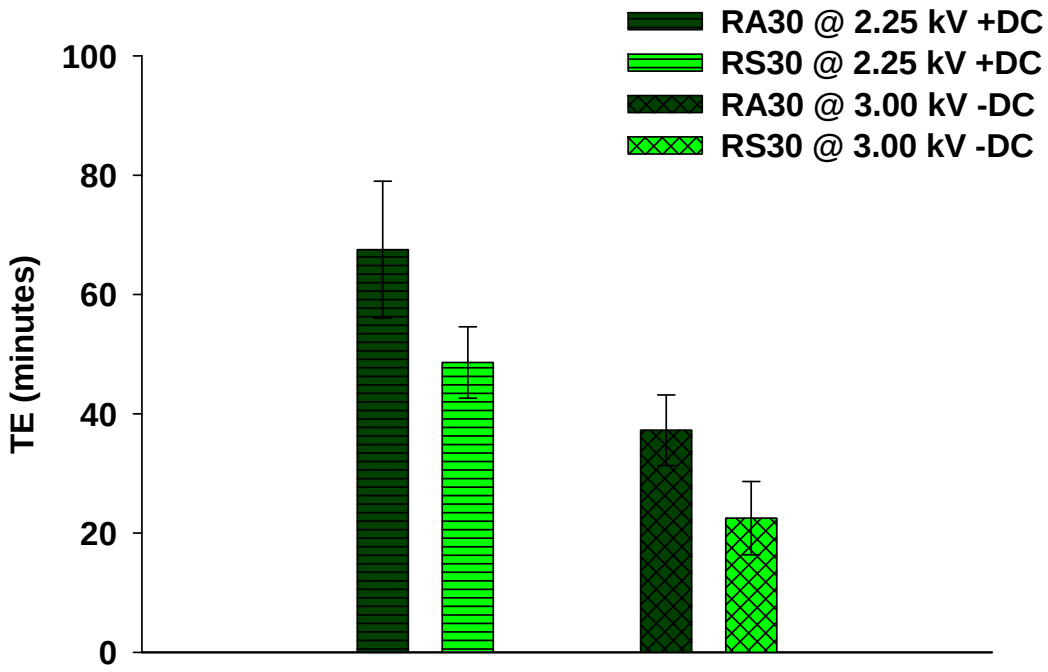

Figure 4.16. TE in minutes for the RA30 and RS30 samples with 2.25 kV +DC and 3 kV –DC.

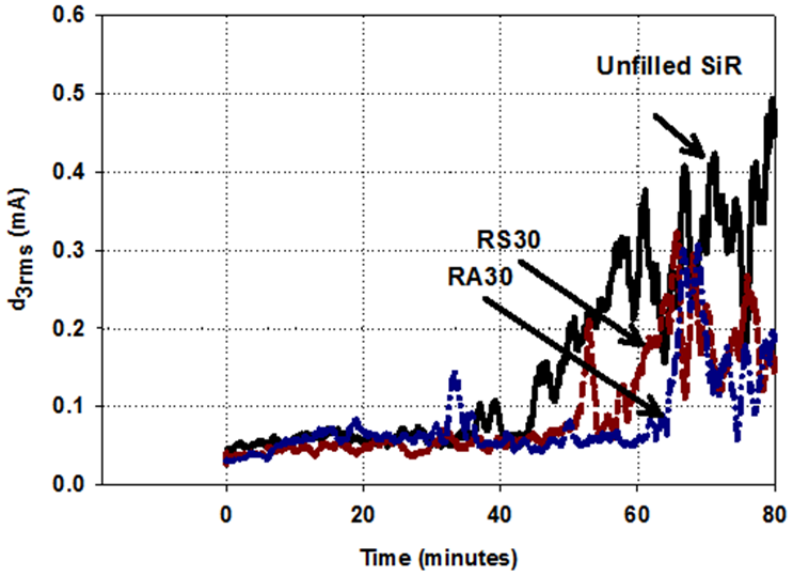

Figure 4.17. Comparison of d_{3rms} patterns with time for unfilled SiR , RA30 and RS30 samples, at 2.25 kV +DC voltage.

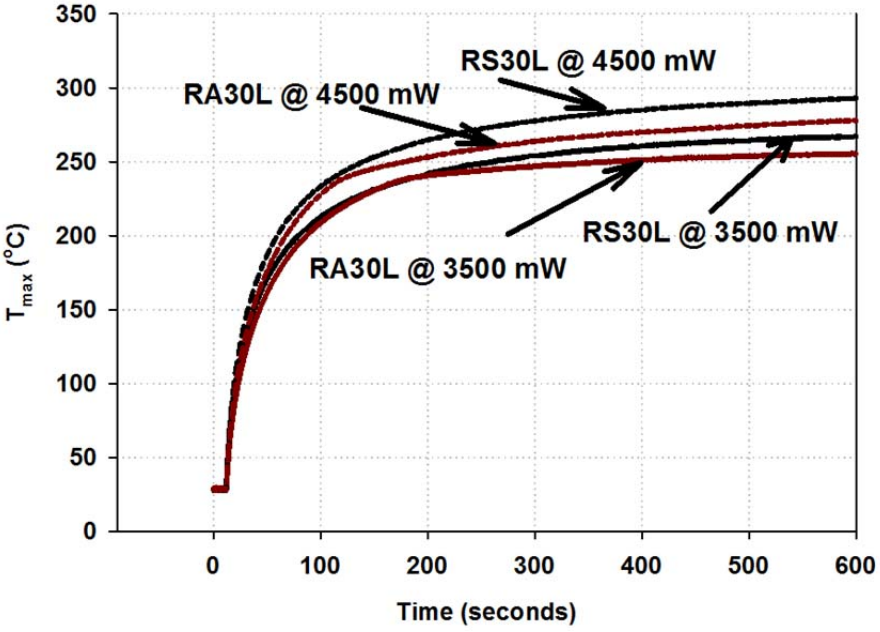

Figure 4.18. T_{max} for RA30L and RS30L samples in laser heating experiments at laser powers of 3.5 and 4.5 W.

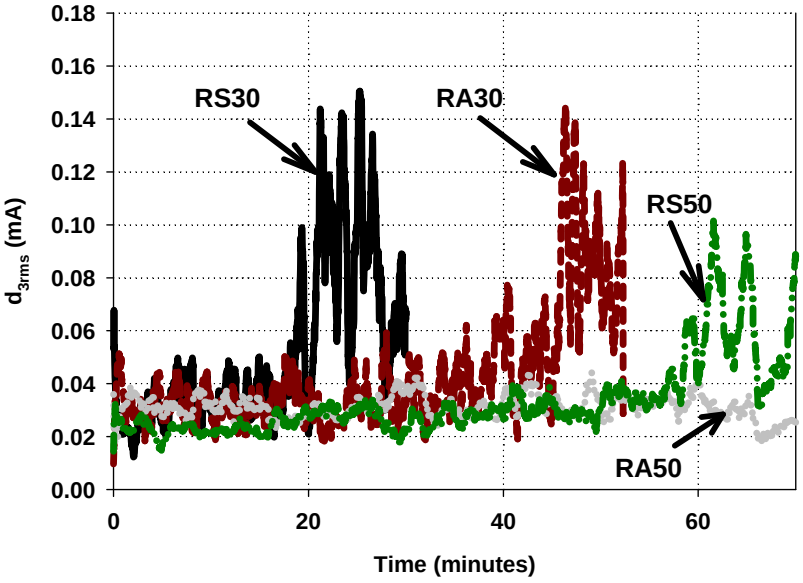

Figure 4.19. Comparison of d_{3rms} with time for RA30, RS30, RA50 and RS50 samples at 2.75 kV +DC.

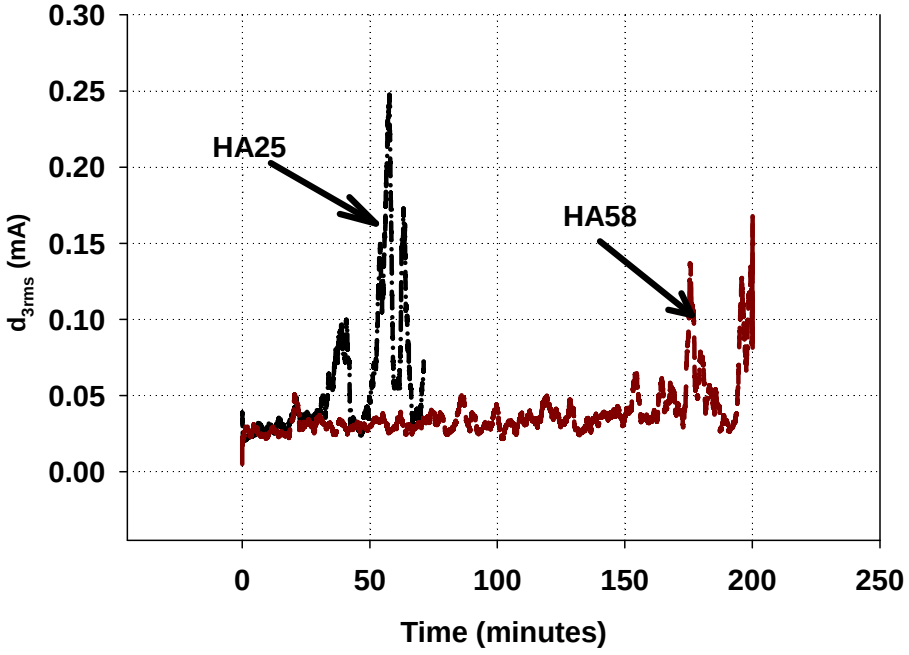

Figure 4.20. Development of d_{3rms} with time for HA25 and HA58 samples under 2.25 kV +DC.

4.8 Analysis of the Surface Temperature in the AC, +DC and –DC Inclined Plane Tests

As previously obtained, different mechanisms were contributing to the development of hotspots, thus erosion inception of SiR in the DC IPT. Therefore, it is very important to investigate for the characteristics of the DBA as indicated by LC. The LC was measured as shown in Figure 4.21, with the cases involving liquid contaminant flow rates of 1 and 1.65 ml/min under AC and DC, to conduct the study at the similar r_p. Table 4.3 shows the corresponding r_p determined using equation (2.3).

Table 4.3. Calculated r_p in the AC IPT.

Flow rate (ml/min)	rp (kΩ/cm)
0.3	73
0.7	51
1	35
1.3	30
1.65	27

By changing the contaminant flow rate, it was noticed that very little change was found in the DBA length. However, a clear distinction in the DBA length was evident with voltage type as shown in Figure 4.22.

The LC was found to be largest under +DC followed by AC and –DC. Figure 4.24 shows the corresponding surface resistance of the DBA showing higher resistivity for the DBA under -DC as compared to +DC and AC, with little difference between AC and +DC. A similar finding has been reported with DBA of longer lengths in flashover studies [69]. The DBA power was found comparable under AC, +DC and –DC at flow rate of 1 ml/min. Figure 4.23 compares the normalized T_{max} for DBA period of one second under AC, +DC and –DC, showing the highest T_{max} under +DC followed by –DC and then AC. Good correlation was obtained between the estimated and the experimental T_{max} with an average r of 0.99 determined by equation , which verifies the analysis conducted.

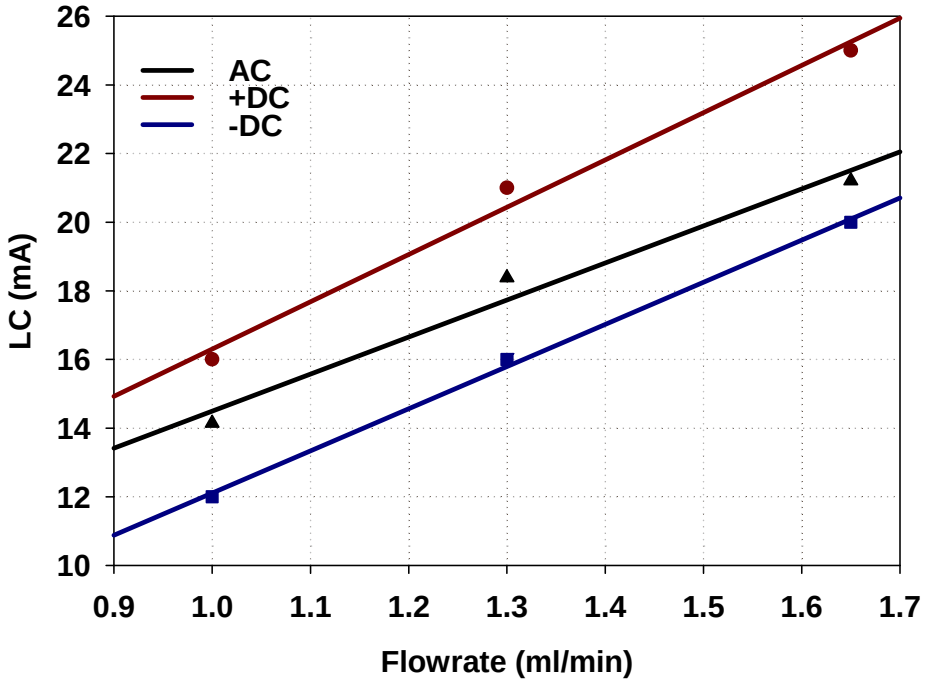

Figure 4.21. LC measured at flow rates of 1, 1.3 and 1.65 ml/min under AC, +DC and –DC.

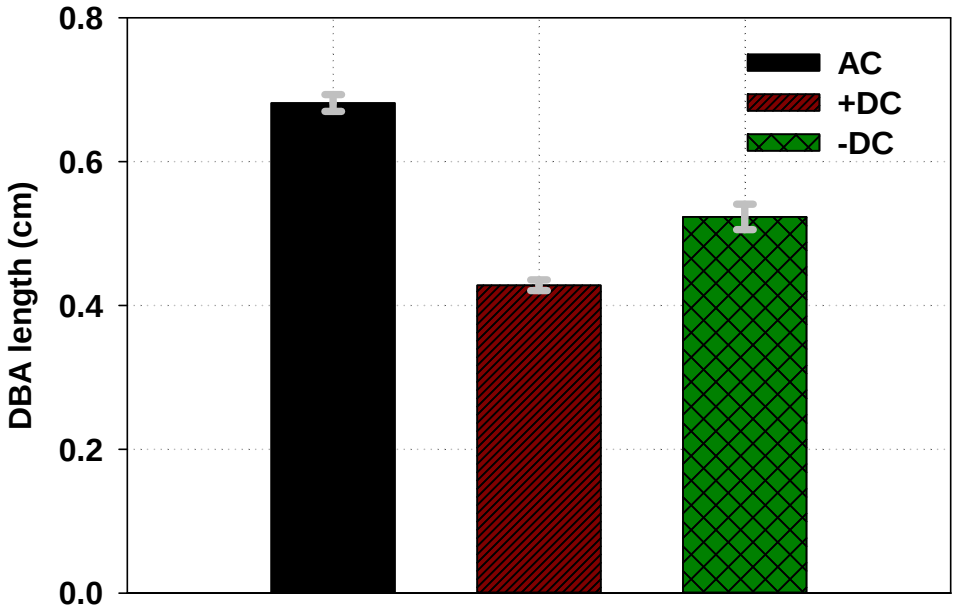

Figure 4.22. Estimated DBA length under 5 kV AC, +DC and –DC.

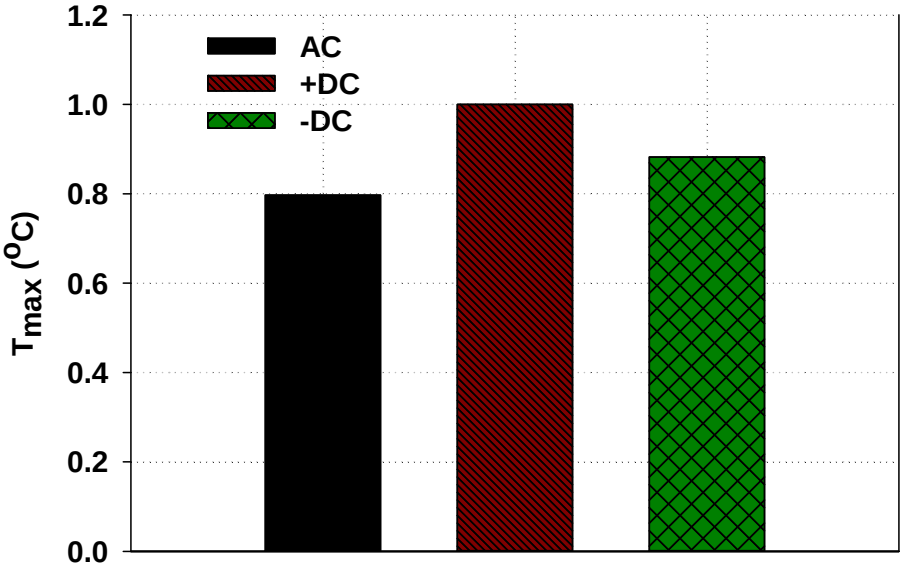

Figure 4.23. Comparison of normlizedT_{max} determined under AC, +DC and -DC for a liquid contaminant flow rate of 1 ml/min.

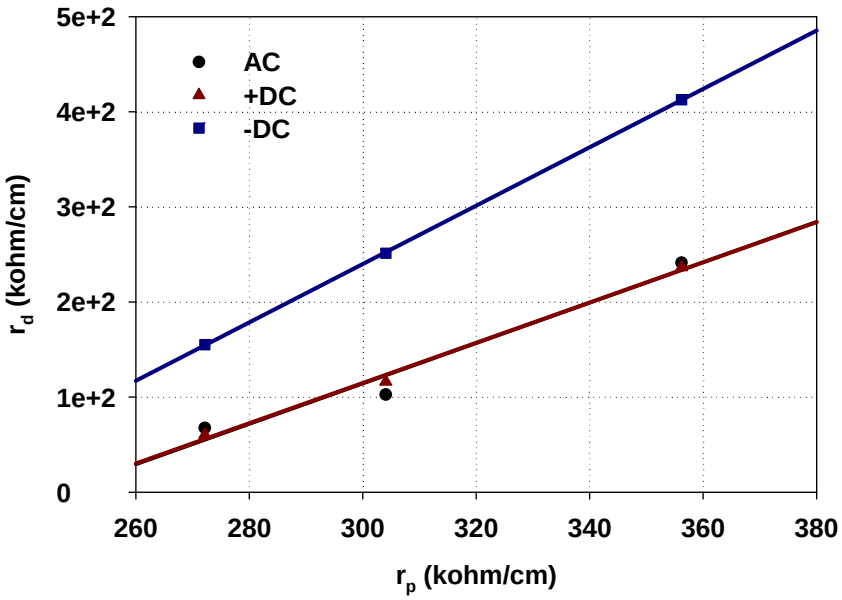

Figure 4.24. r_p versus r_d of the DBA in the AC, +DC and –DC IPTs.

Chapter 5
Discussion

The conducted studies in this research have been targeted mainly towards enabling the development of the DC IPT. Therefore, a mechanistic explanation to the erosion in the DC IPT and the corresponding suppression effect of fillers are provided.

5.1 Erosion of Silicone Rubber Composites in the AC and DC Inclined Plane Tests

5.1.1 AC and DC Erosion Classes

The ITV determined for the unfilled SiR, RA10 and RA30 samples (Table 4.1) has been shown dependent on the voltage type irrespective of the filler loading. Likewise, Chang *et al.* reported the insignificant difference in the ITV for tested SiR composites with different loading levels of ATH in the AC IPT [70]. Ansorge *et al.* have also reported that adding silica filler to unfilled SiR samples in the levels of 20 and 25 wt% does not affect the time-to-failure in the AC IPT [66].

In addition, the ITVs determined in this study is found lower showing more severe DBA under DC as compared to AC, and under +DC as compared to –DC. The ITV has been found by Mathes to be a dependent parameter on the energy dissipated on the tested sample in the IPT [4]. Therefore, based on the findings obtained in this study, the DBA energy with +DC can be defined greater compared to –DC and AC, at the same voltage levels and irrespective with filler loading. Such findings suggest, for a specific base material, equivalent rather than equal voltages has to be determined for the DC as compared to the standard AC IPT.

The AC IPT has been developed by Mathes *et al.* to induce a continuous DBA rooted on the bottom electrode, thereby providing an accelerated and reproducible aging for the tested materials [21]. The eroded paths obtained in this study (Figure 4.1) propagate from the bottom electrode, and the erosion patterns reported throughout the study are reproducible. Both observations have been also reported by Bruce *et al.* [18], which provides a strong basis to develop the DC IPT apparatus similar to that of the AC IPT.

5.1.2 Behavior of Liquid Contaminant under AC, +DC and –DC

Figure 4.2 indicates saturation of LC as an indicator of the DBA in the DC IPT, a similar finding under AC was reported by Jolly as LC saturation is an indication of significant evaporation resulting in intermittent DBA [71]. In the IPT and during the pre DBA stage, the LC flowing in the liquid contaminant does not suffer from disruption and is therefore resistive in nature. When the voltage is increased, however, dry bands can be formed and DBA can take place whereby the rms LC waveform tends to be pulsative in nature. The correlation between the DBA and the satuarion in the LC waveform found in Figure 4.2 [44] can be accordingly confirmed.

In addition, standard deviation of LC can be an indicator of DBA power as it reflects the energy of the waveform variation (distortion) [72]. Standard deviation of decomposed waveforms using the wavelet-multiresolution analysis has been used previously to feature DBA energy [48] and surface pollution severity in clean fog under AC voltages [47]. Figure 5.1 shows the average AC LC at contaminant flow rates of 0.15 and 0.3 ml/min along with the standard voltage ranges as per ASTM D2303, but applied for five minutes. It is seen that the average LC is independent of the applied voltage over the interval of 2 to 2.75 kV at 0.15 ml/min and 3 to 3.75 kV at 0.3 ml/min. A similar pattern under +DC and –DC can be inferred from Figure 4.2 where a saturation in the average current

can be recognized after DBA inception at a specific flow rate of 0.3 ml/min. It is evident therefore that if the standard deviation is an indicator of DBA power, then the average has to be an indicator of the non-discharge current dissipating heat on the liquid contaminant to form dry-bands.

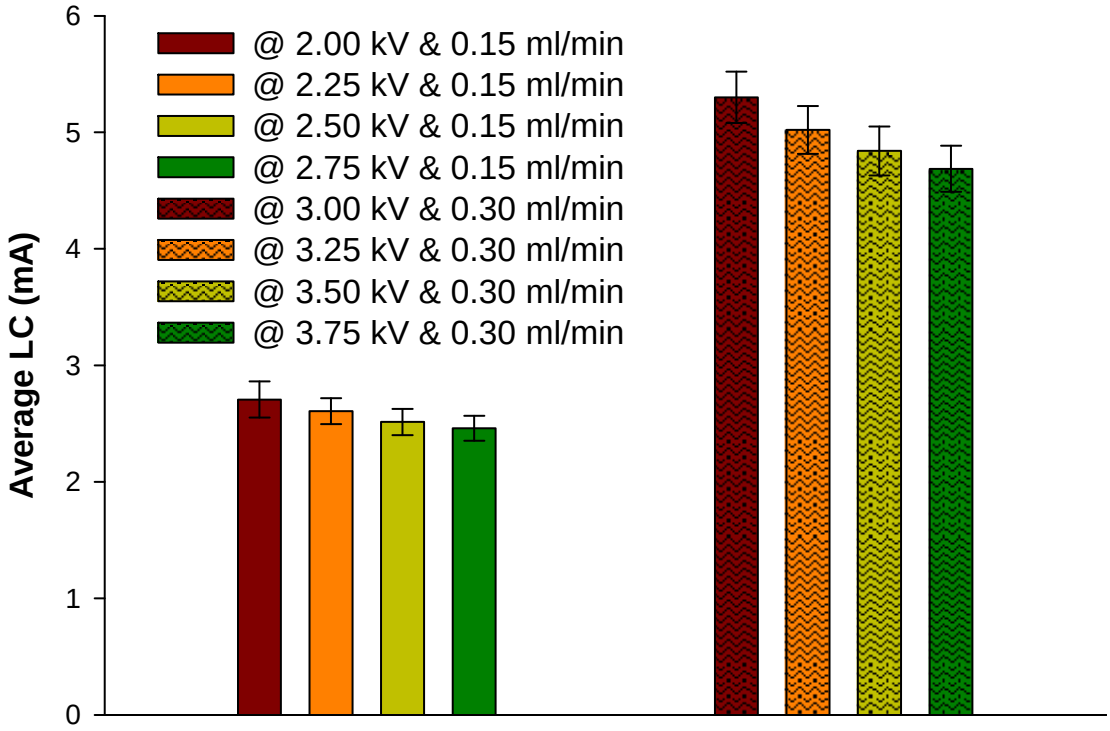

Figure 5.1. Average LC for ASTM D2303 test voltage ranges and at flow rates of 0.2 and 0.3 ml/min.

The inception of discharges takes place at a lower voltage with –DC compared to +DC and AC and this could possibly be attributed to the increased evaporation of the contaminant rivulet and may be the reason for the early saturation in the LC as shown in Figure 4.2. The foam generated in the –DC IPT, as shown in section 4.2, can modify the liquid contaminant characteristics, thereby modifying the inception voltage of DBA. Bruce *et al.* hypothesized the production of hydrogen during electrolysis as reason for the foam production [20].

CHAPTER 5 DISCUSSION

The expulsion of water droplets observed in Figure 4.3 was reported by Vallet *et al.* as an indicator of instability at the triple point (air, solid and liquid contaminant) that comes about due to the electrostatic force overcoming the capillary force [73, 74]. The presence of a surfactant in the contaminant has contributed to the instability at a lower voltage [74]; whereas, the unstable behavior has been reported at later stage of electrowetting.

The DBA current has been reported to be limited by the surface resistance of the contaminated layer [75]. As a result, the least expulsion, thus largest volume of contaminant, obtained under the +DC voltage has led to maximum degree of severity of the DBA and thus minimum ITV. Although more ejection of contaminant under –DC can be inferred as compared to AC, the nature of the DC voltage applied as opposed to 60 Hz AC seems to play an important role in obtaining lower ITV under –DC. Alternatively, Bruce [18] and Vas [20] *et al.* suggested the effect of electrode corrosion as the main reason of the relative difference in the LC levels under the different voltage modes; however, in this part of the study, no significant effect of corrosion was found.

5.1.3 Equivalent DC Voltages

In the light of the lack of information about the DC tracking/erosion classes of materials, new tests for determining these classes still have to be conducted each time a new material composition is investigated under DC. As solid experience of several material classes has been already built for AC, it is beneficial to take the advantage and come up with a parameter that is more generic in obtaining the voltage ratios.

More reliable implementation to energy approach is utilized for obtaining the generic parameter by which the equivalent DC voltages can be determined. As heat ablation of material surfaces is the

consequence of DBA, the non-discharge current of the LC has to be excluded to extract a parameter that correlates with DBA energy. To indicate the DBA energy, the standard deviation of the LC

$$\sigma_i = \sqrt{\frac{1}{N-1}\sum_{n=1}^{N}\left[i[n] - \bar{i}\right]^2}$$

was defined, where N and i[n] are the number of samples acquired and the n^{th} sample of the current, respectively, and $\bar{i}$ is the mean reflecting the non-discharge current component, which can be written as

$$\bar{i} = \frac{1}{N}\sum_{n=1}^{N} i[n].$$

Using standard deviation alone, however, as a DBA energy indicator can be deceiving when comparing signals with different means, i.e wetting current levels. In such case, the standard deviation is a parameter that has to be interpreted with respect to the mean [72], where the average LC has been reported, Figure 4.2, to flow in different levels depending on the voltage mode (+DC and–DC) [18]. Therefore, the CV can be used as a relative indicator to obtain reliable and practical comparison of the DBA energy under AC, +DC and –DC voltages. The coefficient of variation

$$\text{CV} = \frac{\sigma_i}{\bar{i}}$$

was be accordingly determined. In dealing with both DC and AC IPT LC waveforms, it is more practical to use the rms-equivalent for AC waveforms. The rms-equivalent is obtained using a moving one-second window. Thus, for each second, the rms value of the acquired AC waveform

$$\sqrt{\frac{1}{N}\sum_{n=1}^{N}(i[n])^2}$$

was determined. With long duration of voltage application and depending on the voltage mode, residue accumulates on the surface that can affect the severity of the DBA. Thus, an early stage in the DBA is considered in the CV method to avoid the effects of surface residue from affecting the outcome of the method. Therefore, five-minute waveforms are acquired. It is important to note that the CV method determines the energy carried by the discharge current $\left[i[n]-\bar{i}\right]^2$ and looks for equivalent DC voltages producing similar energy rather than forcing an equivalent severity.

A reference DC V_{+DC}^{ref} or V_{-DC}^{ref} voltage level is equivalent to a reference AC V_{AC}^{ref} in the IPT if the induced DC discharge current possesses a CV equal to that of the corresponding AC. Accordingly, the voltage ratios obtained from the CV method can be represented as follows:

$$R_{+DC}^{CV}=\frac{V_{+DC}^{ref}}{V_{AC}^{ref}}.$$

Common reference voltages at 0.15 ml/min and 0.3 ml/min, which are 2.5 kV and 3.5 kV, respectively, are used [23]. Then the equivalent DC voltages to any corresponding AC in the constant voltage methods of the IPT can be found as in equation (2.1)) using the CV ratios (R_{+DC}^{CV} and R_{-DC}^{CV}). To validate the voltage ratios obtained as per the CV method, the percentage difference %Diff between the voltage ratio obtained in the ITV and CV methods are found, for example for the case involving +DC

$$\%Diff_{+DC}=\frac{\left|R_{+DC}^{CV}-R_{+DC}^{ITV}\right|}{\left[\frac{R_{+DC}^{CV}+R_{+DC}^{ITV}}{2}\right]}\times 100\%.$$

Table 5.1 provides the equivalent +DC and –DC test voltages with respect to AC in the CV method. For an AC test level of 2.5 kV with contaminant flow rate of 0.15 ml/min, the equivalent +DC and -

DC test levels are 1.7 kV and 1.9 kV, respectively. Similarly, for an AC test level of 3.5 kV with contaminant flow rate of 0.3 ml/min, the equivalent +DC and –DC test levels are 2.3 kV and 3 kV, respectively. No significant difference can be reported between the equivalent ratios obtained for the two flow rates using the CV methods for both polarities as shown in Table 5.1.

In validating the CV method, the recommended +DC and –DC voltages had a deviation of 1.5% ($\%Diff_{+DC}$) and 1.2% ($\%Diff_{-DC}$), respectively, from the voltage levels determined as per the ITV method. The CV parameter is, therefore, verified to provide a reliable approach by which the equivalent DC voltage can determined. The equivalent –DC voltages obtained using the CV method almost match those reported by Bruce *et al.* for both flow rates, but not under +DC [18]. It seems, therefore, that the CV method has an improved reliability due to its capability of detecting other sources of bias like the relative volume of the contaminant with respect to polarity effect.

Table 5.1. The equivalent +DC and –DC IPT voltages for constant voltage methods along with their ratios with respect to the standard AC voltage, obtained using the CV method.

Flow rate (ml/min)	V_{AC}^{ref} (kV)	V_{+DC}^{ref} (kV)	V_{-DC}^{ref} (kV)	R_{+DC}^{CV} (%)	R_{-DC}^{CV} (%)
0.15	2.5	1.7	1.9	68	76
0.3	3.5	2.3	3	66	85

5.1.4 Erosion Performance of Silicone Rubber under AC and DC Voltages

The relative erosion obtained in Figure 4.6 for the equivalent voltages suggests that, in order to reach a similar performance to that of the AC, a material improvement is needed for the SiR to be employed for DC. This recommendation does not match with Bossi's *et al.* as the authors suggested that no additional improvement is required as long as operational voltages are selected with respect to specific creepage distance (flashover voltages) [76]. The DC flashover voltages found by Bossi *et al.*

for SiR insulators were found equal to 0.75-0.85 of the corresponding AC [76]. Comparable creepage distances to those reported by Bossi *et al.* were, nevertheless, already applied in this study as per the ITV method, and it is recommended that tracking/erosion another factor that has to be added to the withstand voltage criterion in selecting the DC creepage distance.

5.2 The Eroding Dry-Band Arcing Mechanism

The mechanistic observations obtained throughout the study can be summarized in Figure 5.2 showing an example of the LC approximation, its d_{3rms}, and T_{max} with time, along with the corresponding visual appearance of the DBA in the DC IPT. The erosion mechanisms can be accordingly classified into two main sages, the intermittent and the stable DBA stages. In the early stage of the IPT, the DBA is intermittent, as indicated by the pulsative nature of the LC waveform, frequently decreasing below 1 mA in which no arcing develops. This intermittent discharge promotes the EDBA, described as a stable and intense DBA. Extensive analysis into the development of intermittent DBA has been conducted by Bruce *et al.* [18], and the EDBA has been described by Gorur [32] and Mailfert *et al.* [33], yet elucidation on the relation between the intermittent DBA, surface degradation mechanism and the EDBA is needed.

Although no hot spots, thus erosion, can be reported to take place due to the intermittent DBA as respectively shown in Figure 4.13 and Figure 4.8, residue is formed. With T_{max} obtained is < 200 ^{o}C, the residue formed can be attributed to the heat of the DBA leaving silica as residue as described by the Andrinov mechanism of SiR in [11, 12]. Residue formation promotes stable and intense DBA, thereby giving rise to higher T_{max} as shown in Figure 4.7 and eventually the inception of deep erosion shown in Figure 4.8. The stable DBA was identified through a recognizable reduction of non-arcing periods. The statistical analysis shown in Appendix A has also confirmed this behavior described for

the DBA, as similar trend was obtained for to the mean and the LC approximation (Figure A.1). The statistical analysis in Appendix A also indicates an additional ionization taking place in the DBA plasma after the inception of the stable DBA, as an evolution was detected for the skewness and kurtosis showing a change in the distribution of the DBA current as an indication of a change in the ionization mechanism (Figure A.2). The enhanced DBA stability can be justified to take place as a result of the residue slowing down the rate of evaporation of the liquid contaminant in contact with the upper electrode (anode). Gorur *et al.* [32] proposed similar effect for surface deposits of tested SiR in salt fog reducing the rate of evaporation of the contaminant, thereby promoting longer discharge periods [32]. It follows that for a given flow rate in the IPT, the faster accumulation of residue promotes faster inception of the stable DBA, thus evolution of T_{max} and erosion. The faster formation of residue always obtained under –DC as compared to +DC and AC voltages as shown in Figure 4.7 can justify the earlier TE shown in Figure 4.17. Based on Mathes *et al.* [21] work that reported the residue to form with respect to the electrostatic forces during the experiments that led to the development of the standard IPT, enhanced electrostatic precipitation promoting faster accumulation of the residue under DC as compared to AC and under –DC as compared to +DC can be inferred.

On the other hand, more concentrated residue compressing, thus intensifying, the DBA takes place under DC as compared to AC, and under +DC as compared to –DC voltages. The intensification in the DBA is obviously responsible for promoting the heat giving rise to T_{max}. The heat of the DBA is therefore most severe under +DC followed by –DC and then AC. This finding is confirmed by the erosion patterns obtained in Figure 4.8, showing little surface damage to take place under AC as compared to deep erosion under DC, with deeper erosion obtained under +DC as compared to –DC.

CHAPTER 5 DISCUSSION

Bruce [18] and Vas [20] *et al.* proposed electrolysis of the upper electrode giving rise to LC, thus power, to dominate the relative severity of erosion under +DC as compared to -DC. Higher LC is confirmed in this study under +DC as compared to –DC as shown in Figure 4.21, indicating that DBA power can be an influential effect on the relative erosion obtained. However, electrode corrosion does not seem to be the dominant factor, as tiny difference is shown for the linear resistance of the DBA under +DC and AC voltages. In addition, the relative severity of erosion has to be explained taking into consideration the effect of residue formation shown in Figure 4.7, or in other words with respect to the dynamic behavior of the DBA governing the accumulation of residue.

The shorter DBA length obtained under DC as compared to AC, and under +DC as compared to –DC, stresses can be used to justify the accumulation of residue in more concentrated pattern under DC as compared to AC, and under +DC as compared to –DC. The r (found as in equation (2.4)) was obtained between the normalized T_{max} and the L_a to be -0.97, strongly indicating higher T_{max} at lower L_a. It can be inferred that T_{max} is highly influenced by the arc length which determines the corresponding area on which the power of the DBA is dissipated.

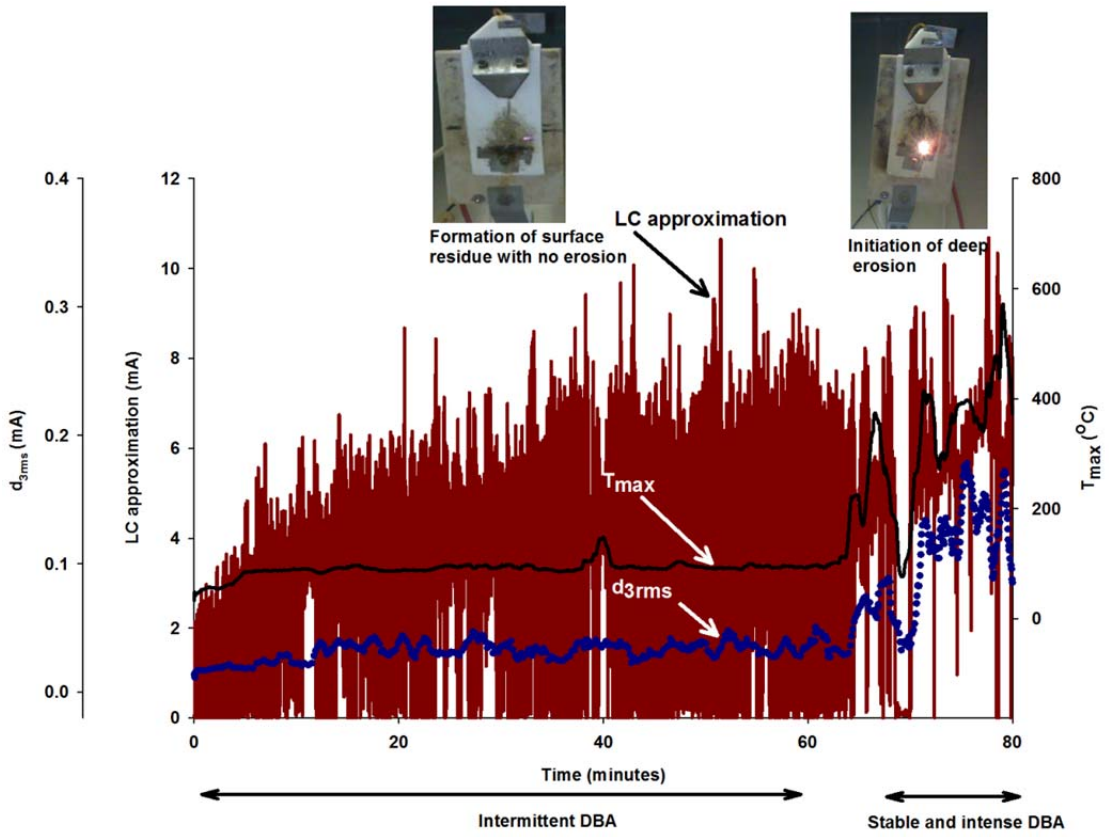

Figure 5.2. Example of the LC approximation, its decomposed d_{3rms} and the corresponding T_{max} in the DC IPT for sample RA30 tested under 2.25 kV +DC.

5.3 The Role of Inorganic Fillers

Based on the aforementioned understanding about the erosion mechanism in the DC IPT, the corresponding thermal effects of fillers are accordingly summarized in Table 5.2. These effects can be used to explain the relative erosion obtained with respect to the effect of fillers type (ATH versus silica) and filler level. Such an understanding of the thermal effects of fillers not only enables comparing erosion of different composites, but also constructs for a reliable and specialized method by which SiR housing composites can be developed using inorganic filler for DC outdoor insulation

applications, rather than simply adding fillers for improved thermal properties of the composites in general.

Table 5.2. Thermal effects of fillers on the suppression of SiR erosion in the DC IPT.

Composite phase	Thermal effect of filler	Effect in the IPT	Indicator in the d3rms
Condensed	Increased thermal conductivity	Delaying the development of T_{max}	Delaying the evolution of d_{3rms}
	Dehydration of fillers increasing heat capacity		
Gas	Dilution of the plasma phase	Increased heat capacity of the plasma phase	Lower magnitude of d_{3rms}

5.3.1 Thermal Effects of Alumina Tri-Hydrate and Silica

As indicated in Table 5.2, the delayed evolution of d_{3rms} observed for both RS30 and RA30 samples as compared to the unfilled SiR (Figure 4.17) can be attributed to an improved thermal conductivity due to the addition of respectively un-hydrated silica and hydrated alumina [50]. In addition, the further delay in hotspots (TE in Figure 4.16 and evolution in T_{max} in Figure 4.17) obtained for the ATH as compared to the silica samples, indicates an additional influential mechanism for the water of hydration to suppress the effect of the residue formation and the DBA heat.

The water of hydration can be also speculated to hinder the physical accumulation of residue, most likely due to the physical cleaning mechanism of the hydrated water [13, 14]. Figure 5.3 shows the temperature profile for RA30L and RS30L samples in the laser heating experiments. Insignificant

difference in the temperature profiles indicates little difference in the thermal conductivities [50]. But the slower evolution of T_{max} with time for RA30L as compared to the RS30L samples shown in Figure 4.18 was evident at about 230 ^{o}C, which is approximately the initial dehydration temperature of ATH in DSC analysis (Figure 5.4). The DSC analysis shows an endothermic dent that begins at 230^{o}C, indicating an increase in the heat capacity of the RA30 samples due to the enthalpy of the dehydration of the ATH. Therefore, the delayed evolution of d_{3rms} shown in Figure 4.17 for the RA30 samples can be also attributed to the enthalpy of the dehydration of ATH.

Figure 5.5 shows the DSC analysis comparing unfilled SiR to RS30 samples in air. The exothermic hump shown for the SiR samples was detected at the same temperature that caused erosion of the samples [37] indicating a thermo-oxidative mechanism of volatile SiR oligomers. Therefore, the reduction in the hump in Figure 5.5 when silica is added indicates a reduction in the volatile oligomers. This reduction is simply attributable to the filler diluting the polymer, thus improving its properties in the condensed phase. In addition, the reduction in the hump shown in Figure 5.5 suggests another dilution effect for the filler to reduce the effect of the combusted oligomers in the plasma phase. Accordingly, the lower magnitudes of d_{3rms} found for the filled as compared to the unfilled SiR (Figure 4.17) can be justified as a result of the dilution of the DBA plasma. The very little difference in the magnitude of d_{3rms} between RA30 and the RS30 samples indicates an insignificant difference in the dilution effect between 30 wt% ATH and silica on suppressing the severity of the DBA plasma.

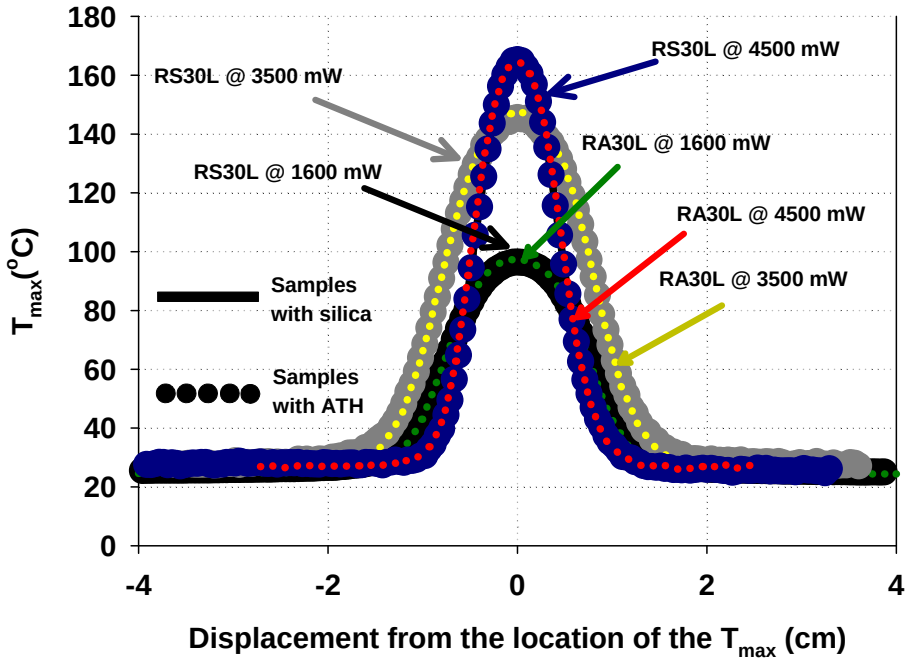

Figure 5.3. Temperature profiles for the RA30L and RS30L samples in laser heating experiments, measurement taken after 30 s of laser power applications.

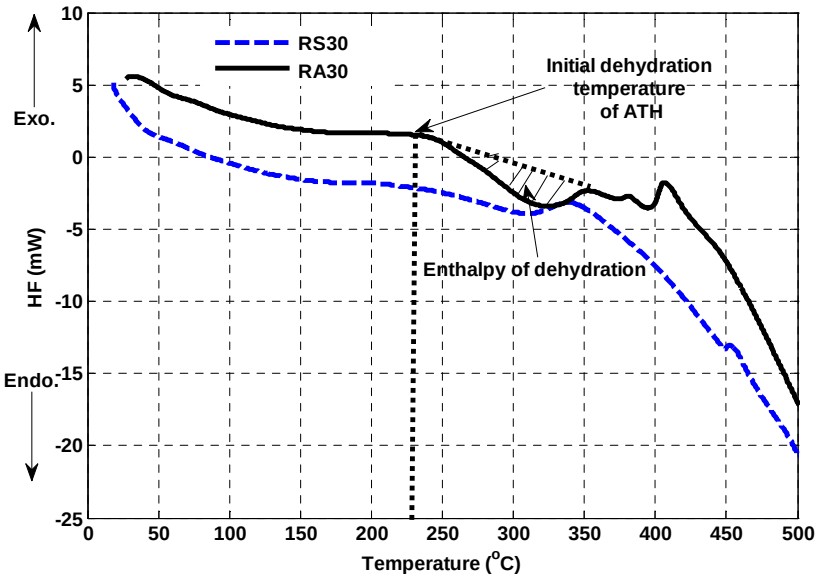

Figure 5.4. DSC analysis of RA30 and RS30 samples in air.

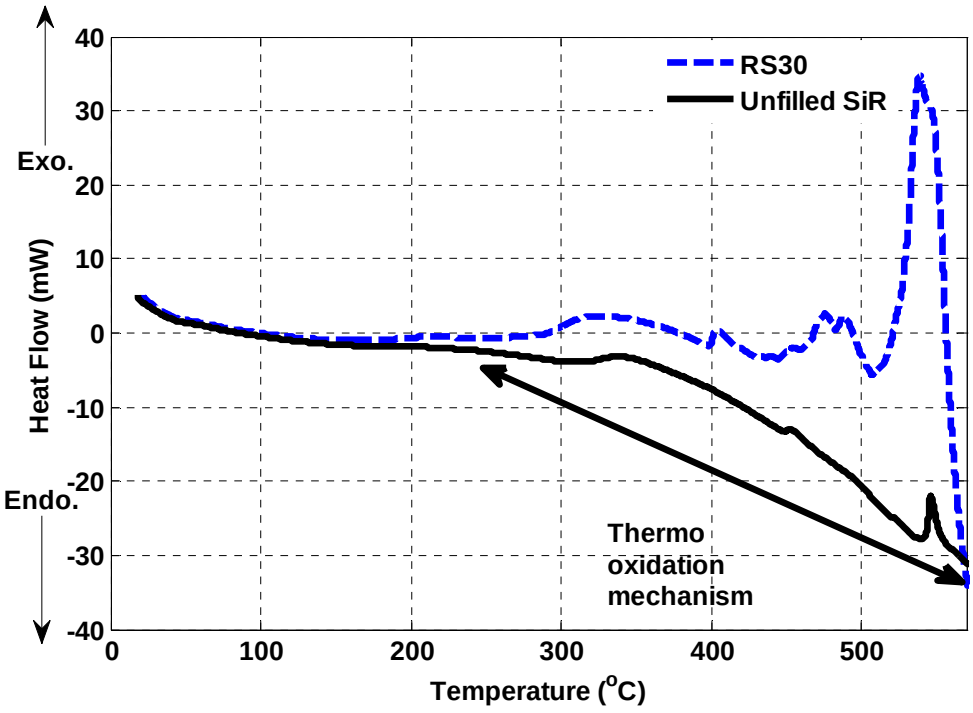

Figure 5.5. DSC analysis of unfilled SiR and RS30 samples in air.

5.3.2 The Effect of Alumina Tri-Hydrate and Silica Levels

The longer time shown for d_{3rms} to develop in the case involving RS50 as compared to the RS30 samples can be attributed to the increased thermal conductivity that is brought about at the higher filler loading [50], thus volume effect of the filler diluting the condensed phase, Figure 5.6. In addition, the relative evolution obtained in Figure 4.18, Figure 4.19 and Figure 4.20 shows the prolonged evolution of the d_{3rms} to be primarily influenced by the filler level, thus thermal conductivity, with an additional influential effect for the ATH.

The higher thermal conductivity has the effect of conducting heat from the region affected by the DBA and distributing the heat over a larger region, thus lowering the temperature. Comparison of temperature profiles in Figure 5.3 and Figure 5.7, respectively shows lower temperature profiles

measured for the RS50L as compared to the RS30L samples during the laser heating experiments, which verifies higher thermal conductivity with higher amounts of silica [50]. Figure 5.7 also shows that the thermal conductivity of RS50L and RA50L is essentially the same as very little difference in the temperature profiles was obtained [50]. However, a lower level of d_{3rms} for the 50 wt% ATH sample suggests yet another mechanism other than thermal conductivity to be present which may be due to dilution of the arc plasma by water of hydration. Similarly, a lower level of d_{3rms} was found for highly filled HTV SiR with ATH as shown in Figure 4.20.

Figure 5.8 shows the DSC analysis of HA25 and HA58 samples in air and N_2. For the HA25 samples, it is evident that the exothermic hump in air is absent in N_2, suggesting a thermo-oxidative mechanism is present during the DC IPT [37, 65]. For the HA58 samples, the exothermic hump is evident in both air and N_2, suggesting an internal oxidation mechanism. An internal oxidation mechanism in highly filled SiR with ATH (>40 wt%) has previously been reported to yield carbon oxides and water, thereby diluting the arc plasma [37]. The diluent gases produced have been accordingly speculated as the water of hydration interacting with the released methyl groups [37, 77].

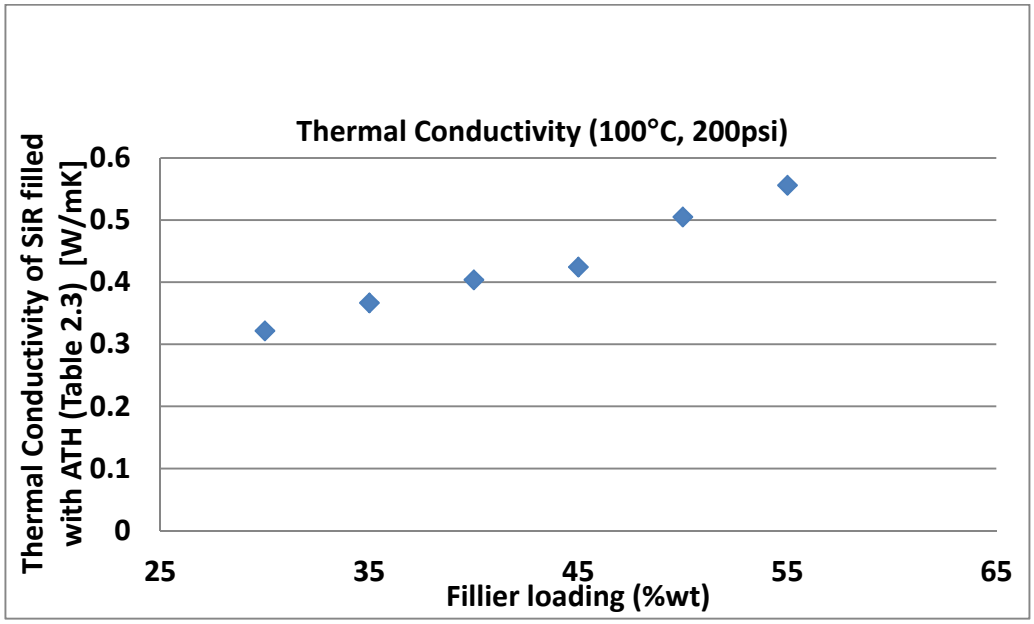

Figure 5.6. Thermal conductivity determined as a function of the filler loading in the ASTM D5470 method.

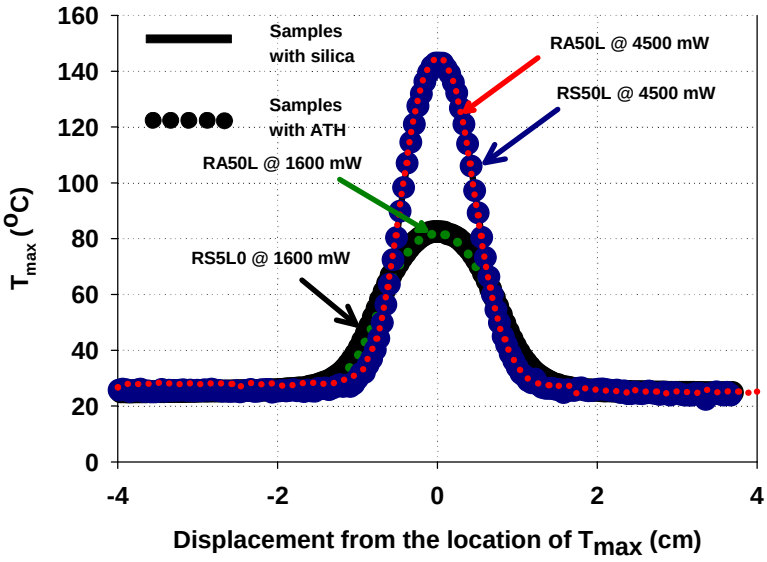

Figure 5.7. Temperature profiles for the RA50L and RS50L samples in laser heating experiments indicating the relative thermal conductivity, measurement taken after 30 s of laser power applications.

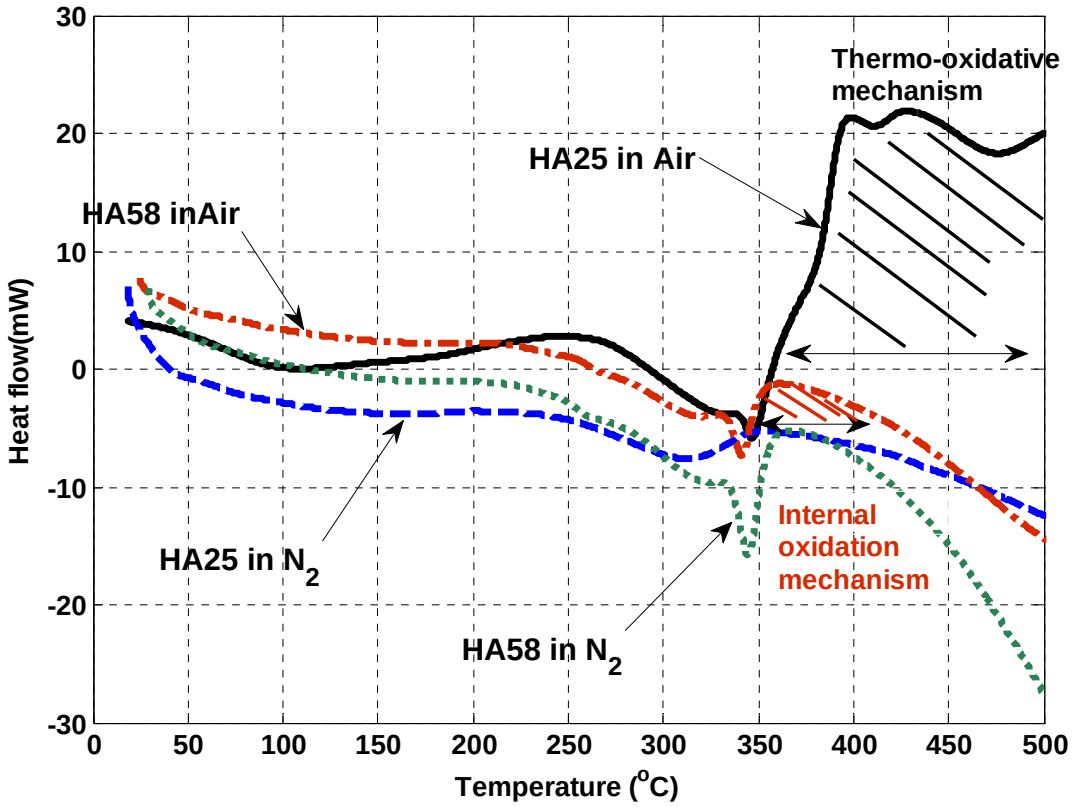

Figure 5.8. DSC analysis of HA25 and HA58 samples in air and N_2 atmospheres showing the internal oxidation mechanism for the HA58 sample.

Chapter 6
Conclusions, Contributions and Future Work

6.1 Conclusions

In this thesis, a thorough mechanistic understanding of the DC DBA as compared to the AC DBA was achieved. In particular, DC as compared to AC DBA characteristics were analyzed by conducting LC measurements prior to and after the inception of DBA. At high test voltages, instability of the contaminant rivulet was found to be an important factor in the development of DBA and, consequently, biasing the test outcomes when equal voltages of rms AC and DC are selected. The ITV in ASTM D2303 was, therefore, proposed as a reliable approach by which +DC and –DC test voltages can be reliably selected. A CV parameter was also proposed as a useful mean of selecting the equivalent DC voltages, and the validity of the parameter was verified experimentally using the ITV test method.

As for the LC study after the inception of the DBA, reduced resistivity for the DBA column was shown under the +DC and AC as compared to the –DC IPTs, giving rise to the magnitude of LC, thus the impinging heat on the tested SiR. This reduction in resistivity was speculated to take place as a result of the produced metallic ions from electrode corrosion under +DC as compared to –DC. On the other hand, minor difference was determined between +DC and AC, indicating the validity of the existing apparatus of the IPT for DC voltages as electrolysis of the test electrodes were not found to bias the IPT outcomes under DC as compared to AC. In addition, the inception behavior of the discharge influencing the length of the DBA was found dependent on the voltage type. Reduced

length was measured for the DC as compared to the AC DBA, with further reduction shown under +DC as compared to –DC voltages. Thermal analysis was accordingly conducted, showing higher hotspot temperatures are promoted with DBA of smaller length.

Erosion in the constant voltage method was investigated under DC by applying the equivalent voltages and compared to AC. Based on this methodology, it was suggested that an improvement in SiR compositions is needed for DC. Moreover, the need to select the creepage distance of polymer insulators designed for AC, yet to be used for DC, with reference to tracking/erosion performance was highlighted.

The study highlighted the importance of investigating the EDBA mechanism, particularly under DC, which may induce severe erosion in the short term in SiR. An investigation into the DBA mechanism leading to erosion of filled SiR in the DC inclined plane test was conducted. Good correlation was obtained between the formation of surface residue, hotspots and the EDBA. The hotspots detected by IR camera correlated well with the temperature of degradation determined by TGA and DSC. To characterize the physical mechanism of DBA, wavelet-based MRA up to seven levels of resolution was applied to the LC waveforms. The analysis showed that both stable and intense discharges characterize the EDBA. A TE parameter was proposed to determine the relative resistance to the formation of residue. Faster accumulation of residue was evident under -DC than +DC, but more concentrated residue giving rise to more stable and intense DBA, thus deeper erosion, was obtained under +DC as compared to -DC. In addition, earlier inception of erosion was obtained for the silica filled- as compared to the ATH filled- silicone, in which the release of the water of hydration was postulated to suppress the residue formation and the effect of the EDBA.

CHAPTER 6 CONCLUSIONS, CONTRIBUTIONS AND FUTURE WORK

The suppression of DBA erosion of silicone rubber by ATH and silica fillers in the DC IPT was accordingly investigated, employing the wavelet based MRA of LC. The d_{3rms} component of the LC as decomposed by the wavelet-based MRA was shown to be an indicator of the effectiveness of the filler type in suppressing erosion by DBA. The addition of ATH or silica filler to SiR increased the thermal conductivity of the composites, prolonging the development of the eroding temperature, and thus the evolution of the d_{3rms}. Additional effect was also obtained for the dehydration enthalpy of ATH, at a filler level of 30 wt%, in suppressing hot spot development. A delay in the evolution of the d_{3rms} as well as reduction in its magnitude was evident with filler level, showing the volume effect of both ATH and silica diluting the SiR. Comparable levels of the d_{3rms} was found between 30 wt% ATH and silica filled composites, which suggests the water of hydration plays a minor role in diluting the SiR but at 58 wt% an internal oxidation mechanism that produces gases diluting the arcing phase appears to suppress erosion.

Table 6.1summarizes the effects determined for silica and ATH fillers to suppress the DBA heat in both the AC and DC IPT. Although similar effects seem to appear in both of the AC and DC IPTs, this study has further proposed LC indicators, $i.e\ d_{3rms}$, through which the effect of fillers are shown during the IPT itself, thereby constructing for the employment of the IPT beyond the validation into the formulation of specialized housing composites.

Table 6.1. The effect of silica and ATH in SiR in suppressing the heat ablation by DBA

Filler type	Filler Effect							
	physical effect on the surface residue		Improving thermal conductivity		Enthalpy of dehydration		Internal oxidation	
	AC	DC	AC	DC	AC	DC	AC	DC
silica	Not reported	d_{3rms}	Salt fog test, Laser and ASTM D5470 [32,50]	d_{3rms}, TGA/DSC and ASTM D5470	Not applied	d_{3rms}, laser and TGA/DSC	Not applied	d_{3rms} and TGA /DSC
ATH	Salt fog test [32]				TGA/DSC [37]		TGA/DSC and internal breakdown voltage experiments [37,77]	

6.2 Contributions

This provides a comprehensive mechanistic framework for the development of the standard DC IPT leading to the development of SiR housing composites for DC outdoor insulation. The proposed framework puts a disciplinary methodology and approach for the understanding of the influential mechanisms on erosion during the IPT. Such understanding could be classified into two stages, (1) understanding the effect of the applied voltage level, polarity, surface condition on erosion leading to the development of the equivalent DC IPT voltages and (2) developing of LC indicators of the EDBA that can be utilized in the understanding of the relative effect of inorganic fillers, leading to the solid designs of SiR housing material specifically for DC outdoor insulation, rather than simply improving the thermal properties of the composite in general. In particular the major contributions of this thesis study can be summarized as the following:

- The DC DBA mechanism as compared to the AC DBA mechanism is understood as an essential step in the development of the equivalent apparatus and guidelines of the standard DC IPT to the existing standard AC. A comprehensive validation to the existing IPT

apparatus, which has been designed for AC voltages, for DC voltages is conducted, showing a modification of the applied DC as compared to the existing standard AC voltages is required, while maintaining the same apparatus.

- The proposed scheme in this study of investigating the eroding DBA mechanism under DC voltages shows the need for improvement of SiR housing composites to withstand stable and intense DBA, which was found to be an essential requirement for DC outdoor insulation applications.
- The role of inorganic filler in suppressing the heat ablation by DBA is understood during the DC IPT, with a LC-based method proposed for this understanding, showing the potential of extending the employment of the IPT beyond the conventional evaluation of composites into the development of case-specific composites for DC outdoor insulation applications.

List of awards, recognition and publications based on this thesis study is given in Appendix 2.

6.3 Future Work

The reproducibility and the repeatability of the determined erosion resistance has been a concern highlighted for the AC IPT; in this study and throughout the literature, the DC IPT has shown the potential of providing relatively reproducible and repeatable outcomes in terms of ranking materials or understanding the DBA mechanism. However, further investigation into the repeatability and the reproducibility of the DC IPT outcomes is required, through conducting round-robin tests and testing wide spectrum of materials.

CHAPTER 6 CONCLUSIONS, CONTRIBUTIONS AND FUTURE WORK

Regulated power supply was used in this study in order to provide a reliable investigation of the fundamental mechanism of the DBA under DC voltages; however, different DC voltage sources with various ripple factors were used in the literature. Such undisciplined use of voltage sources for DC the IPT may affect the reproducibility of the study outcomes in the literature. Voltage sources of the standard AC IPT have been built to produce harmonic-free voltage waveforms at power frequency. Similarly, clear guidelines have to be also provided with respect to DC thorough investigation of the effect of voltage source characteristics such as the ripple factor and voltage regulation.

The use of ATH filler in high levels diluting both the condensed and gas phases of SiR was defined as the prevailing suppression effect of erosion. The use of other hydrated fillers possessing higher enthalpy of dehydration than ATH such as magnesium hydroxide ($Mg(OH)_3$) should be accordingly investigated. The addition of nano-sized fillers with uniform dispersion in the SiR matrix can improve the thermal conductivity immensely, suggesting the potential of the applying nano-sized fillers to suppress the stable and intense DBA obtained under DC stresses.

Cost is another important issue that has to be considered in the development of SiR insulation housing composites. Such a constraint necessitates the quantization of the thermal effects of fillers in SiR in order to optimize composites for commercial use. The superior pollution performance of SiR facilitated its use over other polymeric materials for outdoor insulation; however, investigating erosion of other commonly employed insulating materials in outdoor insulation, such as ethylene propylene diene monomer (EPDM), is important under DC for either further validation of the use of SiR under DC or development of alternative composites for DC.

References

[1] R. S. Gorur, E. A. Cherney and J. T. Burnham, *Outdoor Insulators.* Phoenix, Arizona, USA: Ravi S. Gorur Inc., 1999.

[2] H. Homma, T. Kuroyagi, K. Izumi, C. Mirley, J. Ronzello and S. Boggs, "Diffusion of low molecular weight siloxane from bulk to surface," *IEEE Transactions on Dielectrics and Electrical Insulation,* vol. 6, pp. 370-375, 1999.

[3] Luiz Henrique Meyer, "A study of the role of fillers in silicone rubber compounds for outdoor insulation," PhD dissertation, ECE, University of Waterloo, Waterloo, ON, Canada, 2003.

[4] K. Mathes and E. McGowan, "Electrical insulation tracking—A design-engineering problem," *Electro-technology*, vol. 69, no. 4 pp. 146-151, 1962.

[5] L. Warren, "Testing for tracking [organic insulating materials]," *IEE Colloquium on Insulation Diagnostics-Methods for Determining Quality, Remnant Life and Proof Testing,* 1991, pp. 3/1-313.

[6] K. N. Mathes, L. E. Sieffert, H. P. Walker and R. H. Lindsey, "Methods for Determining the effects of contaminants on electrical insulation," *Transactions of the American Institute of Electrical Engineers,* vol. 68, pp. 113-119, 1949.

[7] S. Hamdani, C. Longuet, D. Perrin, J. Lopez-cuesta and F. Ganachaud, "Flame retardancy of silicone-based materials," *Polymer Degradation and Stability,* vol. 94, pp. 465-495, 2009.

[8] S. Kim, E. A. Cherney, R. Hackam and K. G. Rutherford, "Chemical changes at the surface of RTV silicone rubber coatings on insulators during dry-band arcing," *IEEE Transactions on Dielectrics and Electrical Insulation,* vol. 1, pp. 106-123, 1994.

[9] G. Camino, S. Lomakin and M. Lazzari, "Polydimethylsiloxane thermal degradation Part 1. Kinetic aspects," *Polymer,* vol. 42, pp. 2395-2402, 2001.

[10] G. Camino, S. Lomakin and M. Lageard, "Thermal polydimethylsiloxane degradation. Part 2. The degradation mechanisms," *Polymer,* vol. 43, pp. 2011-2015, 2002.

[11] D. C. Timpe Jr, "Formaldehyde Generation from Silicone Rubber," Technical document, ALCON: Silicone Technologies Division.

[12] D. Timpe, "Silicone Rubber Flame Resistance," *Rubber and Plastics News, pp. 1-6, Jan.1,* 2007.

[13] D. Parr and R. Scarisbrick, "Performance of synthetic insulating materials under polluted conditions," *Proceedings of the Institution of Electrical Engineers,* 1965, pp. 1625-1632.

[14] R. Gorur, E. Cherney and R. Hackam, "A Comparative Study of Polymer Insulating Materials Undern Salt-Fog Conditions," *IEEE Transactions on Electrical Insulation,* pp. 175-182, 1986.

[15] E.A. Cherney, "50 Years in the Development of Polymer Suspension-Type Insulators", *IEEE Electrical Insulation Magazine*, vol. 29, pp. 18-26, 2013.

[16] S. Bossi, A. Pigini, G.P. Fini, A. Porrino, Channakeshava, N. Vasudev, and M. Ramamoorty, "Study of the performance of composite insulators in polluted conditions," *Cigre Report,* pp. 33-104/1-7, 1994.

[17] G. Heger, H. Vermeulen, J. Holtzhausen and W. Vosloo, "A comparative study of insulator materials exposed to high voltage AC and DC surface discharges," *IEEE Transactions on Dielectrics and Electrical Insulation, ,* vol. 17, pp. 513-520, 2010.

[18] G. Bruce, S. Rowland and A. Krivda, "Performance of silicone rubber in DC inclined plane tracking tests," *IEEE Transactions on Dielectrics and Electrical Insulation,* vol. 17, pp. 521-532, 2010.

[19] R. A. Ghunem, S. H. Jayaram and E. Cherney, "Erosion of silicone rubber composites in the AC and DC inclined plane tests," *IEEE Transactions on Dielectrics and Electrical Insulation, ,* vol. 20, pp. 229-236, 2013.

[20] J. V. Vas, B. Venkatesulu and M. Thomas, "Tracking and erosion of silicone rubber nanocomposites under DC voltages of both polarities," *IEEE Transactions on Dielectrics and Electrical Insulation, ,* vol. 19, pp. 91-98, 2012.

[21] K. Mathes and E. McGowan, "Surface electrical failure in the presence of contaminants: the inclined-plane liquid-contaminant test," *Transactions of the American Institute of Electrical Engineers, Part I: Communication and Electronics,* vol. 80, pp. 281-289, 1961.

[22] *Standard Test Methods for Liquid-Contaminant, Inclined-Plane Tracking and Erosion of Insulating Materials*, ASTM D2303, 1997.

[23] *Electrical insulating materials used under severe ambient conditions- Test methods for evaluating resistance to tracking and erosion*, IEC 60587, 2007.

[24] J. Crespo-Sandova, A. Haddad, H. Griffiths and P. Coventry, "Rate of energy absorption as indicator for the tracking/erosion test of silicone rubber," *IEEE Transactions on Dielectrics and Electrical Insulation,* vol. 17, pp. 1772-1780, 2010.

[25] L. H. Meyer, S. H. Jayaram and E. A. Cherney, "Correlation of damage, dry band arcing energy, and temperature in inclined plane testing of silicone rubber for outdoor insulation," *IEEE Transactions on Dielectrics and Electrical Insulation,* vol. 11, pp. 424-432, 2004.

[26] V. Rajini and K. Udayakumar, "Degradation of silicone rubber under AC or DC voltages in radiation environment," *IEEE Transactions on Dielectrics and Electrical Insulation,* vol. 16, pp. 834-841, 2009.

[27] G. Heger, H. Vermeulen, J. Holtzhausen and W. Vosloo, "A comparative study of insulator materials exposed to high voltage AC and DC surface discharges," *IEEE Transactions on Dielectrics and Electrical Insulation,* vol. 17, pp. 513-520, 2010.

[28] T. Gustavsson, S. Gubanski, H. Hillborg, S. Karlsson and U. W. Gedde, "Aging of silicone rubber under ac or dc voltages in a coastal environment," *IEEE Transactions on Dielectrics and Electrical Insulation,* vol. 8, pp. 1029-1039, 2001.

[29] R. Sarathi, S. Chandrasekar and N. Yoshimura, "Investigation of tracking phenomena in outdoor polymeric insulation material under DC voltages using wavelets," *IEEE Transactions on Power Delivery,* vol. 21, pp. 515-517, 2006.

[30] R. Gorur, J. Montesinos, L. Varadadesikan, S. Simmons and M. Shah, "A laboratory test for tracking and erosion resistance of HV outdoor insulation," *IEEE Transactions on Dielectrics and Electrical Insulation,* vol. 4, pp. 767-774, 1997.

[31] V. Moreno and R. Gorur, "Ac and dc performance of polymeric housing materials for HV outdoor insulators," *IEEE Transactions on Dielectrics and Electrical Insulation,* vol. 6, pp. 342-350, 1999.

[32] R. Gorus, E. Cherney and R. Hackam, "The AC and DC performance of polymeric insulating materials under accelerated aging in a fog chamber," *IEEE Transactions on Power Delivery,* vol. 3, pp. 1892-1902, 1988.

[33] R. Mailfert, L. Pargamin and D. Riviere, "Electrical reliability of DC line insulators," *IEEE Transactions on Electrical Insulation,* pp. 267-276, 1981.

[34] S. Rowland, G. Bruce, Y. Liu, A. Krivda and L. Schmidt, "Use of image analysis in DC inclined plane tracking tests of nano and micro composites," *IEEE Transactions on Dielectrics and Electrical Insulation,* vol. 18, pp. 365-374, 2011.

[35] X. Zhang, S. Rowland and V. Terzija, "Increased energy in stable dry-band arcs due to length compression," *IEEE Transactions on Dielectrics and Electrical Insulation,* vol. 17, pp. 473-480, 2010.

[36] K. L. Chrzan and F. Moro, "Concentrated discharges and dry bands on polluted outdoor insulators," *IEEE Transactions on Power Delivery,* vol. 22, pp. 466-471, 2007.

[37] S. Kumagai and N. Yoshimura, "Tracking and erosion of HTV silicone rubber and suppression mechanism of ATH," *IEEE Transactions on Dielectrics and Electrical Insulation,* vol. 8, pp. 203-211, 2001.

[38] S. Kumagai, X. Wang and N. Yoshimura, "Solid residue formation of RTV silicone rubber due to dry-band arcing and thermal decomposition," *IEEE Transactions on Dielectrics and Electrical Insulation,* vol. 5, pp. 281-289, 1998.

[39] G. Heger, H. Vermeulen, J. Holtzhausen and W. Vosloo, "A comparative study of insulator materials exposed to high voltage AC and DC surface discharges," *IEEE Transactions on Dielectrics and Electrical Insulation,* vol. 17, pp. 513-520, 2010.

[40] I. Gutman and R. Hartings, "Single stress and multistress AC/DC tracking and erosion tests for composite insulators," *Nordic Insulation Symposium,* 1999, pp. 271-278.

[41] I. Gutman, K. Halsan, J. Seifert, and W. L. Vosloo, "Pollution and aging performance of DC line composite insulators: Service experience vs. laboratory experience," *World Conference and Exhibition (INMR World Congress) on Insulators, Arresters, Bushings and Cable Accessories,* 2011, pp. 1-11.

[42] J. O. Loberg and E. C. Salthouse, "Dry-band growth on polluted insulation," *IEEE Transactions on Electrical Insulation,* pp. 136-141, 1971.

[43] F. Schmuck, R. Barsch and J. Pilling, "About an improved evaluation of results by the standardized salt-fog procedure for composite insulators," *European Transactions on Electrical Power,* vol. 6, pp. 237-243, 1996.

[44] A. H. El-Hag, S. H. Jayaram and E. A. Cherney, "Fundamental and low frequency harmonic components of leakage current as a diagnostic tool to study aging of RTV and HTV silicone rubber in salt-fog," *IEEE Transactions on Dielectrics and Electrical Insulation,* vol. 10, pp. 128-136, 2003.

[45] A. H. El-Hag, "A new technique to detect dry-band arcing," *IEEE Transactions on Power Delivery,* vol. 20, pp. 1202-1203, 2005.

[46] A. H. El-Hag, "Leakage current characterization for estimating the conditions of non-ceramic insulators' surfaces," *Electric Power System Research,* vol. 77, pp. 379-384, 2007.

[47] S. Chandrasekar, C. Kalaivanan, A. Cavallini and G. Montanari, "Investigations on leakage current and phase angle characteristics of porcelain and polymeric insulator under contaminated conditions," *IEEE Transactions on Dielectrics and Electrical Insulation,* vol. 16, pp. 574-583, 2009.

[48] R. Sarathi and S. Chandrasekar, "Diagnostic study of the surface condition of the insulation structure using wavelet transform and neural networks," *Electric Power System Research,* vol. 68, pp. 137-147, 2003.

REFERENCES

[49] K. N. Mathes, "Surface failure measurements," *Engineering Dielectrics, Electrical Properties of Solid Insulating Materials: Measurements Techniques*, 2B. R. Bartnikas, Ed. Philadelphia: STP 926, Ed. 1983, pp. 289-293.

[50] L. Meyer, S. Jayaram and E. A. Cherney, "Thermal conductivity of filled silicone rubber and its relationship to erosion resistance in the inclined plane test," *IEEE Transactions on Dielectrics and Electrical Insulation,* vol. 11, pp. 620-630, 2004.

[51] L. Meyer, E. Cherney and S. Jayaram, "The role of inorganic fillers in silicone rubber for outdoor insulation alumina tri-hydrate or silica," *IEEE Electrical Insulation Magazine,* vol. 20, pp. 13-21, 2004.

[52] L. E. Schmidt, X. Kornmann, A. Krivda and H. Hillborg, "Tracking and erosion resistance of high temperature vulcanizing ATH-free silicone rubber," *IEEE Transactions on Dielectrics and Electrical Insulation,* vol. 17, pp. 533-540, 2010.

[53] S. Kim, E. A. Cherney and R. Hackam, "Thermal characteristics of RTV silicone rubber coatings as a function of filler level," *Annual Report. Conference on Electrical Insulation and Dielectric Phenomena,* 1992, pp. 713-718.

[54] X. Zhang and S. Rowland, "Stability and energy of low current surface discharges on wet surfaces," *IEEE Transactions on Dielectrics and Electrical Insulation,* vol. 19, pp. 2055-2062, 2012.

[55] S. Bian, S. Jayaram and E. A. Cherney, "Erosion resistance of electrospun silicone rubber nanocomposites," *IEEE Transactions on Dielectrics and Electrical Insulation,* vol. 20, pp. 185-193, 2013.

[56] R. Ghunem, S. Jayaram and E. Cherney, "Statistical indicators of silicone rubber erosion in the DC inclined plane test," *Annual Report Conference on Electrical Insulation and Dielectric Phenomena (CEIDP),* 2012, pp. 737-740.

[57] *Standard test method for thermal transmission properties of thermally conductive electrical insulation materials*, ASTM D5470, 2006.

[58] E. Salthouse, "Initiation of dry bands on polluted insulation," *Proceedings of the Institution of Electrical Engineers,* vol. 115, pp. 1707-1712, 1968.

[59] C. S. Burrus, R. A. Gopinath, H. Guo, J. E. Odegard and I. W. Selesnick, *Introduction to Wavelets and Wavelet Transforms: A Primer*. Prentice Hall Upper Saddle River, 1998.

[60] T. R. Hull, A. Witkowski and L. Hollingbery, "Fire retardant action of mineral fillers," *Polymer Degradation and Stability,* vol. 96, pp. 1462-1469, 2011.

[61] R. N. Rothon, "Effects of particulate fillers on flame retardant properties of composites," *Particulate-Filled Polymer Composites,* pp. 263, 2003.

[62] R. A. Ghunem, S. H. Jayaram, and E. A. Cherney, "Investigation into the Eroding Dry-band Arcing under DC Using Wavelet Based Multiresolution Analysis," *IEEE Transactions on Dielectrics and Electrical Insulation,* accepted, 2013.

[63] R. A. Ghunem, S. H. Jayaram and E. A. Cherney, "Comparative inclined plane tests on silicone and EPDM elastomers under DC," *IEEE Electrical Insulation Conference (EIC),* 2013, pp. 356-359.

[64] S. Ansorge, F. Schmuck and K. O. Papailiou, "Improved silicone rubbers for the use as housing material in composite insulators," *IEEE Transactions on Dielectrics and Electrical Insulation,* vol. 19, pp. 209-217, 2012.

[65] I. Ramirez, E. A. Cherney and S. Jarayam, "Comparison of the erosion resistance of silicone rubber and EPDM composites filled with micro silica and ATH," *IEEE Transactions on Dielectrics and Electrical Insulation,* vol. 19, pp. 218-224, 2012.

[66] X. Zhang, "Ageing of outdoor insulation under low leakage currents ," PhD dissertation, School of Electrical and Electronic Engineering, University of Manchester, Manchester, UK, 2010.

[67] M. El-A Slama, A. Beroual and H. Hadi, "Analytical computation of discharge characteristic constants and critical parameters of flashover of polluted insulators," *IEEE Transactions on Dielectrics and Electrical Insulation,* vol. 17, pp. 1764-1771, 2010.

[68] R. Chang and L. Mazeika, "Analysis of electrical activity associated with inclined-plane tracking and erosion of insulating materials," *IEEE Transactions on Dielectrics and Electrical Insulation,* vol. 7, pp. 394-400, 2000.

[69] D. C. Jolly, "A quantitative method for determining the resistance of polymers to surface discharges," *IEEE Transactions on Electrical Insulation,* pp. 293-299, 1982.

[70] S. W. Smith, "Statistics, Probability and Noise," *Digital Signal Processing: a Practical Guide for Engineers and Scientists*. Burlignton, MA, USA: Elsevier Science, 2003, ch.2, sec.2, pp. 11-34.

[71] M. Vallet, B. Berge and L. Vovelle, "Electrowetting of water and aqueous solutions on poly (ethylene terephthalate) insulating films," *Polymer,* vol. 37, pp. 2465-2470, 1996.

[72] M. Vallet, M. Vallade and B. Berge, "Limiting phenomena for the spreading of water on polymer films by electrowetting," *The European Physical Journal B-Condensed Matter and Complex Systems,* vol. 11, pp. 583-591, 1999.

[73] F. Mugele and J. Baret, "Electrowetting: from basics to applications," *Journal of Physics: Condensed Matter,* vol. 17, pp. R705, 2005.

[74] P. Garcí-Sánchez and F. Mugele, "Fundamentals of electrowetting and applications in microsystems," in *Electrokinetics and Electrohydrodynamics in Microsystems,* vol. 530, pp. 85-125, 2011.

[75] R. Sundararajan and R. Gorur, "Dynamic arc modeling of pollution flashover of insulators under dc voltage," *IEEE Transactions on Electrical Insulation,* vol. 28, pp. 209-218, 1993.

[76] S. Bossi, A. Pigini, G.P. Fini, A. Porrino, Channakeshava, N. Vasudev, and M. Ramamoorty, "Study of the performance of composite insulators in polluted conditions," *Cigre Report,* 1994, pp. 33-104/1-7.

[77] R. Norman and A. Kessel, "Internal Oxidation Mechanism for Nontracking Organic Insulations," *Transactions of the American Institute of Electrical Engineers , Part III.Power Apparatus and Systems,* vol. 77, pp. 632-636, 1958.

Appendix A

Statistical Analysis

The mean, skewness and kurtosis of the distribution of the LC are investigated for possible statistical indicators of the DBA leading to erosion in the DC IPT. During the IPTs, the statistical parameters of the LC were computed over the acquired a 1-seocnd window, thus obtaining more time resolution in the analysis as compared to obtaining generic parameters for the overall distribution of the LC waveform. It should be noted that bias-corrected skewness and kurtosis were computed in the analysis, and the magnitude of the LC was used in the computation of the parameters for the case of negative polarity. The statistical parameters were obtained using Matlab ®.

As examples Figures A1 and A2 show the development of the T_{max} with time along with the statistical parameters determined under +DC and -DC, respectively. A significant rise in the hotspot temperature exceeding 400^{o}C is evident in both silica and the ATH samples and under both polarities. At this stage, it can be recognized that each of the statistical parameters has a correlation with the EDBA.

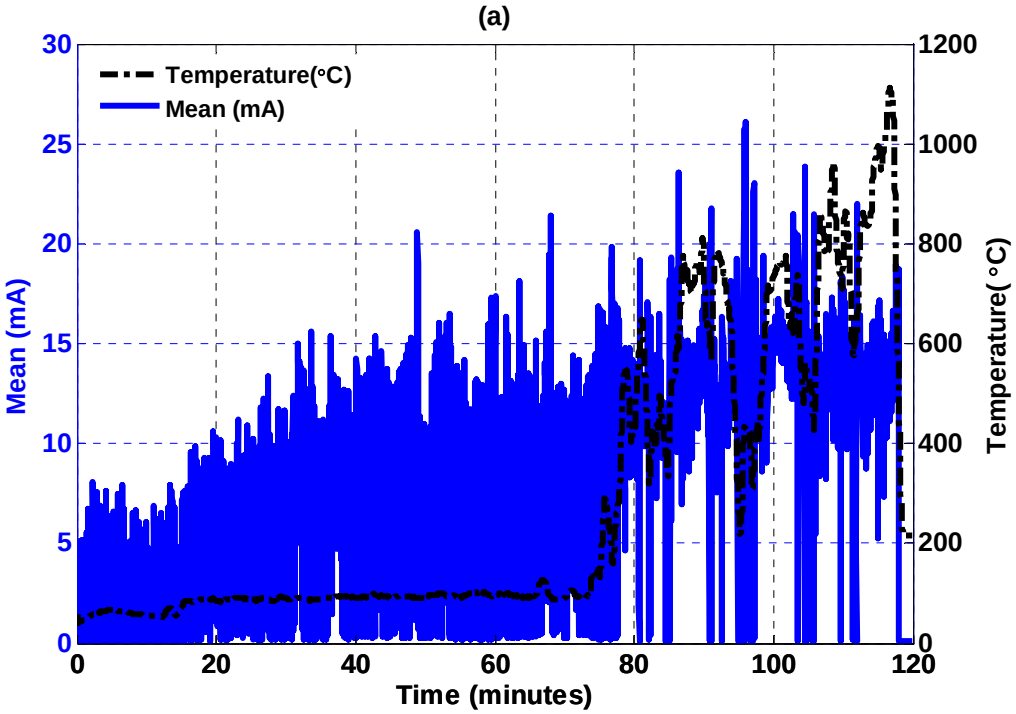
(a)
Temperature(°C)
Mean (mA)
Mean (mA)
Temperature(°C)
Time (minutes)
0
5
10
15
20
25
30
0
200
400
600
800
1000
1200
0
20
40
60
80
100
120

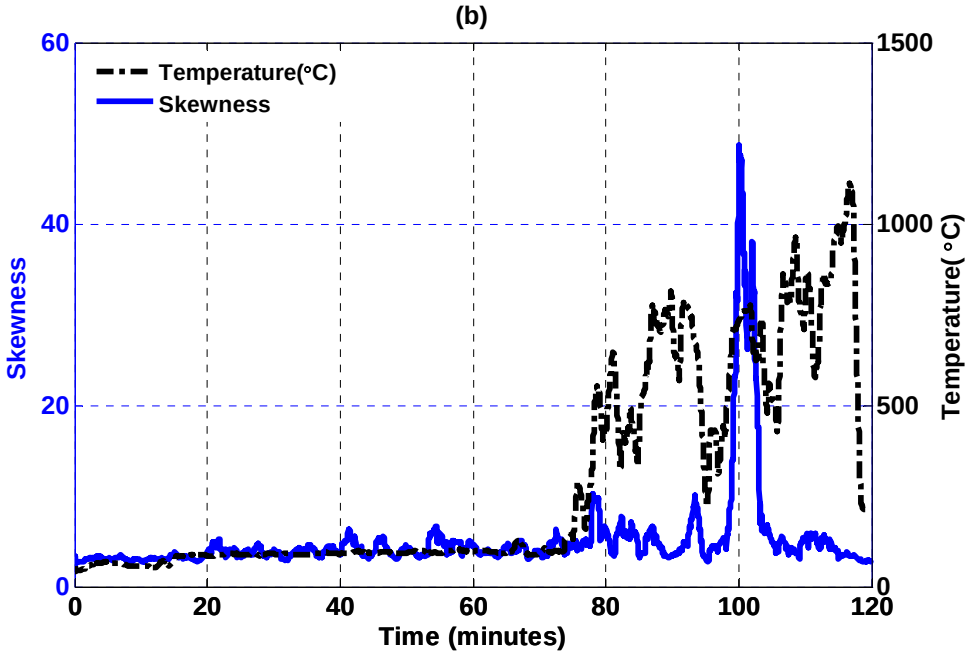
(b)
Temperature(°C)
Skewness
Skewness
Temperature(°C)
Time (minutes)
0
20
40
60
0
500
1000
1500
0
20
40
60
80
100
120

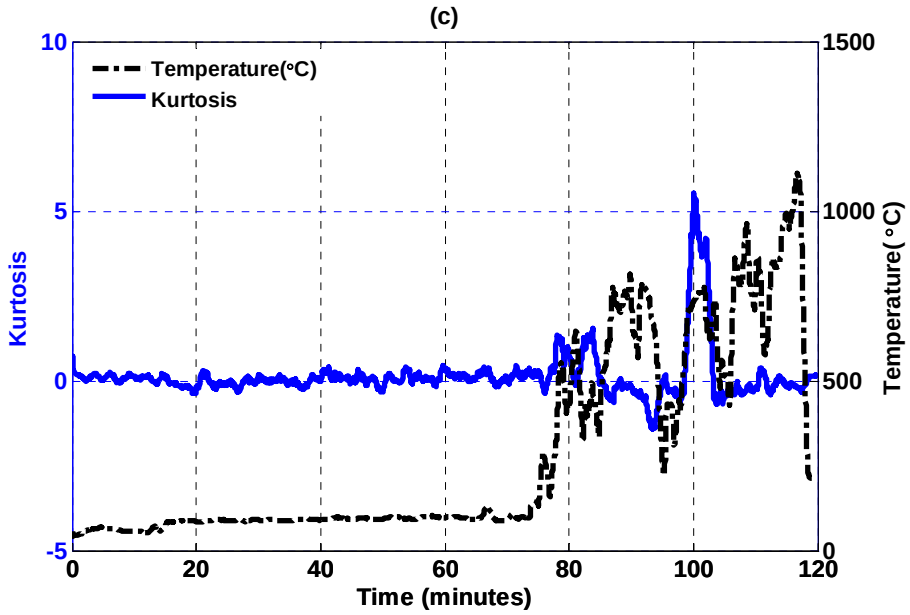

Figure A.1 Typical pattern of development of the T_{max} and the statistical parameters determined; ((a) mean, (b) skewness and (c) kurtosis), with time for the RA30 samples tested under +2.25kV.

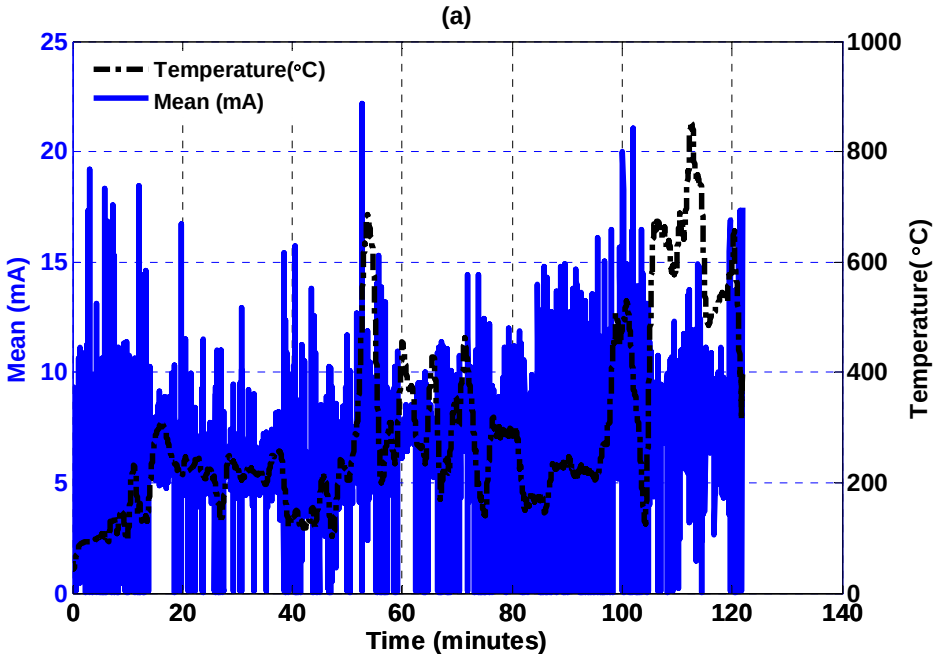

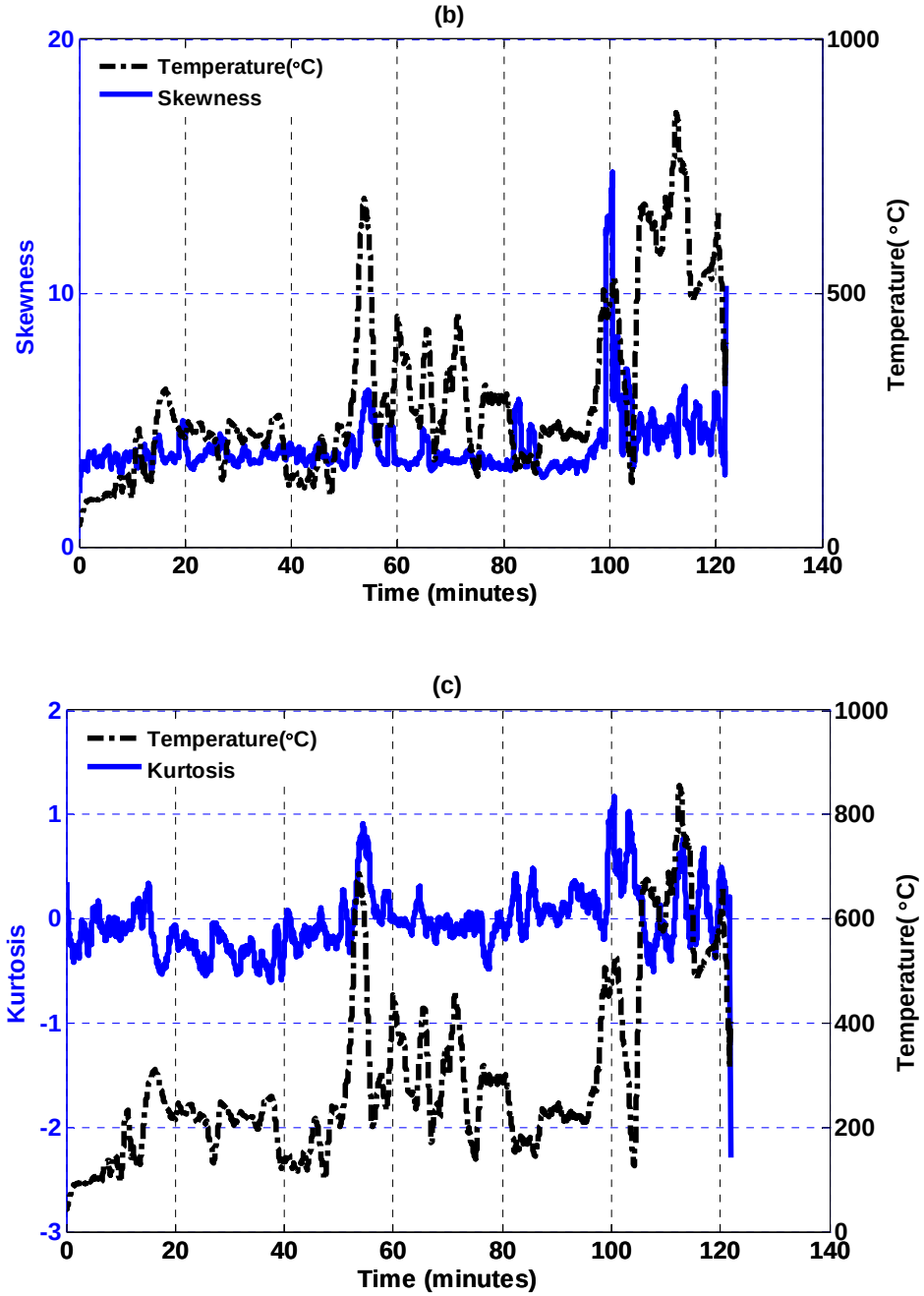

Figure A.2. Typical pattern of development of the T_{max} and the statistical parameters determined ((a) mean, (b) skewness and (c) kurtosis) with time for the RS30 samples tested under -3kV.

APPENDIX A STATISTICAL ANALYSIS

Fewer non-conducting periods of LC, where i[n] <1mA [18], are found to be associated with the EDBA. In other words, significant erosion can be correlated to the occurrence of stable discharges and this must be due to the higher energy dissipated in the longer discharge periods. Skewness and kurtosis are useful indicators of the shape of the LC distribution and skewness is a measure of the degree of the discharge asymmetry with respect to the mean. As shown in Figures A1 and A2, peaks of skewness were obtained at the EDBA stage. Positive skewness was detected throughout the analysis, hence, confirming the occurrence of more discharges with higher magnitudes and thus severeness. Similarly a substantial deviation from zero was obtained for the kurtosis of the discharge, where this deviation indicates a change from a normal distribution. Normal distribution was fitted to the discharge current in the DC IPT [18], but this finding does not seem to be true for all the stages of the DBA as found in this study. It can be rather stated that the discharge current in the DC IPT possesses a normal distribution until the discharge becomes sufficient enough to cause significant erosion on the surface.

Appendix B

Recognition, Awards and List of Papers

B1. Recognition and Awards

1. Part of this study, "A Study of the Direct Current Erosion Mechanism of Polymeric Materials" was awarded the 2012 IEEE dielectrics and electrical insulation society (DEIS) graduate student fellowship and therefore presented in the Conference on Dielectrics and Electrical Insulation Phenomena (CEIDP), October 2013, Shezhen, China.

2. The author of this thesis has been invited to be a member of the IEEE DEIS outdoor insulation committee working in the DC IPT task force, which features parts of this study.

B2. List of Papers in refereed journals

1 **R. A. Ghunem**, S. H. Jayaram, and E. A. Cherney, "Erosion of Silicone Rubber Composites in the AC and DC Inclined Plane Tests," *IEEE Transactions on Dielectrics and Electrical Insulation*, vol. 20, pp. 229-236, 2013.

2 **R. A. Ghunem**, S. H. Jayaram, and E. A. Cherney, "Investigation into the Eroding Dry-Band Arcing under DC Using Wavelet-Based Multiresolution Analysis," *IEEE Transactions on Dielectrics and Electrical Insulation,* vol. 21, pp.713-720, 2014.

3 **R. A. Ghunem**, S. H. Jayaram, and E. A. Cherney, "Suppression of Silicone Rubber Erosion by Alumina Tri-hydrate and Silica Fillers From Dry-Band Arcing under DC," *IEEE Transactions on Dielectrics and Electrical Insulation,* Submitted, December 2013.

B3. List of Papers in refereed conference proceedings

1 **R. A. Ghunem**, S. H. Jayaram, and E. A. Cherney, "Comparative Inclined Plane Tests on Silicone and EPDM Elastomers under DC," *IEEE International Symposium on Electrical Insulation*, pp. 356-359, 2013.

2 **R. A. Ghunem**, S. H. Jayaram, and E. A. Cherney, "Incllined Plane Initial Tracking Voltage for AC, +DC and –DC," *IEEE International Symposium on Electrical Insulation*, pp. 459-463, 2012.

3 **R.A. Ghunem**, S. H. Jayaram, and E. A. Cherney, "Erosion of ATH and Silica Filled Silicone Rubber in the DC Inclined Plane Test," *IEEE international Conference on Properties and Applications of Dielectric Materials*," pp. 1-4, 2012.

4 **R. A. Ghunem**, S. H. Jayaram, E. A. Cherney, "Statistical Parameters as Indicators of Silicone Rubber Tracking/Erosion in the DC Inclined Plane Test," *Conference on Electrical Insulation and Dielectric Phenomena*, pp. 737-740, 2012.

5 **R. A. Ghunem**, S. H. Jayaram, E. A. Cherney, "Suppression of Erosion due to Dry-Band Arcing under DC by Alumina Tri-hydrate Filler in Silicone Rubber," *Conference on Electrical Insulation and Dielectric Phenomena*, pp.20-23, 2013.

B4. List of Non-refereed conference proceedings/presentations

1 **R. A. Ghunem**, S. H. Jayaram & E. A. Cherney "A Detection Method of the Dry-band Arcing in the Inclined Plane Test" 2011 Cage Club Student Conference on High Voltage Engineering and Electrostatics, University of Waterloo, 2011.

2 **R. A. Ghunem**, S. H. Jayaram & E. A. Cherney "Leakage Current Measurements of Wetted Silicone Rubber in AC and DC Inclined Plane Tests" 2013 Cage Club Student Conference on High Voltage Engineering and Electrostatics, University of Waterloo, 2013.